OCEANIC MICROSTRUCTURE OBSERVED NEAR BERMUDA USING A TOWED SENSOR

by

BRUCE ARTHUR MAGNELL

S.B., Massachusetts Institute of Technology

1966

S.M., Massachusetts Institute of Technology

1968

SUBMITTED IN PARTIAL FULFILLMENT

OF THE REQUIREMENTS FOR THE

DEGREE OF DOCTOR OF SCIENCE

at the

MASSACHUSETTS INSTITUTE OF TECHNOLOGY

and the

WOODS HOLE OCEANOGRAPHIC INSTITUTION

June 1973

Signature of Author .....
Joint Program in Oceanography, Woods Hole Oceanographic Institution and Massachusetts Institute of Technology, Department of Meteorology

Certified by .....
Thesis Supervisor

Accepted by .....
Chairman, Joint Oceanography Committee in the Earth Sciences, Massachusetts Institute of Technology - Woods Hole Oceanographic Institution

Lindgren WITHDRAWN FROM DTIC (FOR 30 1973)

MIT Libraries
Document Services

Room 14-0551
77 Massachusetts Avenue
Cambridge, MA 02139
Ph: 617.253.5668 Fax: 617.253.1690
Email: docs@mit.edu
http://libraries.mit.edu/docs

DISCLAIMER OF QUALITY

Due to the condition of the original material, there are unavoidable flaws in this reproduction. We have made every effort possible to provide you with the best copy available. If you are dissatisfied with this product and find it unusable, please contact Document Services as soon as possible.

Thank you.

This is the best available copy.

ABSTRACT

OCEANIC MICROSTRUCTURE OBSERVED NEAR BERMUDA
USING A TOWED SENSOR

by

BRUCE ARTHUR MAGNELL

Submitted to the Department of Meterology on May 4, 1973 in partial fulfillment of the requirements for the degree of Doctor of Science in Oceanography.

Many hypotheses have been advanced to explain the formation of mixed layers in the ocean; the salt finger type of double-diffusive convection, in particular, has received much attention. Because of their uniquely ordered nature, salt fingers should be readily identifiable in the deep thermocline, if in fact they exist there. A relatively limited experiment could thus produce a definitive evaluation of the importance of salt finger convection in the ocean, at least in certain places and at certain times. Such an evaluation, which would help to direct future work on oceanic microstructure, was the primary objective of this thesis.

A secondary and more general objective was to measure the intermittency of mixing events in the ocean; and also, by measuring the RMS gradients of temperature and salinity in such events, to evaluate directly the intensity of vertical mixing.

Since a horizontally-towed sensor is essential if salt fingers are to be observed directly, a new instrument has been designed and built which can resolve fractional-centimeter structures of electrical conductivity while being towed at speeds of several knots. The design of this instrument is described in this report.

The instrument has been towed in deep water near Bermuda. It is believed that salt fingers were observed in the main thermocline on several occasions; but they were so rare as to be negligible in the total vertical mixing. An analysis of one such possible salt finger event is presented.

Numerous other small-scale fluctuations of electrical conductivity were observed, which can be reconciled only with a turbulent model. Intermittency statistics for these events are presented. The eddy diffusivity has been calculated from the data to be approximately 0.075 cm^2/sec.

Thesis Supervisor: Henry M. Stommel

Title: Professor of Oceanography

TABLE OF CONTENTS

ACKNOWLEDGEMENTS 9

GLOSSARY OF TERMS AND ABBREVIATIONS 10

CHAPTER I INTRODUCTION

A. Objectives of the Project 11
B. Instrumentation 12
C. Strategy 13
D. Summary of Results 15

CHAPTER II THE INSTRUMENT

A. The Conductivity Probe 18
B. The Auxiliary Instruments 34
C. Power, Telemetry, and Recording Systems ... 48
D. Towing Vehicle 56
E. Instrument Tests 63

CHAPTER III DESCRIPTION OF THE EXPERIMENT

A. Location 69
B. General Oceanographic Conditions 73
C. Procedure During Experiment 76
D. The Lowerings 78

CHAPTER IV PRELIMINARY DATA ANALYSIS

A. An Overview of the Data Analysis 85
B. Basic Appearance of the Horizontal Microstructure 87
C. Analysis of the Vertical Profiles 91

CHAPTER V HORIZONTAL MICROSTRUCTURE MODELS

A. Model 1: Passive Layers 112
B. Model 2: Salt Fingers 118
C. Model 3: Turbulence 129

CHAPTER VI SIGNIFICANCE OF THE MICROSTRUCTURE

A. Evidence Against Salt Fingers 147
B. Evidence for the Presumption of Turbulence 148
C. Distribution of Microstructure as a Function

of Depth 150
D. Differences Among the Lowerings 150
E. Vertical Mixing Due to Turbulence 155

BIBLIOGRAPHY 158

BIOGRAPHY 161

APPENDIX 1 Optical Methods for Detecting Salt Fingers 162

APPENDIX 2 A Short History of the Project 165

APPENDIX 3 Instrument Details 168

APPENDIX 4 Spectral Analysis Method 180

TABLES AND ILLUSTRATIONS

TABLES IN TEXT pg.

I. Chronology of Field Operations..... 80
II. Analysis of Possible Salt Finger Event..... 123
III. Distribution of Bursts as a Function of Depth..... 151

TABLES IN APPENDIX

A-1 Short History of the Microstructure Project 165
A-2 IRIG Frequencies 177

ILLUSTRATIONS IN TEXT

FIGURE #:

2.1 Single-Electrode Type of Conductivity Probe 21
2.2 Double-Electrode Type of Conductivity Probe 23
2.3 Simplified Cross-Sectional View of Conductivity Probe 25
2.4 Conductivity Probe Electronics (Block Diagram) 27
2.5 Exploded View of Conductivity Probe 32
2.6 Temperature Probe Electronics (Block Diagram) 38
2.7 Vertical Conductivity Gradient Sensor (Block Diagram) 42
2.8 Lower Side View of Gradient Sensor Package 44
2.9 Power, Telemetry, and Recording Systems (Block Diag'm) 49
2.10 View of Completed Instrument in Air (left side) ... 58
2.11 View of Completed Instrument in Air (right side) ... 59
2.12 View of Instrument Under Way 62
2.13 Tank Test Setup 65
2.14 "Smoke Ring" Calibration Record 66

3.1 Chart of Experimental Area near Bermuda 71
3.2 Hydrographic Station, R/V Panulirus II, Sta.#362.... 74
3.3 T - S Relationship for Sta.# 362 ....,..... 75
3.4 Schematic, Lowering 8 81
3.5 Schematic, Lowering 10 82
3.6 Schematic, Lowering 11 83
3.7 Schematic, Lowering 13 84

4.1 Horizontal Microstructure Example from Lowering 13 88
4.2 Vertical Profiles of Gross Temperature and Cond., Low. 8 92
4.3 Vertical Profiles of Gross Temperature and Cond., Low. 10 93
4.4 Vertical Profiles of Gross Temperature and Cond., Low. 11 94
4.5 Vertical Profiles of Gross Temperature and Cond., Low. 13 95
4.6 Vertical Profile of Conductivity Gradient, Lowering 8.... 97
4.7 Vertical Profile of Conductivity Gradient, Lowering 10... 98
4.8 Vertical Profile of Conductivity Gradient, Lowering 11... 99
4.9 Vertical Profile of Conductivity Gradient, Lowering 13... 100
4.10 Relationship of T_z , S_z 103
4.11 Neil Brown CTD Profile (excerpt), 28°02'N, 70°04'W 105
4.12 Enlarged Section of Figure 4.9..... 106
4.13 Neil Brown TD Profile near Bermuda 107

5.1 Section of Lowering 10 Used to Establish the Zero of C' . 115
5.2 Time Record, Event # 14 - 1102 120
5.3 Detail of Figure 5.2 121
5.4 Conductivity Gradient Spectrum, Event # 14 - 1102 - 2 ... 124
5.5 Time Record, Event # 19 - 1340 135
5.6 Detail of Figure 5.5 136
5.7 Conductivity Gradient Spectrum, Event # 19 - 1340 - 2 ... 137
5.8 Time Record, Event # 8 - 1035 138
5.9 Detail of Figure 5.8 139
5.10 Conductivity Gradient Spectrum, Event # 8 - 1035 140
5.11 Time Record, Event # 8 - 1275 141
5.12 Conductivity Gradient Spectrum, Event # 8 - 1275 142
5.13 Composite Spectrum 143

FIGURES IN APPENDIX

A-1 Conductivity Probe: Probe Driver and Current-to-Voltage Converter, Circuit Diagram 171
A-2 Conductivity Probe: 5KHz Demodulator and Differentiator ..172
A-3 Conductivity Probe: Oscillator with Amplitude Stabilization 173
A-4 Cond. Gradient Sensor: Synchronous Demodulator 174
A-5 Cond. Gradient Sensor: Oscillator with A.G.C. 175
A-6 Power Supply and Telemetry Schematic 176

A-7 Signal Splitter, Schematic 178
A-8 Velocity Meter Circuit 179

ACKNOWLEDGMENTS

A project of this complexity could not have been carried out without the generous support of many people.

First and foremost I wish to thank Professor Henry M. Stommel for his extraordinary patience and thoughtful guidance for nearly four years. He provided the initial impetus to get the work started; and he always kept the basic objectives in mind, even during the endless details and frustrations of the field program.

I am also indebted to Drs. Carl Wunsch, Stuart Turner, Melvin Stern, and Herbert Huppert for the essential discussions on salt fingers and oceanic mixing. Dr. Erik Mollo-Christensen provided me with equipment and advice during the data analysis.

I also wish to acknowledge the invaluable assistance during the design and experimental phases of this work of David K. Nergaard, Engineer Extraordinary.

The kindly and helpful personnel of the Bermuda Biological Station helped to make this project possible; special thanks are due to Captain George Taggett of the R/V Panulirus II.

Last but certainly not least, I thank my wife Patricia ("Murph") for her understanding and support during my years as a graduate student.

On a wholly different plane, I owe a large debt of gratitude to the National Science Foundation, which has supported this work under grants number NSF GA - 21172 and NSF GA - 30729 X.

GLOSSARY OF ABBREVIATIONS AND TERMS

C' : voltage representing d/dt (electrical conductivity)

T' : voltage representing d/dt (temperature)

C_g : voltage representing gross conductivity

T_g : voltage representing gross temperature

C_z : voltage representing the vertical gradient of conductivity

T_z : voltage representing the vertical gradient of temperature

Z : depth, usually downward from the surface; or, a voltage representing depth

V : velocity of the instrument package; or data to that effect

ς : density, gm/cc

σ_T : $(\varsigma - 1) \times 1000$

VCO: voltage-controlled-oscillator

FM : frequency modulation

IRIG: Inter-Range Instrumentation Group (a military classification pertaining to telemetry systems)

α : change of density per ^{o}C for sea water

β : change of density per ‰ for sea water

A : change of electrical conductivity per ^{o}C for sea water; also eddy diffusivity

B : change of electrical conductivity per ‰ for sea water

k : wavenumber

ϵ : specific energy dissipation rate for turbulence

ν : kinematic viscosity, cm^2/sec

K : kinematic thermal diffusivity, cm^2/sec

CHAPTER I

INTRODUCTION

A. Objectives of the Project

Within the last decade, it has been found that the vertical profiles of temperature and salinity in the ocean are not smooth, as previously supposed, on scales of meters. Rather there are numerous irregularities in the profiles. In many locations these irregularities, or microstructure, are quite regular, so that the profiles have the appearance of a "staircase".

This type of microstructure is most often found in the thermocline. Stommel, for example, reports that a regular, layered structure existed in the thermocline at several locations near Bermuda. (Cooper and Stommel, 1968).

Much attention has recently been given to the question of the creation and maintenance of these layers. One or more active processes must be at work locally, although perhaps intermittently; otherwise, diffusion would be expected to smooth out the profiles within a relatively short time. Moreover, these active processes certainly are associated with or result in vertical mixing; and although the gross ocean-wide magnitude of vertical mixing may be surmised from considerations of the thermohaline circulation, its details on the local level are quite obscure.

The "salt-finger" type of double-diffusive convection, which will not be described in detail here (for a physical explanation, see Stern, 1960) has been suggested by several investigators as

a possible cause of layering in the thermocline in the Central Atlantic. M.E. Stern and J.S. Turner have demonstrated in the laboratory that salt fingers can produce a layered structure, having relatively sharp "interfaces" between turbulent mixed "layers". (Stern and Turner, 1969). Salt finger convection is an attractive explanation of the layers in the ocean for several reasons: (1) it is a purely local phenomenon, using the potential energy stored in the destabilizing salinity field to produce a downward flux of buoyancy; (2) it can be shown that if salt fingers are reasonably commonplace, the effective kinematic diffusivity may be large enough to account for nearly all the vertical mixing in the ocean (Turner, 1967). But there have been no previous direct observations of salt fingers in the ocean, and no way to determine whether or not salt finger convection is in fact important.

This project is intended to provide more information about the oceanic microstructure in general, and in particular to detect the presence of salt fingers if they exist.

B. INSTRUMENTATION

Since salt fingers are vertical columns of water moving alternately upwards and downwards, it is necessary to use a horizontally-towed sensor in order to detect them directly. An instrument has been built to do this; it is comprised in essence of two major parts: a specially designed microstructure probe which is capable of resolving fractional-centimeter structures

at speeds of several knots; and an auxiliary instrument package which provides the necessary background information to establish the context in which the microstructure is observed. All the instruments are mounted on a towing "fish" which maintains the correct attitude and direction as it is towed. Data is transmitted to the surface and recorded.

The microstructure probe measures electrical conductivity. The reasons for the choice of this parameter are discussed in detail in the Appendix and in Chapter II: The Instrument. The design of the conductivity instrument and its performance are discussed in the first part of Chapter II. An effort was also made to measure temperature with the same resolution and speed of response as the conductivity probe, but it was not successful. The temperature probe is discussed in Chapter II as well.

The auxiliary instruments measure the local vertical gradients of electrical conductivity and temperature, as well as depth and velocity. The necessity of measuring the local gradients, using a differential type of sensor, is a consequence of using a horizontally-towed instrument. A sensor was designed and built to perform this function. The auxiliary instruments are also discussed in Chapter II, as is the design of the fish itself.

C. STRATEGY

The waters around Bermuda were selected as the location for the experiment. In addition to its con-

venience and accessibility, two main scientific factors dictated the choice of Bermuda. Firstly, it was thought to be important to use the instrument in a place where distinct layering had actually been observed; such a location would maximize the probability of finding salt fingers. Secondly, the Bermuda area has been extensively surveyed over the years by a variety of different oceanographic methods; and although it is known that conditions around the island can change very rapidly, nevertheless it was thought that these previous surveys would aid greatly in interpretting the microstructure data. This was all the more important since this project had not the resources to undertake even a limited hydrographic survey.

The general procedure during the field operations at Bermuda was to steam out to the 1000-fathom depth contour south of the island, and there commence towing the instrument in a southerly direction at speeds of 2 to 4 knots. The 1000-fathom depth line marks the bottom of the steep part of the island slope; and in order to avoid any risk of the instrument striking the bottom, all the tows were done in water of at least this depth. During a tow, the instrument was made to ascend and descend slowly, relative to its forward progress, so as to survey the water column vertically. "Yo-yo" experiments, in which the instrument is alternately raised and lowered over a limited depth range, were also performed, in order to determine the horizontal extent of certain features. The data was monitored in real time to permit immediate evaluation,

and to permit active investigation of interesting features.

A total of about 10 hours of useful data will be presented for analysis here. Detailed descriptions of these lowerings and of the general oceanographic conditions in the area are given in Chapter III: Description of the Experiment.

D. SUMMARY OF RESULTS

The vertical profiles were observed to contain microstructure in all the lowerings, in the form of considerable variations in the vertical gradients of conductivity and temperature. In the main thermocline, there were seen in almost every lowering several well-mixed layers from 2 to 20 meters thick. Gradient peaks of 5 times the mean local gradient were commonplace (measured over a 30 centimeter vertical separation); these gradient regions were typically 1 or 2 meters thick in the thermocline. Gradient maxima of greater than 10 times the mean gradient were occasionally observed. But no regular steplike structure, such as that found by Cooper and Stommel (1968), was seen during this investigation.

The relatively uniform water above the main thermocline (the so-called 18° water) also was observed to contain vertical microstructure, although the peak gradients were considerably less, and the well-mixed regions there were thicker.

These vertical profiles are consistent with previous observations near Bermuda and in the deep ocean,

and suggest that conditions in the towing region were typical of deep-ocean microstructure; the nearness of the island is not thought to be a direct cause of the observed microstructure in most cases.

Numerous "bursts" of high-frequency conductivity signal were observed during the tows. It will be demonstrated in Chapter V that these bursts must represent small vertical structures in the ocean, not thin horizontal layers. They must therefore be due to one or another dynamically active process.

The bursts were observed primarily in the main thermocline and in the surface thermocline; bursts were not observed in the 18° water in most lowerings. By far the largest and most sustained bursts occurred in the surface thermocline, but these are somewhat difficult to interpret since the actual structure of the water near the surface is obscure and variable. A total of about 50 significant bursts were observed in the main thermocline.

A few of these bursts may have been caused by salt fingers. But most of the bursts are too wideband in wave number to be definitely identified as salt fingers. Consequently, it is concluded that, although salt fingers do exist in the thermocline, they are probably not a major factor in the vertical mixing near Bermuda. Turbulent mixing processes, possibly due to overturning or shear from internal waves, are thought to be more important. Relatively large-scale shear due to the mean flow, especially in the vicinity of an island, may also be a cause of the turbulence in some cases.

Bursts were observed less than 1 percent of the time in the thermocline, and not at all in the 18° water (except on one anomalous lowering). Computation of an eddy diffusivity, averaged over the thermocline, yields a value $A=0.075$ cm^2/sec. The eddy diffusivity in the 18° water is apparently zero.

Significant differences were observed between lowerings, which yield additional circumstantial evidence regarding the origin of the microstructure.

The horizontal extent of turbulent patches is found to be as great as 600 meters, with thicknesses of about 1 or 2 meters of active turbulence.

CHAPTER II

THE INSTRUMENT

A. THE CONDUCTIVITY PROBE

1. FUNDAMENTAL CONSIDERATIONS

Consideration was given to two basic methods of measuring oceanic parameters on a very small scale, namely, optical methods and electrical conductivity (in conjunction with temperature). The optical system was rejected, for reasons which are detailed in Appendix 1.

Electrical conductivity is a function of temperature, salinity, and pressure; unlike the refractive index, however, it is an increasing function of both temperature and salinity. Therefore conductivity is a good indicator for salt fingers, which are characterized by downward-moving fingers of higher temperature and salinity and upward-moving fingers of lower temperature and salinity. The temperature, salinity, and pressure (depth) coefficients of conductivity are typically: (Gregg and Cox, 1971)

$$\frac{\partial C}{\partial t} = +0.96 \ \text{mmho}\cdot\text{cm}^{-1}/^{\circ}\text{C} \ ; \ \frac{\partial C}{\partial S} = +0.99 \ \text{mmho}\cdot\text{cm}^{-1}/{}^{0}/_{00}$$

$$\frac{\partial C}{\partial z} = \frac{\partial C}{\partial P} \cdot \frac{dP}{dz} = 4 \times 10^{-6} \ \text{mmho}\cdot\text{cm}^{-1}/\text{cm}$$

It is not possible to separate both temperature and salinity information from conductivity alone, but the required temperature and salinity resolution of about .001°C in 30 C and .001 0/00 in 35 0/00 implied that a conductivity resolution of 1 part in 30,000 would be adequate. This is a feasible resolution from

an electronic point of view, even at low excitation levels. The major problem was to design a sufficiently quiet and stable sensor.

The required volume resolution or cell size is 1 cm. diameter. This requirement is unfortunate because the most stable noise-free type of conductivity sensor is the inductive variety, which would have to be no larger than 2 or 3 millimeters overall in order to sense 1 cm. structures. The difficulty of constructing and maintaining such a tiny sensor was considered to be formidable; and furthermore, the impossibility of flushing water through it rapidly enough to achieve high frequency response was evident. Therefore an electrode-type probe, which can more readily be made small, was the only alternative.

The required frequency response depends upon the speed at which the instrument is being towed through the ocean. At three knots (150 cm./sec.), for example, the frequency response of the probe would have to be 300 Hz in order to resolve half-centimeter conductivity variations. The major limitation to the frequency response lies not in the electronics but in the speed with which the probe can be flushed with water. Conductivity measurements are purely electrical in character and do not involve thermal time constants or other physical sources of delay.

SINGLE-ELECTRODE PROBES

The ordinary type of electrode probe (referred to hereafter as the single-electrode type), illustrated

in Figure 2.1, suffers from several major deficiencies. Firstly, its sensitivity depends critically upon maintaining the lowest possible contact resistance near the spherical surface of the probe. The voltage measured between the electrode and ground is composed of the voltage drop in the water, which is the desired quantity, plus undesirable voltages arising from the flow of electrons from the metal electrodes to the sea water. The ground plane electrode is assumed to be so large, and the current density over its surface so small, that no significant voltage develops there. Such is not the case at the small spherical electrode, however, where the current density is high and the area relatively small. The actual volume resistivity of sea water is mainly resistive in character, having only a small capacitive reactance; but the contact impedance is highly capacitive due to polarization of the water, and therefore frequency sensitive. The electrode is commonly constructed of or coated with porous platinum (platinum-black) to maximize its surface area, and is excited by the highest practicable frequency to minimize the effect of the polarization. However, the performance of the electrode is seriously degraded by fouling, even by microorganisms, because such growths drastically reduce the effective surface area. Furthermore, a fouled probe can be restored to its original sensitivity only by being soaked in acid; occasional recoating with platinum black is also necessary. Such difficulties precluded the use of this type of probe in a deep ocean-going instrument.

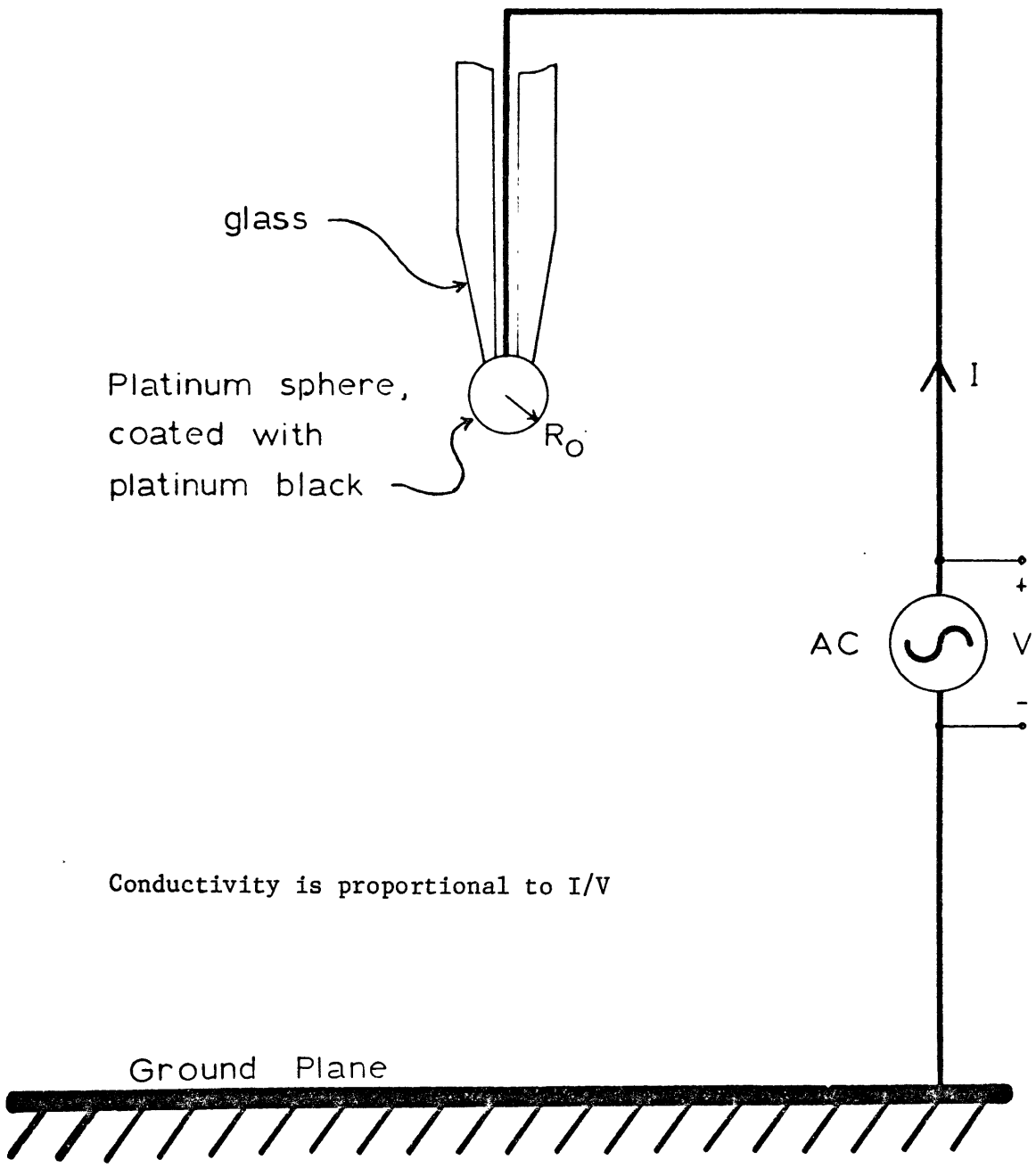

Figure 2.1 Single-Electrode Type of Conductivity Probe

DOUBLE-ELECTRODE PROBE

Acting upon a suggestion by Neil D. Brown, (private communication), the author investigated the properties of double-electrode conductivity probes. Such a probe, illustrated schematically in Figure 2.2, has two electrodes in addition to the large ground contact. One electrode supplies electrical current, which flows in the water to the ground plane but is constrained to issue through a small orifice. The second electrode, which is connected to a very high impedance amplifier, measures the voltage between the ground and the orifice. The current-supplying electrode may have any desired size and shape since its contact impedance is unimportant. The voltage-measuring electrode draws negligible current; moreover it may have a relatively large surface area in contact with the water even though its opening at the orifice is small. The effect of its contact impedance is thus negligible, and an accurate and stable measurement of the resistivity of the sea water path between the orifice and ground may be made.

This type of probe eliminates the most serious objections to the single electrode probe; therefore it was chosen for the microstructure sensor.

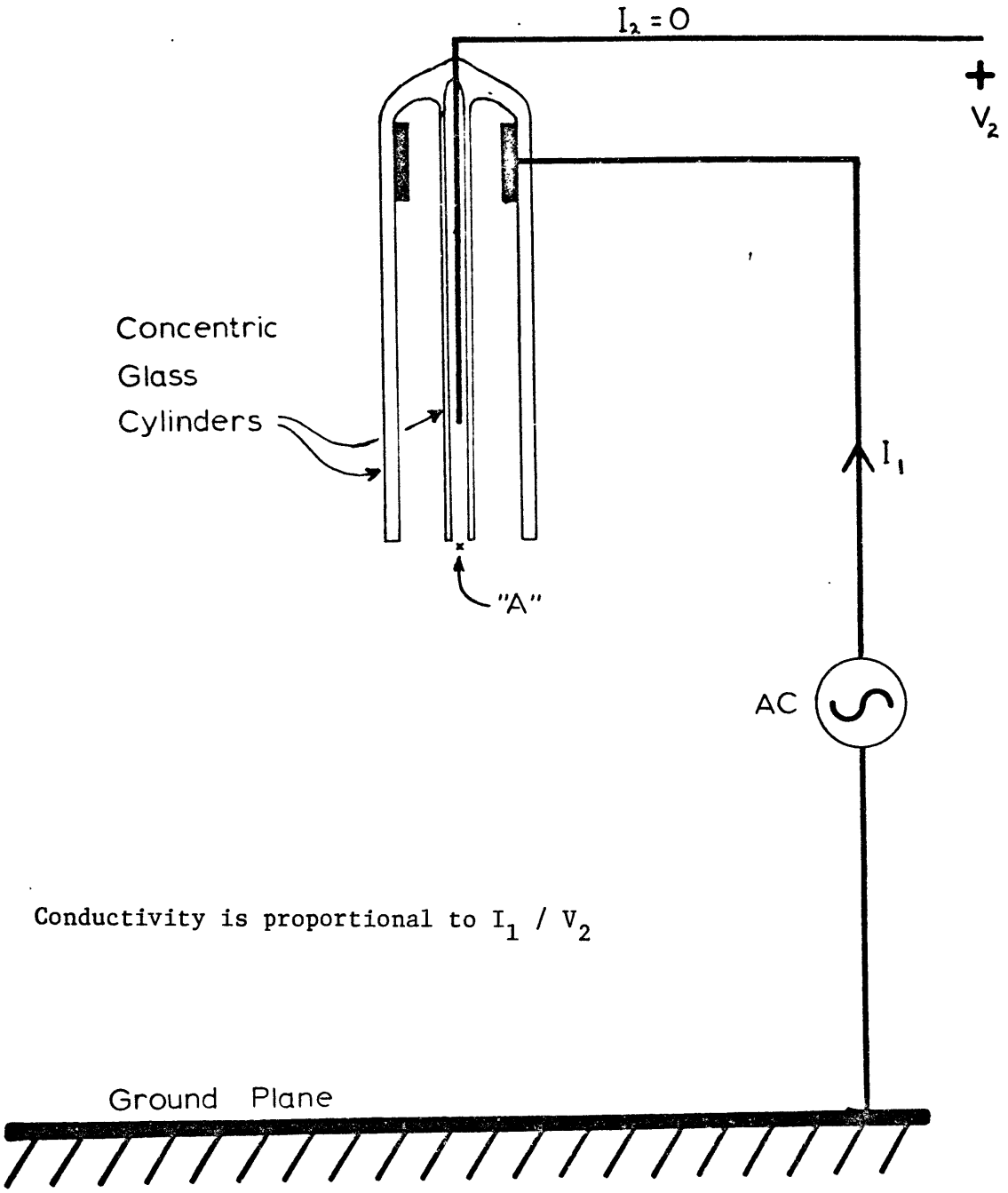

Conductivity is proportional to I_1 / V_2

Figure 2.2 Double-Electrode Type of Conductivity Probe

2. PROBE DETAIL

The physical design of the probe was determined primarily by the requirements that the probe should traverse undisturbed water and that its response should be fast. To meet these requirements the probe was designed as a long, thin pointed object mounted on the instrument so as to precede all other parts. Conductivity is measured in a small volume of water ahead of the probe tip. Provision also had to be made for active flushing of the probe tip so as to prevent the formation of a stagnation layer.

Figure 2.3 illustrates the details of the design. Important features to note are: (1) The probe is excited by A-C current (5 KHz), which flows from the cylindrical current-supplying electrode through the annulus to the large outer ground electrode. The current density is highest at the outlet of this annular orifice, decreasing approximately as radius $^{-2}$ away from the tip. Thus most of the voltage drop occurs very near the probe tip; (2) The voltage is measured between the center of the annulus and ground. Negligible current flows in the inner electrode tube; that is, the potential is the same everywhere inside the inner cylinder, and is equal to the potential at the probe tip; (3) The current density is uniform and vanishingly small over the surface of the ground electrode, and hence no error voltage arises there.

3. ELECTRICAL CONSIDERATIONS

Conductivity, being the inverse of resistivity, is

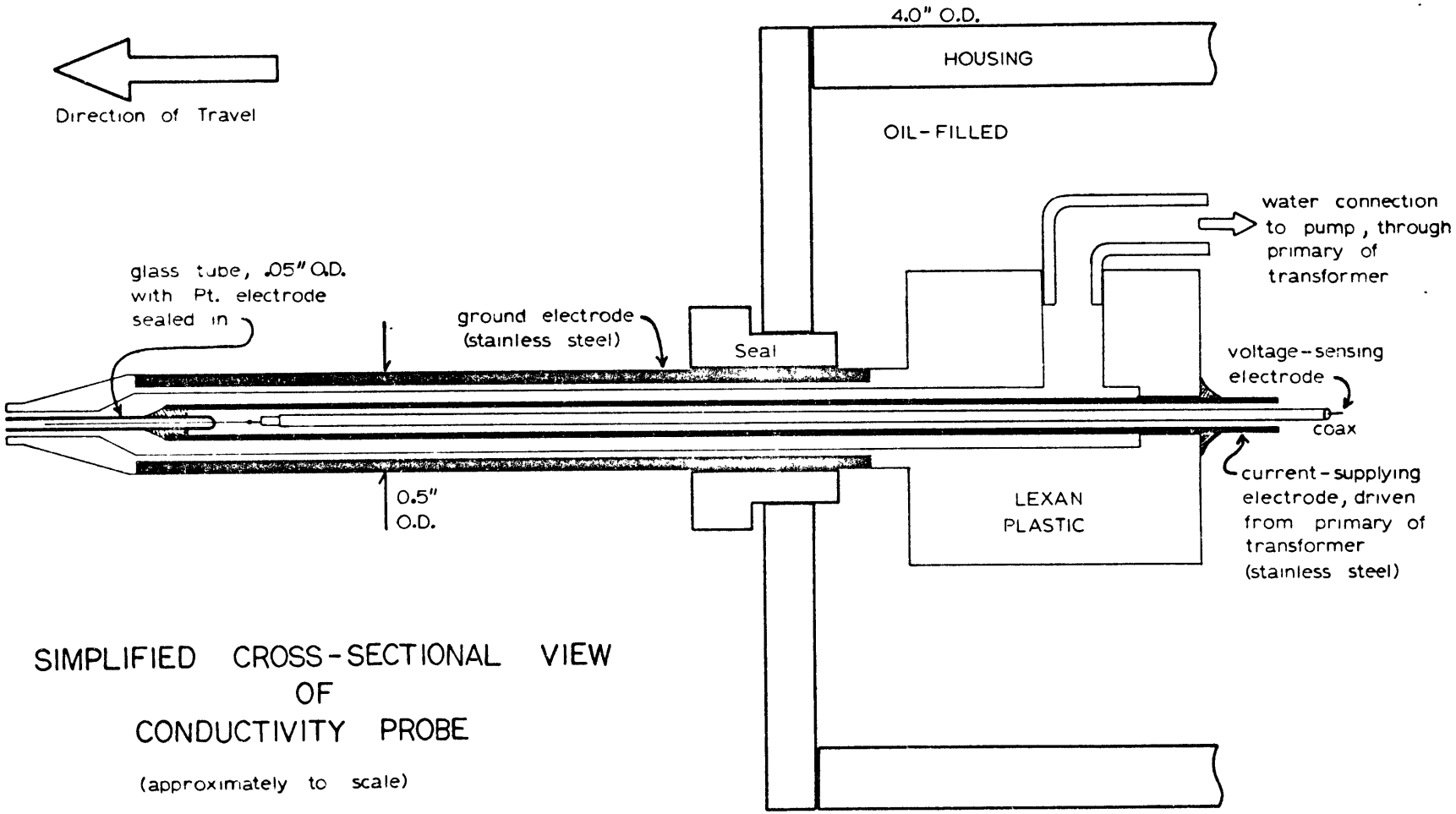

SIMPLIFIED CROSS-SECTIONAL VIEW OF CONDUCTIVITY PROBE

(approximately to scale)

FIGURE 2.3

proportional to the ratio of current to voltage applied across a fixed-geometry sample. This suggests that an electrical output directly proportional to conductivity may be obtained if the amplitude of the voltage is held constant and the current is measured. Therefore a circuit was designed having the probe in the feedback loop of an operational amplifier as shown schematically in Figure 2.4; see also the circuit diagram, Appendix 1, Figure A-1. A constant-amplitude A-C voltage is applied to the amplifier's non-inverting (+) input, and the voltage-measuring electrode is connected to the inverting (-) input. The amplifier's output is connected, via a current-sensing transformer, to the current electrode of the probe. The amplifier, having very high gain, will supply whatever current is necessary through the probe to make the voltage at the (-) input track the voltage at the (+) input. The impedance in the probe between the current-supplying electrode and the orifice is unimportant (provided that the amplifier is capable of driving it within its linear operating region).

Since it is vital to the correct operation of this probe that the voltage-measuring electrode should have a very high impedance, consideration has been given to minimizing capacitive coupling between this electrode and all other points. The connection between the (-) terminal of the amplifier and the electrode was made, as shown in Figure a1, with coaxial cable, whose outside conductor was driven by the input oscillator. This cable extended as far as possible toward the

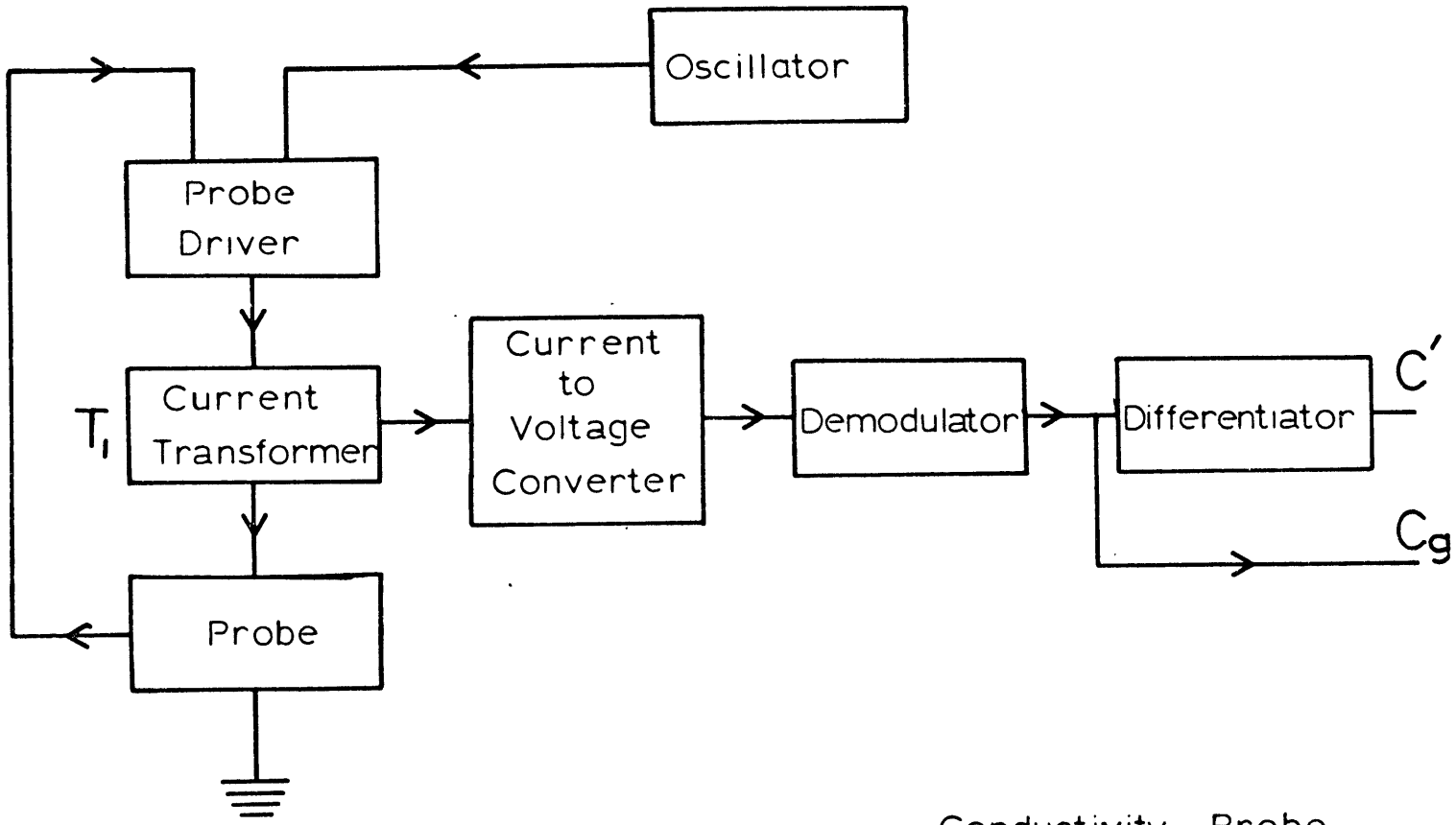

Conductivity Probe

Block Diagram

FIGURE 2.4

voltage-measuring electrode, leaving less than two inches of unshielded wire.

Lastly, it was necessary to design a special transformer to measure the electrical current flowing through the probe. The necessity of flushing water through the probe (discussed in more detail in the next section) means that there will be two electrical paths to ground from the current-supplying electrode, the second path being through the pumping system. Therefore some means had to be found to measure only the current flowing out of the probe. For this purpose a special transformer, shown schematically in Figure A1, was constructed, whose primary winding is a coil of stainless-steel tubing (four complete turns) through which the sea water flows. One end of this tubing coil is connected to the probe, the other end to the pump. The amplifier output is connected to the pump end of the winding, so that the magnetic flux linking the core is proportional only to the current flowing through the probe. The secondary winding consists of 100 turns of copper wire; its connection and the associated electronics will be described later in Section 5 of this chapter.

The core of the transformer was a high-permeability laminated iron "C" core (2 mil laminations). This construction was preferred over a ferrite core because the laminated core could be exposed to high ambient pressures in an oil-filled housing with no risk of a change in its properties.

4. PROBE FLUSHING

Laboratory tests on a prototype probe revealed the necessity of continually drawing water through the annulus. If this was not done, the water in the vicinity of the probe tip would become heated and its conductivity thereby raised. Small changes in the water velocity past the probe tip would then result in large spurious signals (ventilation noise). Moreover a stagnation layer tended to form on the blunt tip of the probe when it was being moved forward, which degraded the sensitivity and the response speed in an unpredictable way. For these reasons it was necessary to design a water-pumping system to suck "new" water into the annulus continuously.

The flushing rate was determined primarily by the necessity of completely avoiding any stagnation layer on the probe tip, regardless of the velocity of the instrument. At the same time it was not desirable to suck too much water through the probe since that would destroy the spatial resolution. The criterion thus was that the entire volume of water intersected by the cylindrical tip of the probe should be sucked through it. (Refer to Figure 2.3 for dimensions). This of course implies that the pumping rate must be proportional to the towing velocity. The nominal rate was calculated to be $(0.1) \cdot V$ ml/sec. where V is the speed of motion in cm/sec.

The method chosen to accomplish this was to mount at the rear of the instrument carriage a large propeller, turned by the motion of the instrument through

the water, coupled to a constant-displacement pump. The propeller was made sufficiently large (30" dia.) that the drag of the pump was small, and therefore the propeller turned at a rate proportional to the velocity. A commercial bronze gear pump was used because it offered the best combination (in a constant-displacement per revolution type pump) of uniform non-pulsating pumping and low friction. The smallest pump (and the highest RPM) consistent with reasonable propeller blade pitch was chosen in order to minimize leakage, which is a major problem of gear pumps turning at low speeds.

Towing tank tests demonstrated that the pumping rate was not in fact proportional to the velocity, owing to leakage in the pump and drag on the propeller. The rate, however, was within 20% of nominal at all velocities tested; and in the absence of a more accurate pumping scheme, it was regarded as acceptable. Consideration had been given to a velocity-controlled, electrically powered pump; but the high power consumption, electrical noise, and complexity of such a system ruled it out.

5. SIGNAL-CONVERSION ELECTRONICS

The output of the probe (regarded hereafter as incorporating the probe-driving amplifier), is an A-C current whose amplitude is proportional to conductivity; this signal is available from the secondary winding of the special transformer. The signal-conversion electronics shown in Figure 2.4 consists of the following: (1) a current-to-voltage converter which converts the

A-C current flowing in the secondary of the transformer to an A-C voltage; (2) a bandpass filter to remove noise outside the frequency band of the A-C signal; (3) a demodulator, incorporating a precision rectifier and a low-pass filter, to convert the A-C voltage into a low-frequency signal proportional to conductivity; and (4) a differentiator, which takes the time derivative of the conductivity signal (up to 500 Hz).

The necessity of differentiating the conductivity signal arises out of the fact that the energy spectrum in the ocean decreases rapidly toward higher frequencies, whereas the higher frequencies (corresponding to small structures) are the desired quantity. Since the dynamic range and signal-to-noise ratio of the telemetry and recording systems are limited, it is necessary to pre-emphasize these higher frequencies by differentiating the signal before transmitting it; otherwise the higher frequencies will be lost or degraded.

6. MECHANICAL CONFIGURATION

The mechanical design of the microstructure sensor is shown in Figure 2.5. The conductivity probe is mounted so as to project about six inches beyond (forward of) a stainless steel end cap which forms part of the ground plane. Behind this cap is an oil-filled housing, enclosing the special sea-water transformer and the coaxial cables, which is connected to an external oil-filled bellows in order to keep the housing at ambient pressure. Mounted behind this housing is the pressure housing containing the electronics; bulk-

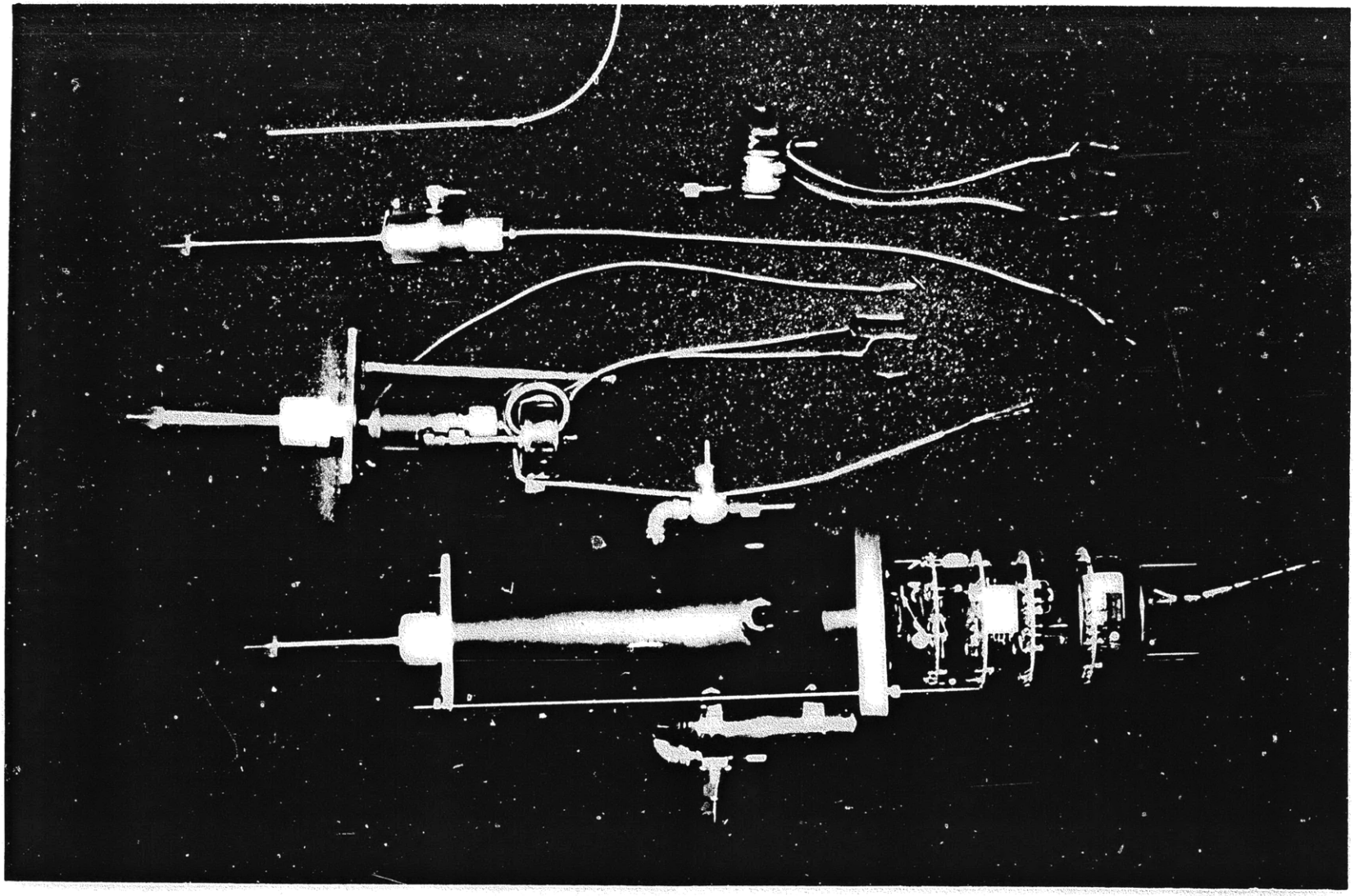

FIGURE 2.5 Exploded View of Conductivity Probe
Object at upper right is the special transformer with sea-water loops (see text)

head feedthrus provide connection between the electronics and the wiring in the oil-filled section.

7. OUTPUT SPECIFICATIONS OF CONDUCTIVITY PROBE INSTRUMENT

Two signals are taken from the conductivity microstructure sensor and transmitted separately. One is the voltage proportional to conductivity (referred to hereafter as "gross" conductivity, Cg), and the other is the time derivative of the conductivity signal (referred to as C'). In each case it should be understood that symbols such as Cg and C' refer to voltages which in turn are proportional to that particular physical variable.

The sensitivity at the Cg output is +0.077 volts per mmho·cm^{-1}. The Cg output was intended primarily as a check on the operation of the instrument, since it was felt that the inherently spiky C' signal might not give a clear indication of an instrument malfunction. This instrument was not intended to be an accurate absolute conductivity sensor; hence no effort was made either to provide a convenient output sensitivity, or more importantly to stabilize the instrument against small changes in sensitivity and level due to varying ambient temperature and pressure. To have done so, particularly in the case of temperature stabilization, would have required a vastly greater effort, probably involving quartz or glass probe construction and ultrastable electronics. This effort was not thought to be justifiable because the instrument was intended primarily to observe small-scale horizontal variations in

conductivity.

The sensitivity of the C' output is 0.034 volts per mmho.cm^{-1}/sec. The lack of absolute stability of the conductivity signal, Cg, results in a small gain error in C', which is less than 1%.

B. AUXILIARY INSTRUMENTS

The conductivity-type microstructure sensor described above is intended to be the primary instrument for detecting the presence of microstructure. But in order to interpret and understand any signals (or the lack of signals) from the conductivity probe it is necessary to know the context in which they occurred. Thus it was considered desirable to measure simultaneously: (1) temperature; (2) vertical gradient of conductivity; (3) vertical gradient of temperature; (4) depth; and (5) forward velocity. A brief description follows of the design consideration of each of these instruments. Details on the actual performance of the instruments are given at the end of each section.

1. SELECTION AND DESIGN OF THE TEMPERATURE PROBE

Ideally, temperature should be measured at the same location at which the electrical conductivity is measured, and with sufficiently good precision and frequency response to enable the calculation of salinity on the microscale. This would require temperature accuracy down to 0.001°C and a frequency response extending up to several hundred hertz. Temperature, however, is inherently more difficult to measure rapidly

than conductivity, because it involves the diffusion of heat; in particular, temperature probes for use in salt water must be electrically insulated from the water, commonly by glass encapsulation, which is not conducive to fast response.

Metal film resistance probes were considered first. These are commercially available in the form of tiny quartz fibers plated with a thin metal film and insulated with another layer of quartz only a few angstroms thick. Their frequency response extends to about 100 Hz without compensation, and they have the stability and linearity common to larger metal resistance thermometers. But they have two serious drawbacks, namely: their low sensitivity, and their low resistance. The former means that the percentage change in resistance per degree is low (typically 0.5% per ^{o}C) which is not serious in itself provided that sufficient excitation voltage can be applied. The low resistance, however, implies that the excitation voltage must be kept very low in order to avoid self-heating of the probe and consequent sensitivity to velocity (ventilation noise). It can be easily calculated, for example, that in order to resolve temperature differences of $10^{-3o}C$ it would be necessary to resolve voltage differences of about 0.15 microvolts (assuming 1 K probe resistance and 1 micro-watt power level). To resolve such infinitesimal voltages at frequencies ranging from zero to one hundred hertz is beyond the capability of commercially available amplifiers (at least those which will fit into an underwater housing). Therefore the metal film probe was regretfully abandoned.

Thermistor-type probes are the remaining alternative. Even the smallest thermistors (0.010 inches in diameter) are considerably larger and slower than the metal-film types, but fortunately they offer much higher sensitivity (typically 5% per degree) and very much higher resistance (available up to several megohms). These factors result in a sensitivity of about 50 microvolts per 10^{-3}°C, for frequencies up to about 30 Hz. The slowness of the response can be electronically compensated to frequencies above 100 Hz; this is possible because up to that frequency the resolution-level signal is above the total noise level. Laboratory experiments disclosed that the response to a thermal "step" could be as short as five to ten milliseconds, with compensation.

The circuit used is a resistance bridge with a low-drift D-C amplifier, whose output is (approximately) proportional to temperature. The design sensitivity is 0.667 volt per degree C (0 - 30°C is full scale). This output is known as Tg ("gross" temperature) and is analogous to Cg, in that it was not thought necessary to stabilize the sensor against the effect of pressure, nor to remove the small non-linearity present in this type of sensor.

The D-C coupled section is followed by the frequency compensation circuit, which is designed to boost the overall gain at frequencies above 30 Hz at a rate of 20 db per decade up to 300 Hz. Above 300 Hz the gain rolls off to prevent oscillation and excessive sensitivity to noise.

Lastly, there is a differentiator circuit which produces a T' signal analogous to C'. Its output is 0.55 volts per ^{o}C per sec., for frequencies up to 300 Hz. Above that frequency the gain rolls off. A block diagram of the entire temperature electronics is shown in Figure 2.6.

The mechanical design was determined largely by the need to put the thermistor as close as possible to the conductivity probe without interfering with the free flow of water around it. Furthermore it was desirable to make the thermistors interchangeable, since they are easily broken. Therefore each thermistor is mounted at the end of a 1/8 inch diameter stainless steel tube which is shaped and positioned so that the thermistor is as close as possible to the tip of the conductivity probe. The other end of this tube leads into a small pressure housing containing a calibrated resistor; the entire assembly constitutes half of the bridge circuit. The small housing is mounted on the body of the conductivity probe. The electronics are located elsewhere (in the power supply cylinder) and connected by waterproof cable to the thermistor housing.

Each thermistor was matched with a resistor, such that the ratio of resistance was correct at 15 degrees Centigrade. Matching was accomplished by immersing the thermistors in a circulating water bath held at 15 degrees, and adjusting a resistance trimpot until the bridge balanced. Each thermistor and resistor was then assigned a number. The thermistors, being all of the same type, have the property that the proportional

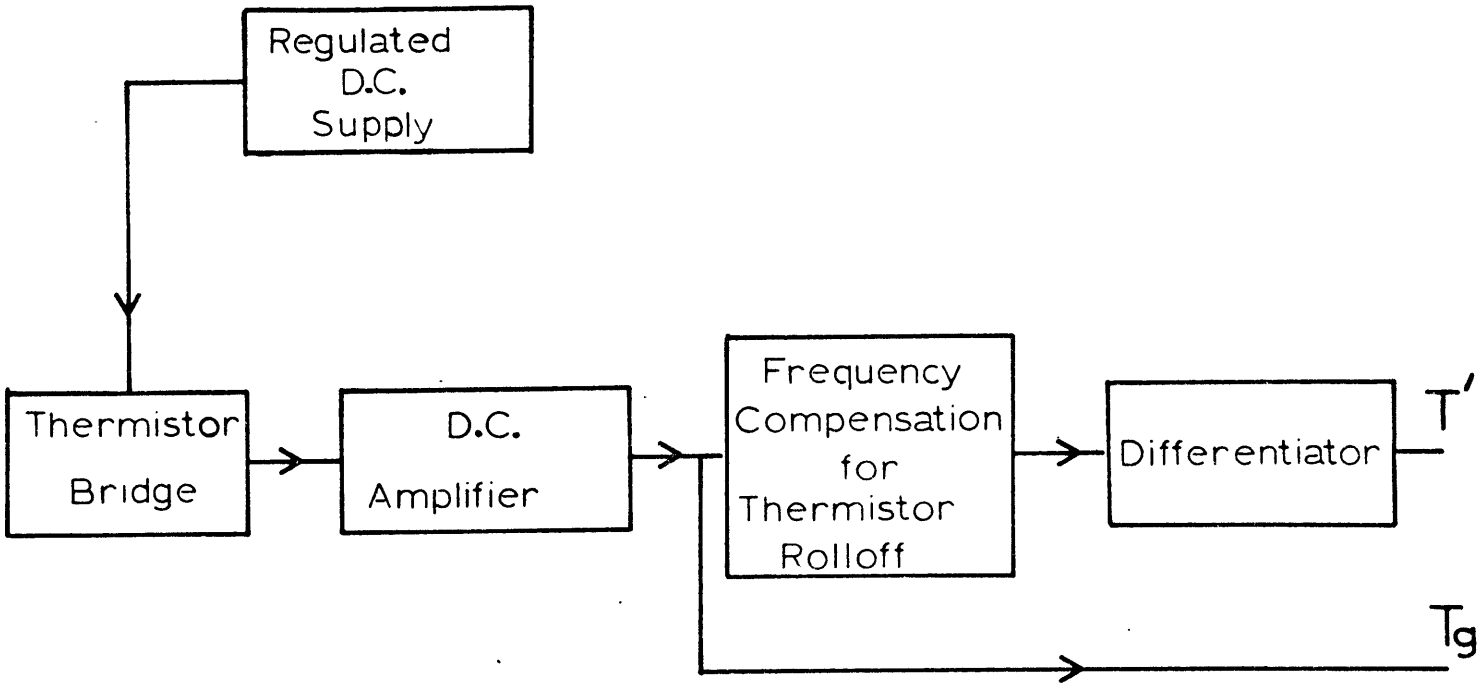

Temperature Probe

Block Diagram

FIGURE 2.6

change in resistance per degree is the same for all units, although the actual resistance at 15 degrees may vary by 20 percent from unit to unit. Thus the combined thermistor-resistor pair constitutes one-half of the bridge circuit, having the property that both the zero point (at which the bridge balances) and the sensitivity do not change if a different pair is substituted. This allowed complete interchangeability of thermistors without the necessity of recalibration each time one broke.

In practice, the T' signal was contaminated by noise of large amplitude. The tiny thermistors functioned rather well as gross temperature sensors, as will be seen in the next chapter, except for the inevitable breakage problem; but the differentiated and frequency-compensated T' signal contained large amounts of high frequency energy, mostly rather narrowband. Whether this oscillation arose in the thermistor itself or in the circuitry following the D-C amplifier is not known. The differentiation and compensation circuits, which have an inherent tendency to oscillate, were specifically designed and checked beforehand to ensure their stability, even under overload conditions. Suspicion therefore points toward the thermistor itself as the origin of the noise. A microphonic condition due to the strumming of the cable may have been responsible, aggravated by the high impedance (1 Megohm at 20 C) of the thermistor, and the relatively long wire between it and the amplifier.

This problem was perceived during the sea trials.

Efforts were made to solve it, but none succeeded. However, it was carefully determined that no correlation existed between this T' noise and the vastly more infrequent bursts of signal on C'.

2. VERTICAL CONDUCTIVITY GRADIENT SENSOR

For the purpose of the investigation it was essential to measure the local vertical gradient of electrical conductivity and/or temperature. It is expected, for example, that if salt fingers are an important causative agent for the formation of layers in the thermocline, then they will be found primarily on the interface separating these layers; hence a test for salt fingers would be a significant correlation between the occurence of microstructure and the presence of sharp local maxima in the vertical gradient.

This instrument, being intended for horizontal towing, requires a differential type of sensor. The "gross" conductivity cannot be relied upon to give a clear indication of the local gradient unless the instrument is being raised or lowered at a uniform rate.

The instrument to be described below was constructed by a different investigator, Dr. John C. Van Leer, for another microstructure project; the design criteria are not necessarily those of the author.

The differential conductivity sensor measures the difference in conductivity between two vertically separated heads (in this case, 30 cm. apart). The heads need not be very small, so use was made of ordinary inductive-type conductivity sensors (manufactured by

the Bissett-Berman Corporation for use in their S.T.D. instrument). Amplitude-stabilized A-C excitation (at 10 KHz) is applied equally to the primary windings of the sensors, and a differential amplifier senses the imbalance current in the secondary windings. Assuming that the sensitivity of the heads is the same, this imbalance current is due solely to a difference in conductivity between the heads. A synchronous demodulator with a low-pass filter converts the A-C signal into a slowly-varying D-C level proportional to the local gradient. A block diagram of the system is shown in Figure 2.7.

The sensitivity of the instrument is 20 volts per mmho$\cdot$cm^{-1} ($\pm$.5 mmho$\cdot$cm^{-1} full scale), which, with a vertical separation of 30 cm. between the heads, corresponds to 0.6 volts per μmho$\cdot$cm^{-1}/cm. This differential technique yields an accurate estimate of the gradient only for vertical scales larger than 30 centimeters. Conductivity variations occuring on smaller scales will yield gradient estimates that are too low.

It should be noted that the zero of the conductivity difference depends upon the tracking of the heads. The sensitivities of the two heads must always be identical; otherwise the difference between them will contain a signal proportional to conductivity itself. An error due to this cause was discovered during the investigation, and will be discussed in more detail in Appendix 3.

The conductivity gradient sensor is installed in the same package as the temperature gradient sensor,

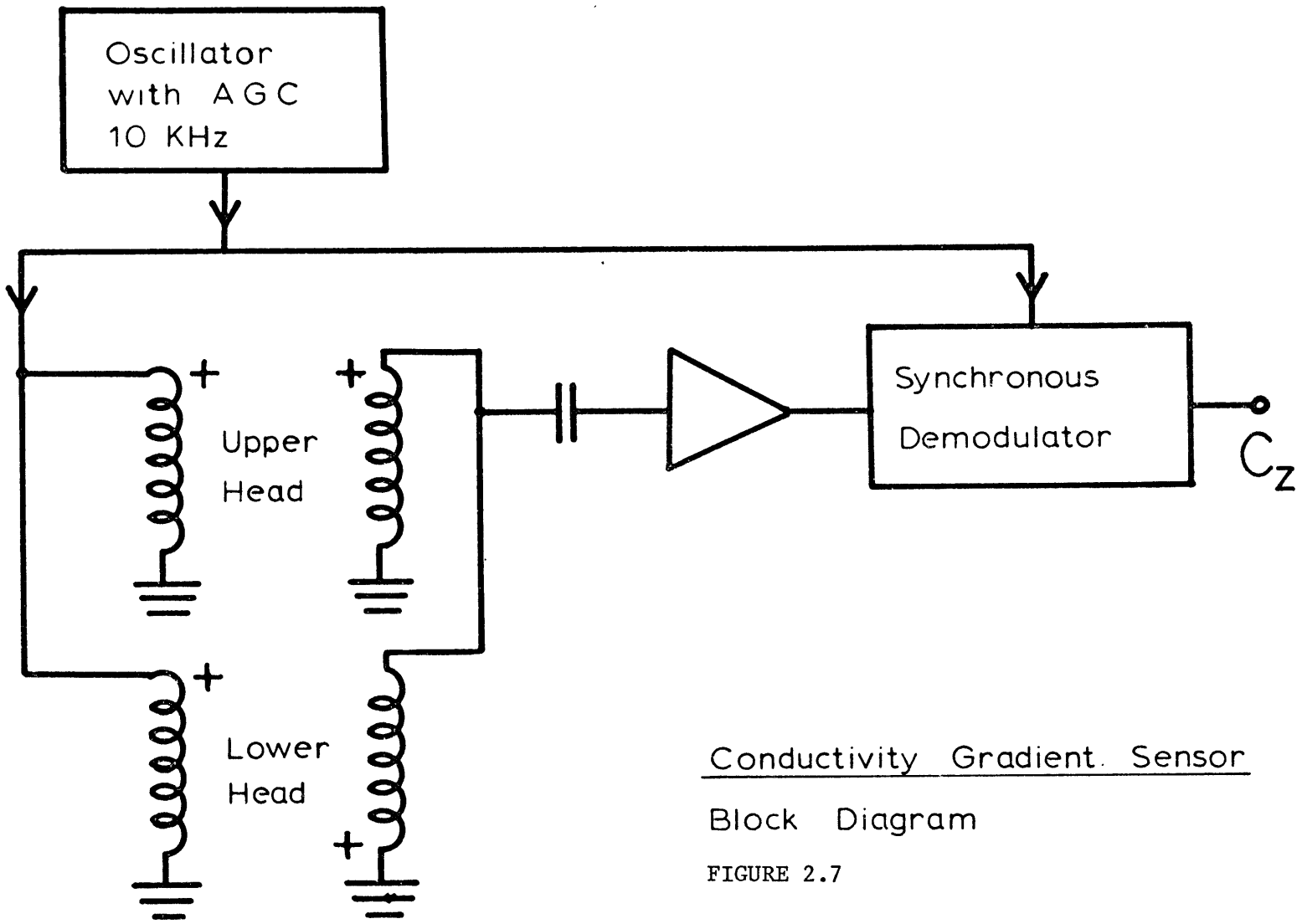

Conductivity Gradient Sensor

Block Diagram

FIGURE 2.7

and share a common power supply. This package was mounted alongside, but aft of, the microstructure sensor, so as to sample undisturbed water but not interfere with the flow past the microstructure probe.

The entire gradient-sensing package is illustrated in Figure 2.8.

3. VERTICAL TEMPERATURE GRADIENT SENSOR

For the temperature gradient sensor a thermopile design was chosen, because of its inherent lack of zero error. The voltage generated by a thermopile whose junctions are vertically separated is proportional only to the temperature difference between the junctions.

A thermopile comprising 90 pairs of iron-constantan junctions was used in order to achieve maximum resolution of the temperature gradient. The junctions are located in tiny (.047" dia.) stainless steel tubes which protrude from a pair of flat cylindrical heads. The tubes are in the form of semi-circular loops; each loop contains two junctions which are insulated from the tube by a thin insulating sleeve.

The heads are mounted 30 centimeters apart on hollow oil-filled tubes which contain the wires. The output wires are led through a pressure bulkhead to the amplifier. This entire assembly mounts forward of and in line with the conductivity gradient sensor. Refer to Figure 2.8 for the illustration.

The electronics for the temperature gradient sensor are simple, consisting of one chopper-stabilized

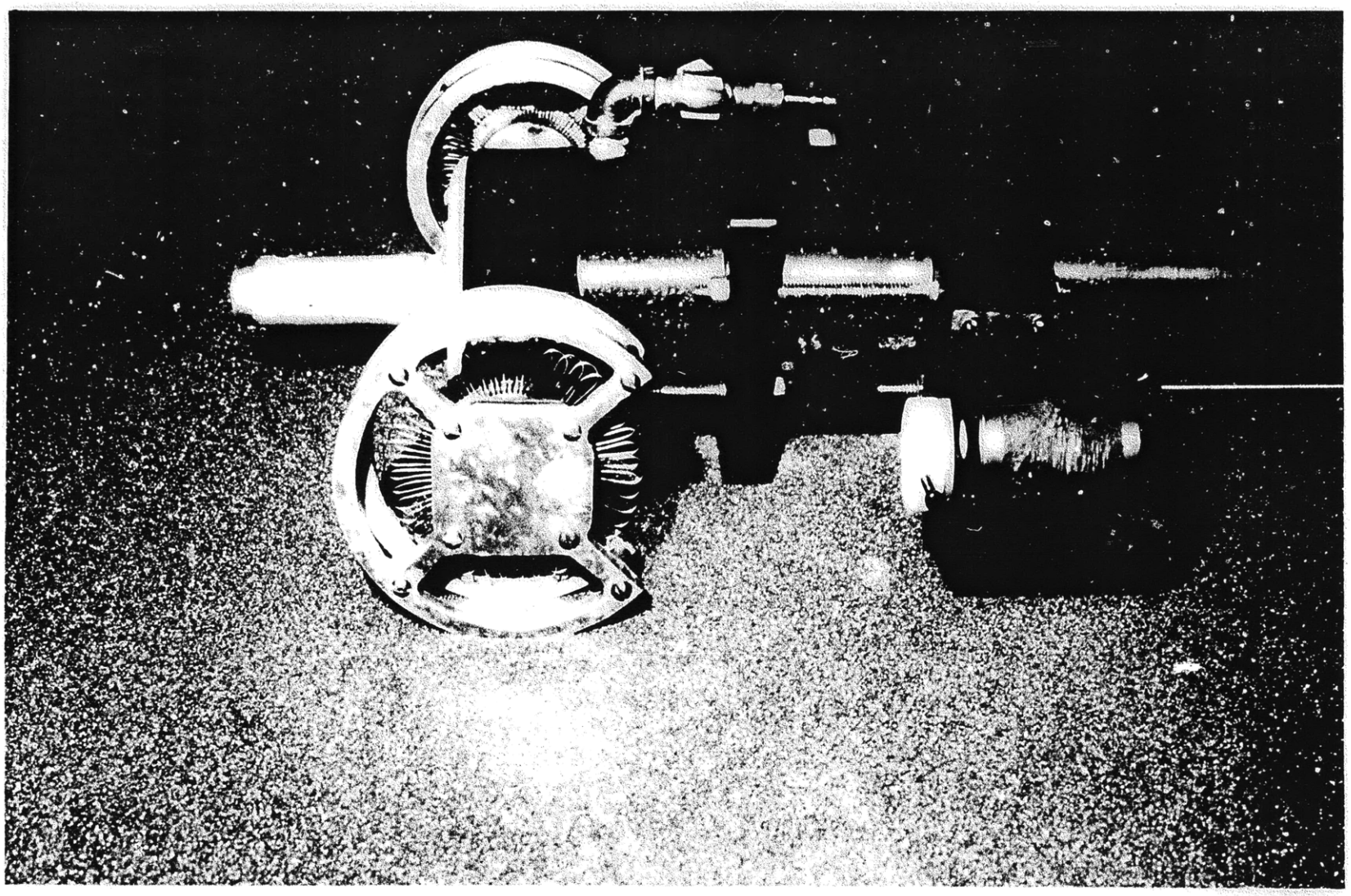

FIGURE 2.8 Lower side view of gradient sensor package
Conductivity sensors lie to the right; temperature sensors to the left

D-C amplifier. The output sensitivity is 20 volts per degree Centigrade (±0.5 C full scale) which corresponds to a gradient sensitivity of 0.6 volts per 10^{-3} °C per cm. The resolution of the instrument is 5 x 10^{-4} °C, and its response time was designed to be approximately 50 milliseconds.

Due to an oversight during the modification of this instrument from its previous configuration, the frequency response was degraded. The intent of its designer was to extend the frequency response of the amplifier to about 40 Hz; in fact, however, the amplifier as used after modification had a frequency response of only 0.2 Hz. The result is that the Tz signal is somewhat "smeared" and the amplitude of its peaks is reduced.

Were it not for the presence of higher frequency noise, primarily due to the telemetry and recording systems, this error could have been corrected almost completely in later analysis. A matching filter to do this was built and tested, using the defective amplifier itself to provide the lagged response. This system, which boosted the gain at higher frequencies, proved capable of restoring the lost frequency response up to about 20 Hz. But unfortunately the response had to be limited in practice to about 1Hz if the noise (which is also boosted) was not to become excessive. This improvement, while noticeable, was not entirely satisfactory, since the Cz signal was not similarly frequency limited.

Consequently, it has not been feasible to calculate

the salinity gradient from the temperature and conductivity gradients, as originally intended. However, the temperature gradient signal has proven to be extremely valuable as a means of verifying the reality of observed conductivity gradient features, since temperature and conductivity gradients are qualitatively similar.

4. VELOCITY METER

Clearly it is necessary to know the velocity of the instrument package, so as to be able to convert the data from a function of time to a function of spatial position. For this purpose a simple impeller-type velocity meter was chosen. The meter has small magnets attached to the backsides of two of its blades; a pickup coil attached to the meter housing produces two pulses per revolution. These pulses are amplified and transmitted. The circuit used is shown in Appendix 3.

The principal advantage of an impeller-type meter is that it produces pulses which are (approximately) constant-distance. These pulses provide a handy distance scale when displayed on a strip-chart record in conjunction with other variables. Furthermore, pulses are much easier to transmit accurately than an analog voltage would be; telemetry requirements are much less critical.

The velocity meter was tested by towing the entire instrument at various calibrated speeds. The towing carriage used for this purpose would not safely go

faster than about 85 cm/sec., which was only half of the desired range, and only one-third of the maximum velocity actually attained during the sea-going experiment. Fortunately the velocity meters (of which there were three to allow for breakage) exhibited a reasonably constant number of revolutions per centimeter traveled (13.0) except at low speeds.

5. DEPTH

Depth is measured with a Bissett-Berman pressure gauge. This commercially available unit has a range of 0 - 2200 p.s.i.g., corresponding to 0 - 1500 meters. The unit contains its own FM oscillator, working in the frequency band of 9712 - 11288 Hz.

C. POWER, TELEMETRY, AND RECORDING SYSTEMS

1. POWER

The instruments require altogether about 20 watts. The operational amplifiers used in many of the circuits require +15 and -15 volts with respect to ground (sea water). Other instruments operate from +27 volts, such as the depth sensor.

D-C power is sent down the cable from the surface ship. Owing to the great length of cable, a high-voltage power supply is required to drive the necessary current (1.1 amperes D-C) into the cable. The actual voltage required depends of course upon the particular cable used; in this investigation about 150 volts was necessary.

The main power in the instrument is established by a 27 volt zener diode in the power supply cylinder. The D-C current from the surface is applied to this diode. All of the circuits draw their power from this 27 volt supply, and the zener diode sinks the excess current so as to maintain the correct voltage. Some circuits operate directly on 27 volts; +15 and -15 volts (regulated) for the remaining circuits are provided by DC-to-DC inverters which operate from 27 volts. A block diagram of the entire power, telemetry, and recording systems is shown in Figure 2.9. A circuit schematic of the power supply (and the telemetry oscillators which are described in Section 2 is shown in Appendix 3.

Each instrument requiring +15 and -15 volts is supplied from a separate inverter, so as to provide maximum power-supply isolation between instruments,

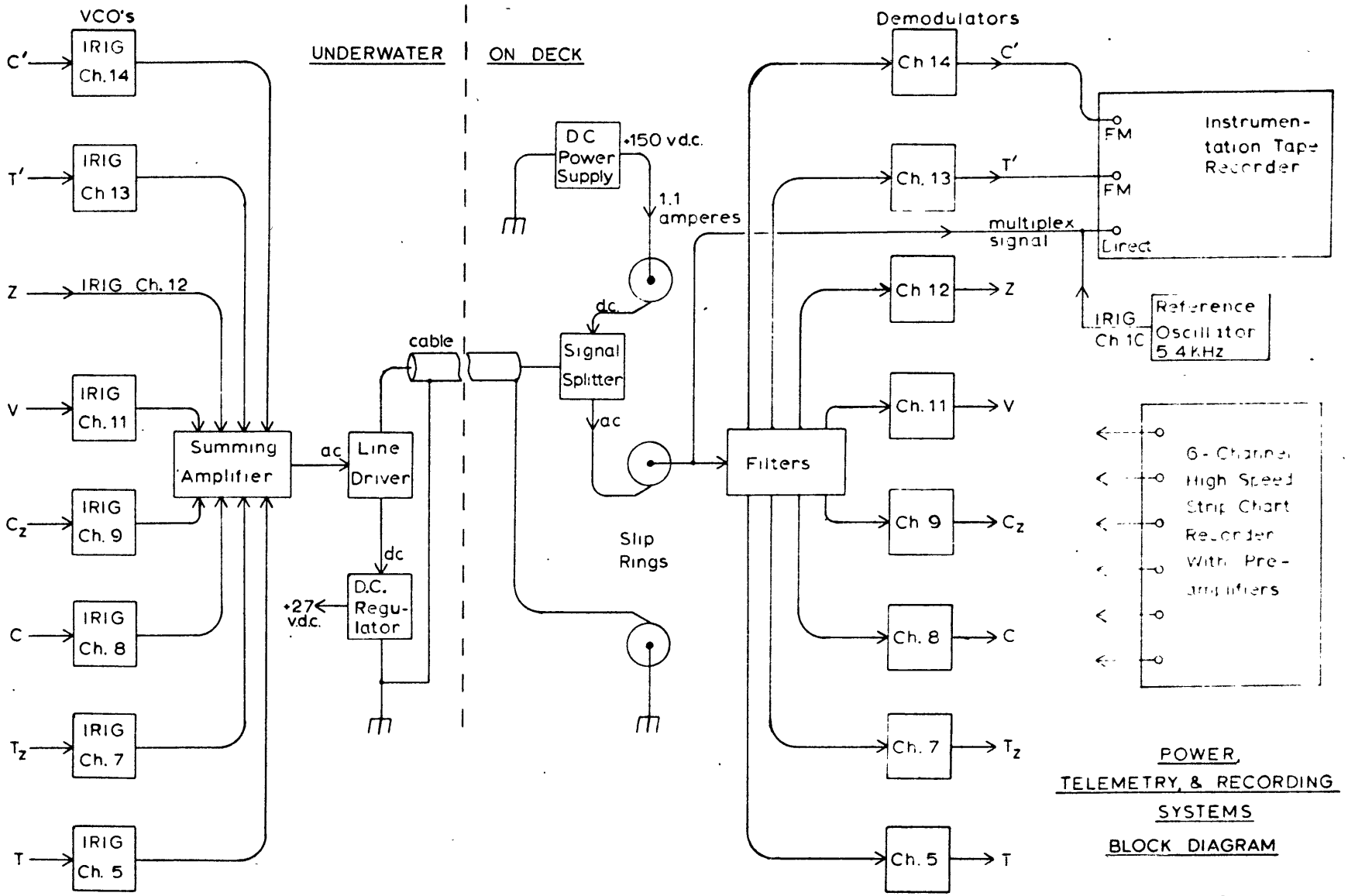

POWER, TELEMETRY, & RECORDING SYSTEMS BLOCK DIAGRAM

FIGURE 2.9

and also to prevent a fault in one instrument from affecting others.

It will be noted that this system is somewhat inefficient. The power supply at the surface produces about 180 watts, of which only 32 reach the input to the power supply cylinder on the instrument, the remainder being dissipated in the cable. Approximately 12 watts are dissipated in the zener diode and the inverters. Moreover, of the 20 watts actually supplied to the circuits, about two-thirds (12 watts) is required to power the amplifier which drives telemetry signals up the cable to the surface. Thus the cable is by far the greatest source of inefficiency.

2. TELEMETRY SYSTEM

For this instrument the telemetry system must simultaneously transmit eight variables (C', T', Cgross, Tgross, C_z , T_z , V, Z) to the recording system aboard the surface ship. C' and T' must have trams-mission bandwidths from D-C to 500 Hz; the others need only D-C to 40 Hz or less.

Clearly, if a nine-conductor oceanographic cable were available, it would be possible to transmit each signal and the power over a separate conductor; then a telemetry system, as such, would be unnecessary. But multi-conductor cables are not readily available, and are extremely expensive and bulky. Moreover if the cable is long there is a strong likelihood of "cross-talk" between conductors. Therefore a telemetry system had to be designed which could transmit all the signals

simultaneously over a single-conductor cable, while also allowing D-C power to be sent down the same conductor from the ship to the instrument.

Narrowband, frequency-modulated, frequency-multiplex telemetry was selected. Briefly, this system converts each analog variable into a narrowband frequency-modulated sine wave, whose maximum frequency deviation is ± 7.5% of its center frequency. The center frequencies are chosen such that there is no frequency overlap. The sine waves are then summed electronically, producing a composite or multiplex signal which, by means of a power amplifier, is superimposed upon the D-C voltage from the surface ship.

The conversion of the information from its original analog form to FM is accomplished with voltage-controlled oscillators (VCO's), which are contained in the same pressure housing as the power supply. The outputs of the VCO's are summed in an amplifier and sent up the same cable used for D-C power, by means of a series line driver circuit. A block diagram of this system has been shown in Figure 2.9. Refer to Appendix 3 for circuit details. Provision is also made for sending the multiplex signal through a separate conductor, if multi-conductor cable should be available.

Commercially available oscillators are used (Bosch-Arma Model 1270 BY-1). These were tested in the laboratory for frequency stability, and were found to have a temperature coefficient of -0.76×10^{-4} per degree C. Thus these oscillators are expected to drift less than 1.3% with respect to full scale over the entire oceanographic temperature range of 5-30 degrees C.

In terms of analog output voltages, which are ±10 volts full scale for all channels, the VCO frequency drift amounts to 0.26 volts over the full 5 - 30 degree C. range. Referring to Figure 3.2, p. 74 , it may be seen that the actual temperature range encountered in this experiment was no more than 16 degrees C. (0 - 1000 meters); the corresponding VCO drift should amount to no more than ±0.16 volts with respect to the value at the surface.

The effect of this VCO drift upon the data may be more or less serious depending on the signal variations and the required accuracy. For the Cg data, which varies by only 1.2 volts over the entire depth range, a telemetry oscillator drift of 0.16 volts is significant indeed; and this must be borne in mind when inspecting the Cg data. For the Tg data, on the other hand, which varies by about 11 volts over the 0 - 1000 meter depth range, the VCO error is an order-of-magnitude less serious. For the Tz and Cz data, the VCO drift amounts to 0.027 degrees C. per meter and 0.027 mm o $cm.^{-1}$ per meter respectively; these are approximately equal to the mean gradients in the deep thermocline. For the velocity signal, which consists of a series of pulses, the drift has no significance. The depth sensor contains its own oscillator, and hence is not subject to these considerations at all. The all important C' signal, being a time derivative, is essentially A-C coupled anyway; however, this telemetry drift (plus other drifts) make it much more difficult to integrate C' later.

The original analog signals are recovered at the

surface. First the telemetry signals are separated from the D-C current. This is done by a signal-splitter, to be described later in this section. Then the various frequencies are separated from the composite signal by bandpass filters; and lastly each frequency is demodulated to produce a replica of the original analog input. The overall telemetry system gain is adjusted to one (i.e., voltage input=voltage output). The demodulator is shown schematically in Figure 2.9.

Standard IRIG frequency bands are used. Table A-2 in Appendix 3 lists the center frequencies used, together with the upper and lower frequency excursions.

Slip rings are of course a necessity at the winch, in order to get the signals off the rotating winch drum. Slip ring brushes, however, can be a major source of noise, particularly if they are carrying heavy current. Therefore, in order to avoid degradation of the multiplex signal by slip ring noise, a "signal-splitter" circuit was employed, which mounted on the winch drum on the cable side of the slip rings, so that the A-C and D-C flow through separate brushes. The circuit, shown in Appendix 3, consists of a large filter choke and capacitor, through which the D-C current flows. This filter provides clean, noise-free D-C and a high A-C impedance. A capacitor provides A-C pick-off.

3. RECORDING SYSTEM

The information coming up the cable from the instrument must be recorded in two separate ways. Firstly, it must be recorded on magnetic tape in the simplest and most direct way possible so as to be fully recover-

able in the future. Secondly, it must be recorded on a chart recorder so as to be immediately visible in real time.

TAPE RECORDER

The frequency-modulated signals coming up the cable are in a form suitable for recording directly on magnetic tape. Essentially, the method chosen is to record the entire multiplex signal on a single direct-record channel. A constant-frequency reference signal (5.4 KHz - IRIG Channel #10) is added to the multiplex signal before recording; this reference provides a means of eliminating the undesirable effects of tape speed variations upon playback.

Unfortunately, however, the linearity of most tape recorders is only fair, which tends to contaminate the higher frequencies with distortion products of the lower frequencies. Therefore, in order to produce the cleanest recording of the valuable C' and T' signals, it was decided to record these signals separately, each on its own channel of the four-channel recorder.

Moreover, if the 22.0 KHz and 14.5 KHz FM signals, which contain the C' and T' information, were to be recorded without modification, it would be necessary to use a high tape speed (15 inches per second). The signals, however, are narrowband and the modulating frequencies do not exceed 500 Hz, so that the wide bandwidth of the 15 i.p.s. tape speed is unnecessary. Therefore, in order to conserve tape, it was decided to record the analog (demodulated) C' and T' signals at

3 3/4 i.p.s. via separate FM-record channels on the tape recorder. Refer to Figure 2.9 for a block diagram of the recorder connections.

Recordings made with this system may be played back to recreate the experiment exactly as it occurred. The multiplex signal from the recorder is connected into the demodulator, which processes the FM signals to obtain all the original variables except C' and T'. Demodulation is done with respect to the reference frequency (5.4 KHz) to eliminate the effect of tape speed variations. The C' and T' signals are obtained directly from the tape recorder.

STRIP-CHART RECORDER

Any of the eight variables can be displayed on the strip-chart recorder. A six-channel machine was used because an eight-channel one was not available; but the lack of the full channel complement has not been a serious defect. The strip-chart recorder is meant to be an on-line monitor, enabling the investigator to inspect the data (in a somewhat crude fashion). Such inspection is vital to the successful conduct of the experiment: not only can the investigator detect instrument malfunction, but more importantly he can alter the course of the experiment if an interesting feature or event should occur.

The strip-chart recorder also enables the investigator to select interesting events for further analysis. Horizontal microstructure is an intermittent phenomenon, and the record is bound to contain large stretches where-

in nothing happened. The infrequent places where microstructure occurs must be marked and later analyzed one by one, and the strip-chart record provides this important first step in the data analysis.

The machine used in this project is a Brush Instruments Co. Model 260. The essential requirements were, firstly, that the instrument be capable of recording high-speed signals (above 100 Hz), and secondly, that it have a wide range of useful chart speeds. For example, it was found to be convenient to run the chart recorder at speeds of less than one centimeter per minute during the experiment, to provide a "picture" encompassing several hours of operation; yet in order to get a detailed look at a microstructure event it is necessary to run the recorder at speeds as high as 25 centimeters per second. Inkless recording is mandatory under these conditions.

The recorder is used in conjunction with a Sanborn Co. eight-channel pre-amplifier.

D. TOWING VEHICLE

The towing vehicle or "fish" is the carriage on which the instruments and components are mounted. Its primary function is to hold the instruments in the correct orientation as the instrument package moves through the water. In particular, the C' and T' sensors must always protrude ahead of the instrument package so that they will sample undisturbed water. Moreover, since the vehicle is relatively light, the fish must actively pull itself downward if it is to be towed at

great depths. The necessity of this downward lift did not become apparent, however, until sea trials commenced.

There are four separate instrument housings of substantial size: (1) the conductivity microstructure sensor; (2) the gradient sensors; (3) the depth sensor; and (4) the power supply and telemetry unit. In addition there are two smaller objects, namely: the velocity meter and the temperature probe. Lastly there is the rather large pump-and-propeller assembly described in Chapter III.

Wherever possible the larger units were installed in long, thin cylindrical pressure housings. These are mounted with their axes parallel to the direction of motion so as to minimize drag.

The complete instrument is illustrated in Figures 2.10 and 2.11 (without diving planes). Note that the conductivity sensor (with the temperature and velocity sensors attached) is mounted furthest forward, with the gradient sensor package further aft and to the side. The other cylinders are mounted underneath and out of the way. The pump and propeller are at the extreme after end. The cable is attached, as shown, somewhat forward of amidships. The fish is steered and made to tow correctly by the combined effects of the vertical stabilizing fin (not shown) and the drag of the propeller.

The diving planes consist of simple, flat, rectangular plates (14 inches by 12 inches each) attached to the frame of the vehicle opposite the point of

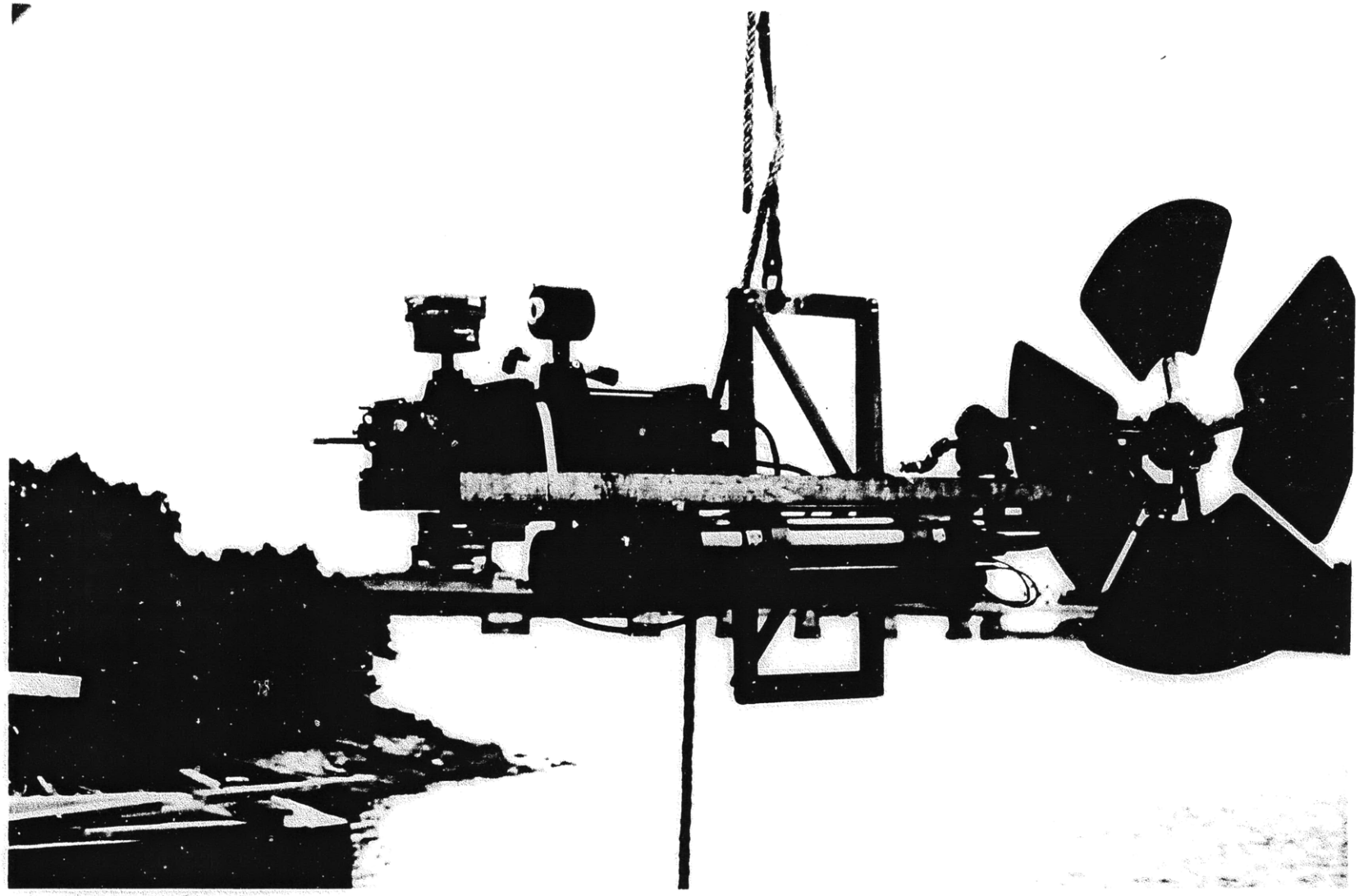

FIGURE 2.10 View of Complete Instrument in Air (left side). Without fins or stabilizer.

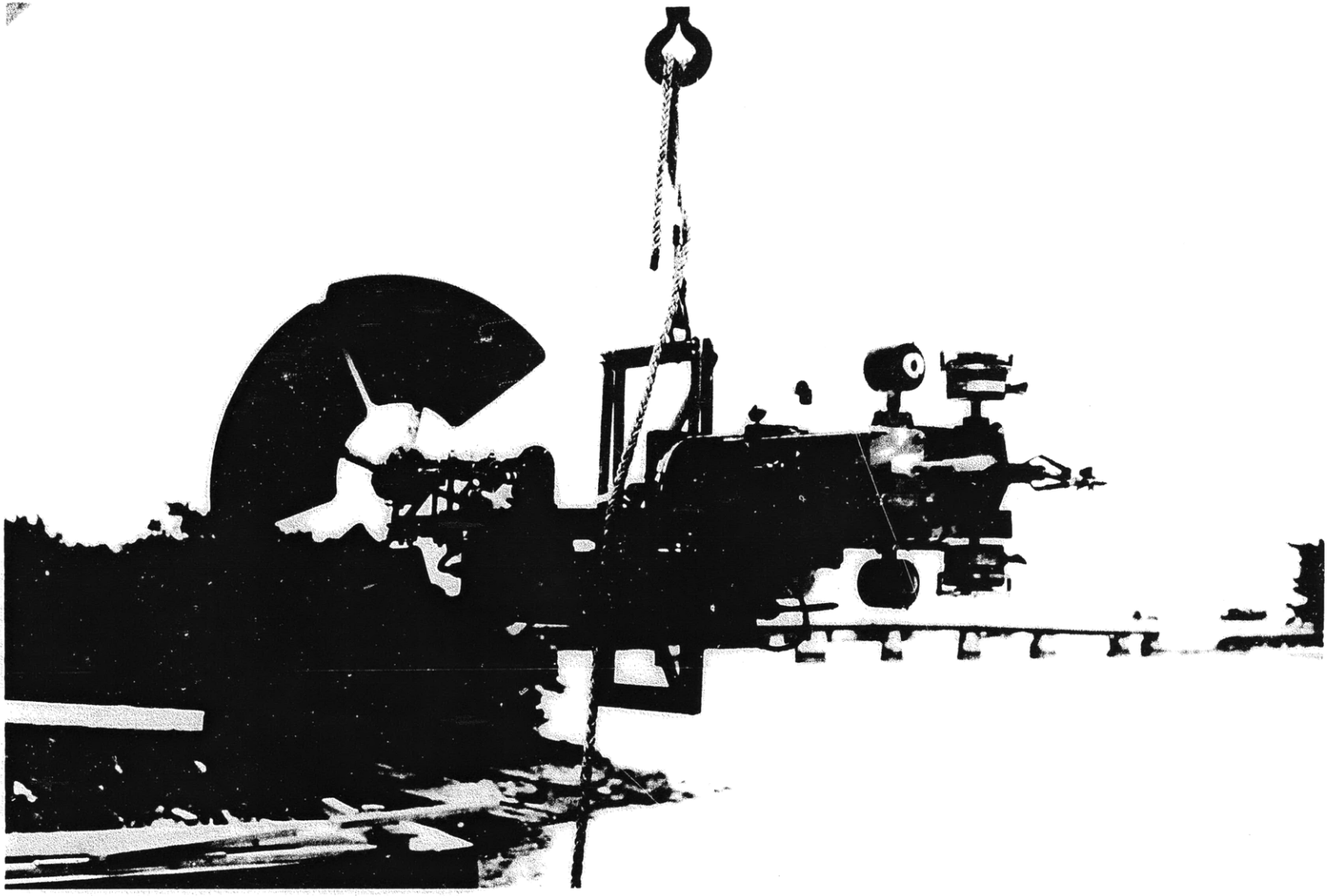

FIGURE 2.11 View of Complete Instrument in Air (right side).

attachment of the cable. They are mounted parallel to the frame. A horizontal fin, placed as far aft as possible, maintains the angle of attack of the vehicle at 5 degrees (tail up).

The fish tended to tow in a slightly "tail-up" attitude even without the fins, because the point of attachment of the cable was above the center of drag, as can be clearly seen in the Figures. This arrangement was necessary to avoid fouling the cable on the delicate instruments during launching and recovery. Rather than try to overcome this tendency with the tail fin, it was decided to adopt the tail-up position as the normal attitude, and depend upon the tail fin only to maintain that attitude.

Sea trials revealed the necessity of incorporating diving planes or wings to increase the downward force on the cable, thereby enabling the instrument to go deeper for a given length of cable. This was an important objective, since the cable used was only 1500 meters long. Without diving planes, the instrument could not be towed steadily at depths greater than 600 meters, at least not at speeds which our research vessel, the R/V Panulirus II, could achieve. The Panulirus has diesel engines and fixed-pitch propellers and cannot steam slower than about three knots, even with a head wind.

The wings were constructed of one-eighth inch steel plate, having a total area of 340 square inches. A simple calculation, assuming a maximum velocity of 250 centimeters per second, 5 to 10 degree angle of

attack, an aspect ratio between 1:1 and 1:2, and a lift coefficient C_L of 0.3, (Prandtl, 1952) gave a net downward "lift" of only 50 pounds. In comparison with the 100 pound weight of the instrument, this dynamic force would not seem large enough to be worth the bother. Larger planes, however, would offer a serious risk of excessive strain on the cable due to the rolling of the ship, particularly if the instrument should be near the surface. Flat plates certainly do not have the optimum lift-to-drag ratio; however, the instrument itself is not streamlined, so that its drag is much larger than the drag of the wings anyway. Therefore the effect of the wings is to multiply the lift-to-drag ratio of the instrument by about 1.5 at maximum speed.

At any rate, wings of this size were tried and found to have a beneficial effect on the performance of the vehicle. Depths of 800 meters were achieved at steady speeds; moreover, the sensitivity of the instrument's depth to slight changes in ship speed decreased.

A horizontal stabilizer fin was mounted at the rear of the frame, just forward of the propeller, to control the angle of attack of the wings. It performed its function well; the vertical angle between the frame and the streamline of the flow was much more nearly constant than it had been previously. This may have resulted in a further reduction of the net drag of the instrument.

The completed instrument in the water and under tow is portrayed in Figure 2.12.

FIGURE 2.12 View of Instrument Under Way

E. TANK TESTS

Preliminary tests of the completed instrument were carried out in a fifty-foot long salt water tank at Woods Hole Oceanographic Institution. This tank was equipped with a towing carriage to support and propel the instrument. The tank had previously been filled with a highly-stratified salt solution (NaCl, not sea water) of approximately 20 0/00 salinity. This was by no means an ideal test fluid; but the time available would not permit of draining, cleaning, and refilling the tank, and then allowing it to equilibrate, the harbor water at that time (April 1972) being less than 50°F. Moreover, the problem of biological fouling in the stagnant, warmed sea water might have proven severe. For these reasons the existing water was retained.

The water tended to stratify itself if left undisturbed because the bottom of the tank, which rested in a concrete foundation, was considerably colder than the walls; initially the temperature difference between top and bottom was 10 degrees Centigrade, and even after the tank had been stirred thoroughly a temperature difference of several degrees would re-establish itself overnight. These large gradients, combined with the low average salinity, often produced confusing results from the instruments, particularly the gradient sensors. Consequently, the performances of these sensors was not thoroughly investigated in the tank.

CONDUCTIVITY PROBE TESTS

The most extensive tests were carried out upon the conductivity sensor to verify its sensitivity and speed of response. Simple tests, such as sprinkling salt crystals into the water, allowing them to sink, and then running the instrument through the trails they left, demonstrated that the sensor was capable of resolving structures of fractional-centimeter size. Such tests, however, were too crude to check the instrument's response quantitatively.

More quantitative measurements were obtained by injecting vortex rings of water differing from its surroundings across the front of the stationary probe. These "underwater smoke rings" provided a more-or-less controllable means of varying the conductivity rapidly enough. The setup is illustrated schematically in Figure 2.13. A typical record of a C' signal resulting from a "smoke ring" is shown in Figure 2.14. The conductivity of the water issuing from the jet could be altered by adding fresh water to a sample of tank water. The copper coil shown in Figure 2.13 was intended to prevent any temperature difference from arising between the ambient water and the "smoke rings". It was also necessary to draw water through the probe by the action of a siphon, to prevent formation of a stagnation layer, which would have been highly velocity sensitive.

It became apparent as the testing proceeded that reproducible results were difficult to obtain for small conductivity variations. The design sensitivity of the probe is 3 parts in 10^5; and thus to measure its resolution level, the temperature would have to be known

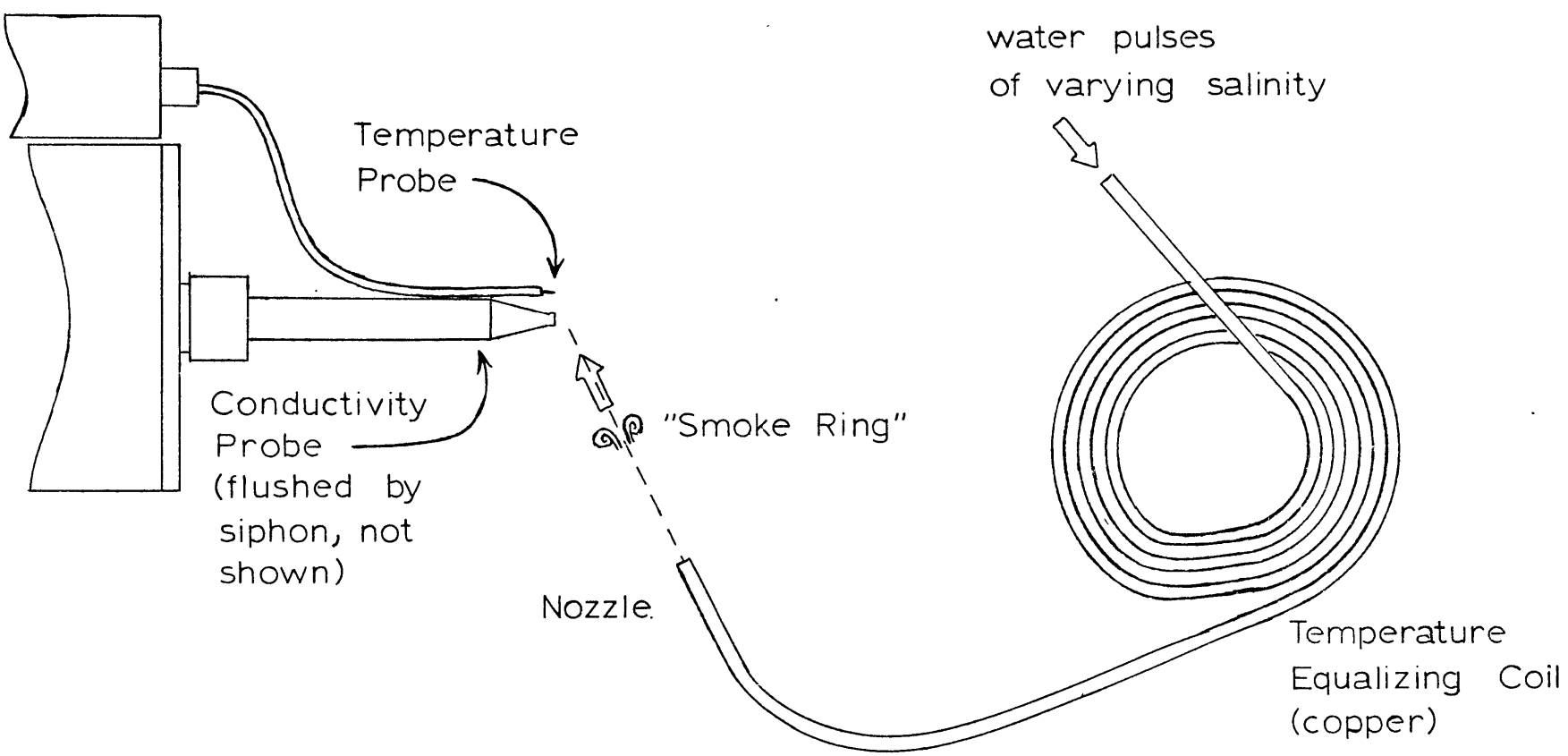

TANK TEST SETUP

FIGURE 2.13

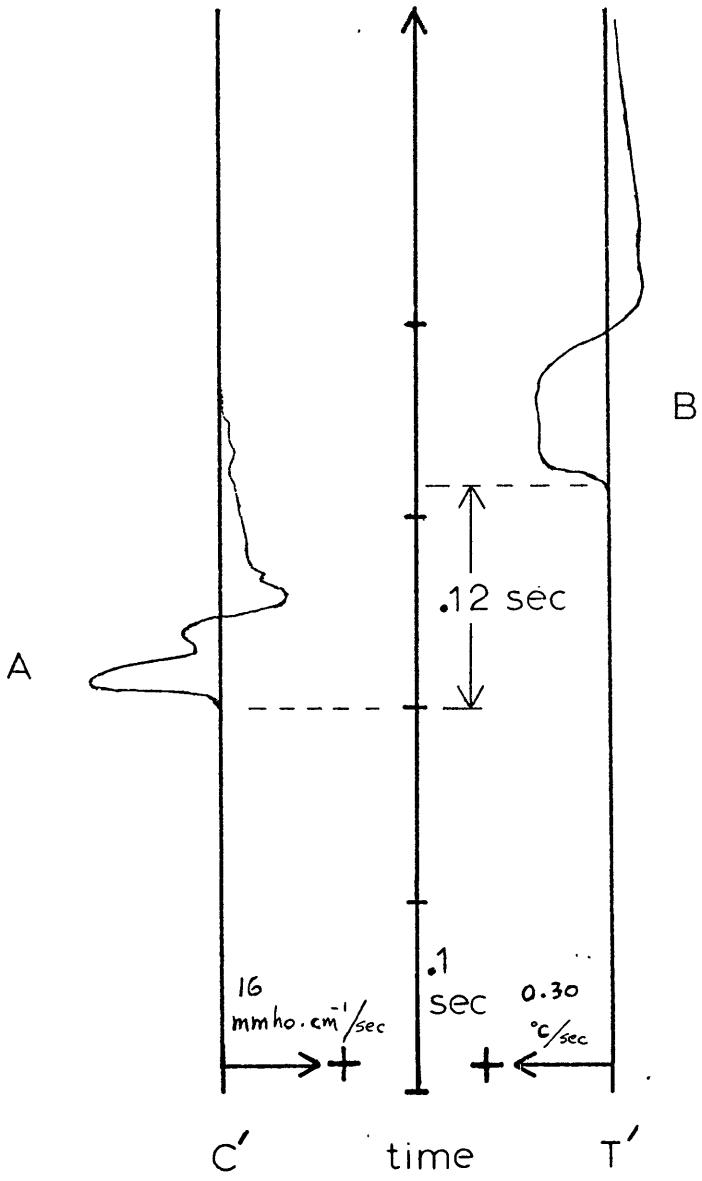

Tracing of excerpt from run of 22 April 1972.

Passage of 1 "smoke ring" vortex past C and T probes.

Initial Composition of "smoke ring" (at Nozzle):

$S = (0.95)S_o$ where S_o = ambient salinity = 15.5 ‰

T = unknown (not equilibrated)

$\Delta S = -0.78$‰ from initial conditions

$\Delta S = -0.43$‰ calculated from area under A and B above, and from Riley and Skirrow (1965).

Spatial Extent of "smoke ring" : less than spacing between C and T probes, which is 0.8 cm.

FIGURE 2.14 TANK TEST CALIBRATION RECORD

to that accuracy. Such temperature control, however, was impossible in this large, unevenly-heated, convecting body of water, copper coils notwithstanding. Moreover, the spatial resolution of the probe was seriously degraded in this setup because of its stationarity. Sucking water from a still tank through a stationary probe produces a much more diffuse and accelerated flow pattern than that which results from sucking water through a moving probe. This had the result of smearing the "smoke rings" as they approached the stationary probe, thereby producing a lower rate-of-change of conductivity than would have been the case if the probe were moving but the rings stationary.

Nevertheless, the tank tests demonstrated that the conductivity probe could resolve small structures; the signal level at the output due to the intersection by the probe of a 1 cm. diameter conductivity structure is about 90% of the signal due to the intersection of a much larger structure. The sensitivity of the instrument agreed with the design value within the errors of the tank test setup.

SEA TRIALS

Owing to scheduling difficulties and the need for deep water, sea-going trials of the instrument were not undertaken in New England waters. Instead the trials were combined with the data-gathering expedition itself, which was based at the Bermuda Biological Station. The vessel used was the R/V Panulirus II, a 65 foot twin-diesel boat equipped for research.

Normally it is not good practice to attempt to combine trial runs with data gathering; electronic equipment is rarely cooperative enough. But in this case shore-based laboratory facilities were available at the Biological Station, and Panulirus made day trips out to sea. This arrangement was extremely satisfactory both for the trials and data collecting, except for the necessity of shipping all the required supplies to Bermuda.

CHAPTER III

DESCRIPTION OF THE EXPERIMENT

A. LOCATION

Several investigators have reported finding a step-like structure of temperature and salinity in the main thermocline near Bermuda. This region is characterized in general by the fact that both temperature and salinity decrease with depth in the permanent thermocline, conditions which favor the salt finger type of double-diffusive convection; and it has been proposed that salt fingers may account for the formation of the layers and sharp interfaces. The purpose of this investigation was to gather more information on the nature of such microstructure, and in particular to see if salt fingers could be found between the layers. Bermuda is therefore a suitable if not unique place to use the microstructure instrument.

Bermuda offers certain practical advantages to the oceanographer. The 1,000-fathom depth line is only six nautical miles off the south shore of the islands. Day trips using relatively small vessels are thus entirely feasible, in contrast to New England waters, where the continental shelf extends 200 miles offshore, and where larger, sea-going vessels are mandatory. The climate is generally favorable in Bermuda, although it can be quite rough especially in the winter and spring. (This advantage, however, is offset to some extent by the use of small ships which require better weather for any particular operation than larger ships). Bermuda is also fairly easy to get to by air. Most importantly, ex-

cellent shore-based laboratory facilities are available at the Bermuda Biological Station. The combination of onshore laboratories with a small ship for day trips is ideal for a project such as this one which involves instrument "debugging" and trial runs as well as data gathering.

The area near Bermuda is certainly not unique in having microstructure; indeed, many other parts of the ocean exhibit more clearly defined steps in the vertical profiles than do the waters near Bermuda. But in view of the advantages of operating from Bermuda, the known existence of microstructure in the thermocline there, and the availability of numerous oceanographic observations of various kinds made in the vicinity, it was decided that Bermuda was the best place to carry out the experiment.

A chart of the Bermuda Islands is shown in Figure 3.1, indicating the place southeast of the island where most of the deep-sea work of this investigation was done. Most of the data to be analyzed in this section were gathered there in June, 1972.

On each of the cruises, the R/V Panulirus II steamed around the eastern end of the island, and then south-east into deep water. The launching and towing of the instrument commenced when the 1000-fathom depth contour was passed. This point, which is about 6 nautical miles southeast of St. David's Light, is marked on the Bermuda chart, Figure 3.1. The instrument was towed at the slowest speed at which the ship had adequate steerageway; this naturally depended upon the

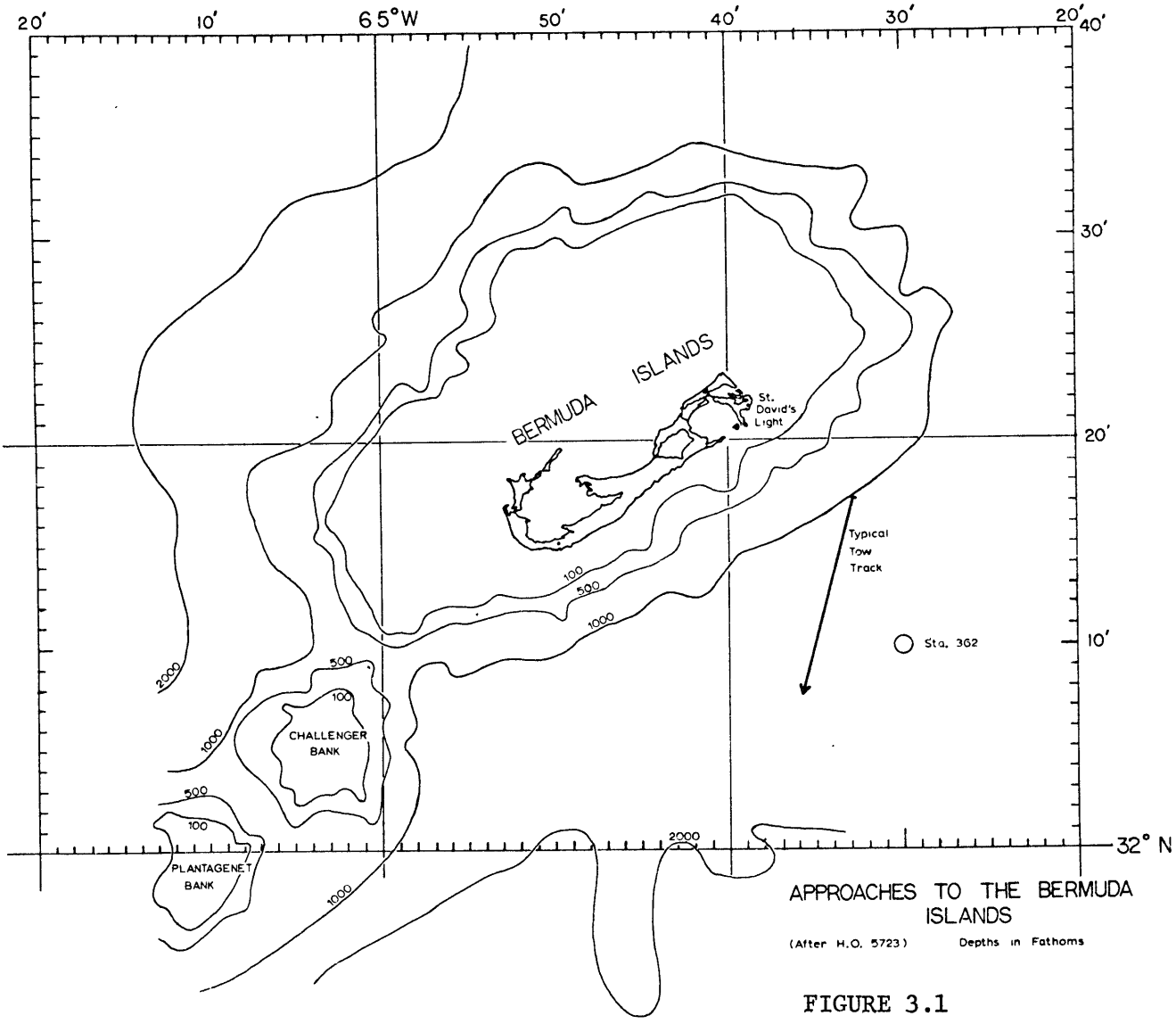
20'
10'
65°W
50'
40'
30'
20'
40'
30'
20'
10'
32° N
BERMUDA ISLANDS
St. David's Light
Typical Tow Track
Sta. 362
CHALLENGER BANK
PLANTAGENET BANK
100
500
1000
2000
APPROACHES TO THE BERMUDA ISLANDS
(After H.O. 5723)
Depths in Fathoms

FIGURE 3.1

wind velocity. The direction of the tow was determined by the wind direction; it was found that if the wind were kept on the starboard bow, the ship's motion was least offensive; and moreover the course, speed, and wire angle could be held steady with a minimum of correction. This resulted in a southerly course, away from the island, because the wind was almost always out of the southwest. A typical towing track is also shown in Figure 3.1.

No towing operations were conducted in water of less than 1000 fathoms, primarily as a safety precaution. When towing in the thermocline, it was necessary to let out the entire 1500 meters of available cable; and if the ship should stop for some reason, the instrument would descend to that depth. Considering the navigational uncertainties and the steepness of the island slope at that point, it was decided not to tow in less than 1000 fathoms.

Owing to the slowness of the R/V Panulirus II, and the necessity of making day trips, it was not feasible to venture around the island to sample the microstructure on the other sides. It required one-and-one-half hours steaming from the Biological Station dock merely to cross the nearest 1000-fathom contour, south-southeast of St. David's Light; to have steamed around to the northwest side would have required a several-day trip. But there was no a priori reason to suppose that the microstructure would be any less pronounced on the southeast side, so it was decided to concentrate on that area.

B. GENERAL OCEANOGRAPHIC CONDITIONS

Figure 3.2 is a vertical profile of temperature, salinity, and conductivity as a function of depth; the data are from hydrographic station #362 taken by R/V Panulirus II, the research vessel of the Biological Station on 7 June, 1972. This hydrographic station was taken, as shown in Figure 3.1, at the approximate location of the microstructure work. The T-S relation for this station is plotted on Figure 3.3, along with lines of constant density and electrical conductivity. From these figures it is clear that temperature is the primary influence on the conductivity, and that conductivity is a monotonically decreasing function of depth in the large scale.

It should be noted that the detailed distribution of temperature and salinity in the upper layers of the ocean is quite variable. Certainly the surface salinity minimum of Figure 3.2 is not a permanent feature. Other Panulirus stations show surface salinities ranging from 36.20 to 36.70; it evidently depends upon the recent history of the weather. In fact, the entire upper layer, from the surface down to the 18-degree water, is rather confused, and may contain substantial temperature and salinity inversions.

The area around Bermuda has been surveyed extensively by hydrographic methods, and also by the use of moored current meters, Swallow floats, parachute drogues, vertical current meters, and a temperature micro-profiler. Wunsch (1972), for example, has conducted an extensive investigation of the flow around the island. He

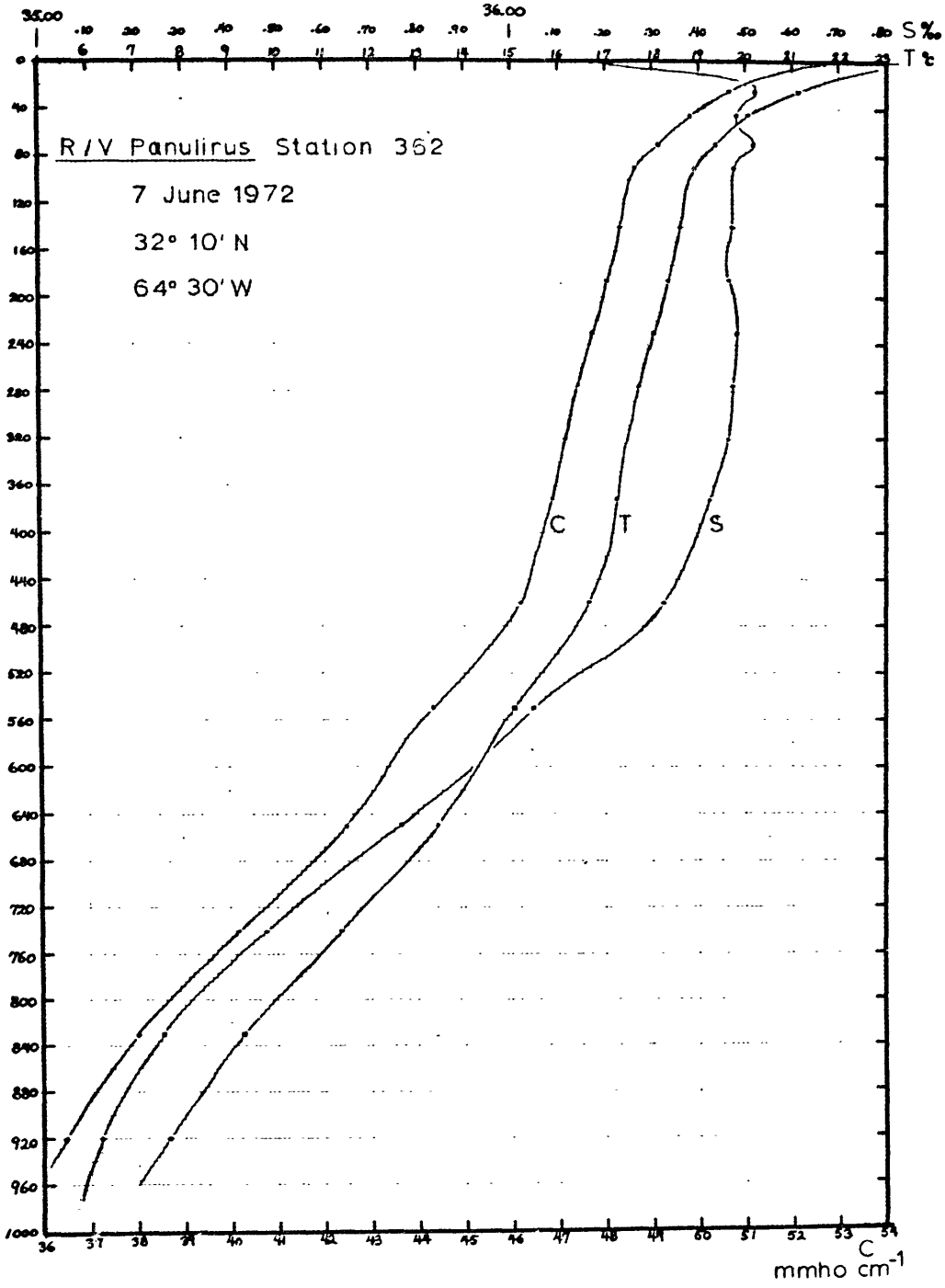
35.00
36.00
S ‰
T °c
R/V Panulirus Station 362
7 June 1972
32° 10' N
64° 30' W
C
T
S
C
mmho cm-1

FIGURE 3.2

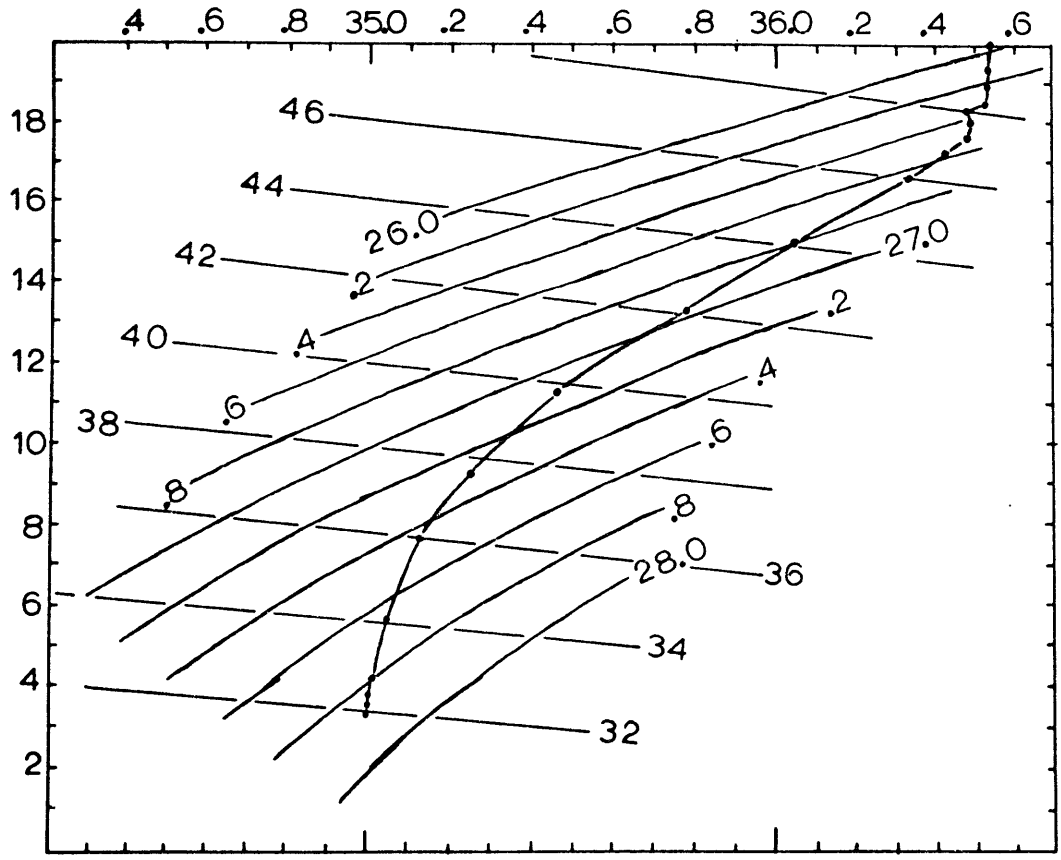

T-S Relationship for R/V Panulirus II Sta. 362
7 June 1972 32° 10'N 64° 30'W
With Isopleths of Electrical Conductivity

FIGURE 3.3 (after Sverdrup, Johnson, and Fleming, 1942; also Riley and Skirrow, 1965)

found, in essence, that "microstructure", loosely defined as a steplike structure in vertical profiles of temperature and salinity, appears to increase as the island is approached. He found furthermore that this microstructure is not uniformly distributed azimuthally around the island; rather it seems to be most pronounced on whichever side of the island lies to the right of the mean flow. But the direction of the mean flow can vary abruptly; it has been observed at various times to flow out of the west, northeast, and southwest.

The direction of the mean flow past Bermuda is not known for the period June - July, 1972, when this work was carried out.

In the same paper, Wunsch also asserts that there appears to be more structure within the 18 degree water (200-400 meters depth) than in the water above or below.

C. GENERAL PROCEDURE DURING EXPERIMENT

As had been expected, it proved to be very difficult to tow the instrument at a constant depth. The large amount of cable, hanging on a wide catenary between the ship and the instrument, meant that unattainably precise control of the towing speed and direction were essential if constant depth were to be maintained.

Active depth control using the winch was tried and found wanting, largely because of the slowness of response of the system to changes in cable tension. There was also an extreme communication problem between the ship's lab and the winch; to effect a change in the

winch speed, the author was obliged to leave the lab and shout his request into the winch operator's ear in order to be heard above the noise of the engines.

Constant-depth towing was not the most desirable procedure anyway, since it provided little information about conditions in the water above or below the instrument. The optimum procedure was to tow the instrument at a shallow vertical angle. This was best accomplished by running the winch slowly in or out, making occasional changes in its speed to compensate for variations in ship speed.

The rolling and surging of the ship introduced difficulties, especially when the cable was being run out. Under these conditions the velocity of the cable was at a minimum, being the difference between the ship's speed and the winch speed. Consequently, changes in the ship's speed had a much greater effect on the cable tension when the cable was being let out than when it was being hauled in. The pump which flushes water through the conductivity probe proved to be sensitive to these speed changes, so that the lowering had to be kept very slow. This in turn decreased the depth stability.

The procedure adopted to combat these difficulties was to lower the instrument quite rapidly to the maximum desired depth, ignoring any data taken during this lowering. Then the instrument was raised steadily at a moderate rate. A reasonably steady monotonic ascent could be achieved in this way. Vertical velocities of 15 to 30 centimeters per second in combination with for-

ward velocities of 100 to 200 centimeters per second were typical.

Exceptions to this policy of steady ascent were made on occasion. "Yo-yo" type experiments were done, in which the instrument was repeatedly raised and lowered through an interesting feature. The rate of lowering was kept rather low in order to prevent stoppage of the pump; nevertheless the sudden change in cable tension as the winch reversed direction often caused spurious signals on C'.

The six-channel high-speed strip-chart recorder with electrostatic writing was used to monitor the data as it unfolded in real time. The variables monitored were usually C', T', Cz, Tz, V, and Z. This chart record was manually marked with numbers corresponding to the tape footage indicator, so as to be able to locate events again later without having to play back an entire tape.

D. THE LOWERINGS

The lowerings of the instrument were made during the period 4 June - 6 July, 1972. A total of 13 separate lowerings were made, on 7 short cruises of the R/V Panulirus II. The first few lowerings must be regarded as trial runs for the purpose of "debugging" the instrument. Persistent leakage in the underwater electrical connectors was the major problem; and this problem continued intermittently throughout the series of lowerings.

A calendar of events covering the period of the

lowerings is shown below in Table I. The lowerings which provided useful data are indicated by asterisks (*). A profusion of excessively windy days and major storms, both of which are rather unusual in Bermuda in June, were the major cause of delays. Relatively calm weather was essential, since severe motion of the ship had a serious effect on the performance of the towed sensor package.

The four useful lowerings are shown schematically as a function of time in Figures 3.4 through 3.7. Only useful sections of the lowerings are shown. Certain parts of each lowering are generally not useful, particularly down-going sections where the instrument tended to stop dead in the water momentarily owing to the roll and surge of the ship. But there are exceptions, however, such as the down-going portion of Lowering 11, which was made on an extraordinarily calm day. Occasional instrument malfunction, and time-outs for tape changing, caused the remaining gaps.

The locations of the "bursts" of microstructure on the C' conductivity record are indicated on the lowering diagrams by numbered arrows, except where the microstructure was too dense. The first two digits of each number indicate the tape reel number, and the last four digits indicate the approximate tape footage at which the burst occured.

TABLE I

CHRONOLOGY OF FIELD OPERATIONS - BERMUDA 1972

(lowerings marked with * contain useful data)

JUNE	
4	Lowering 1
7	Hydro. Station #362
9	Lowering 2; 3; 4
10	Lowering 5
16	Lowering 6; 7; 8*
28	Hydro. Station #363
29	Lowering 9
JULY	
3	Lowering 10*; 11*
6	Lowering 12; 13*
9	Return to Boston

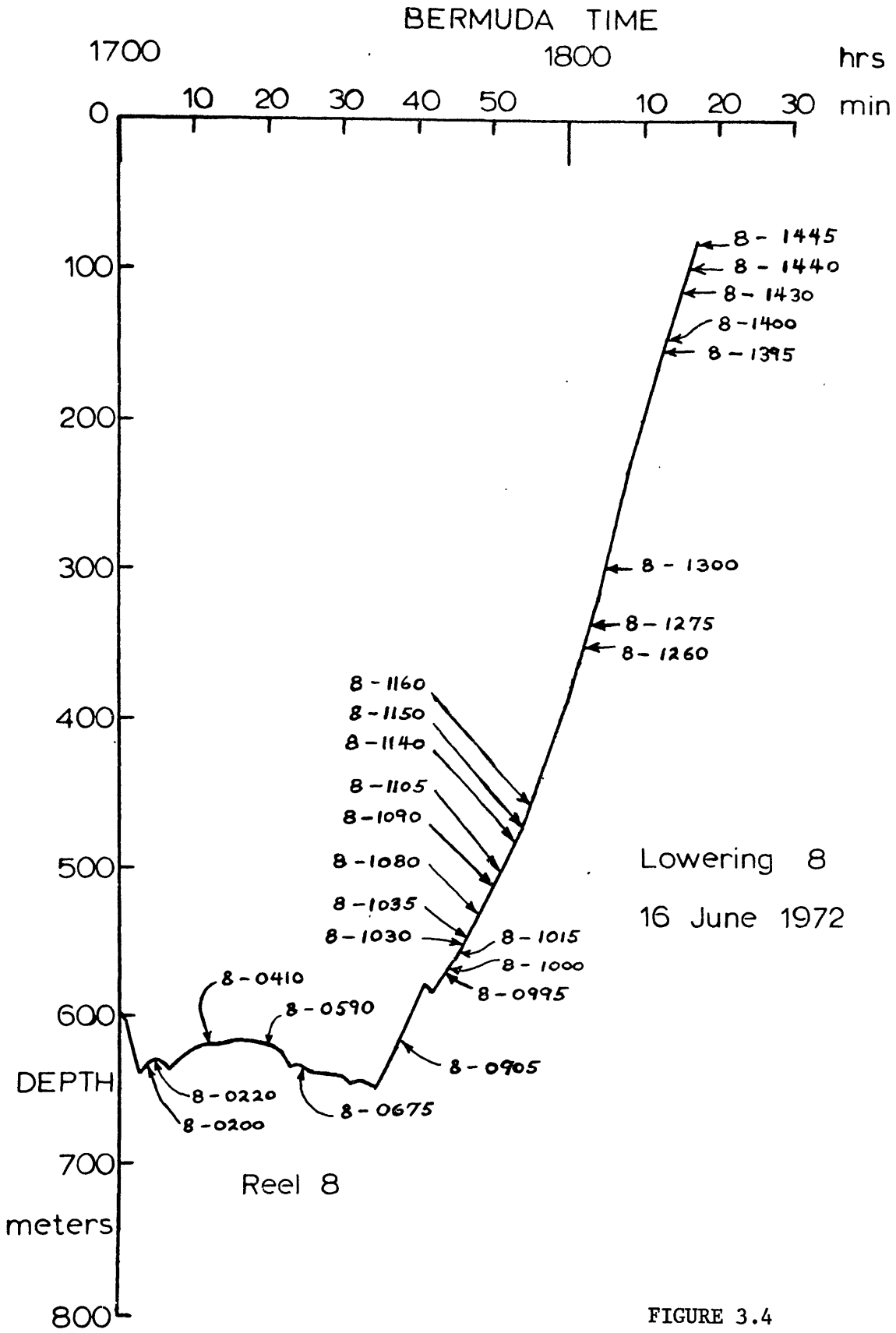
BERMUDA TIME
1700
1800
hrs
0
10
20
30
40
50
10
20
30
min
100
200
300
400
500
600
700
800
DEPTH
meters
8 - 1445
8 - 1440
8 - 1430
8 - 1400
8 - 1395
8 - 1300
8 - 1275
8 - 1260
8 - 1160
8 - 1150
8 - 1140
8 - 1105
8 - 1090
8 - 1080
8 - 1035
8 - 1030
8 - 1015
8 - 1000
8 - 0995
8 - 0905
8 - 0675
8 - 0590
8 - 0410
8 - 0220
8 - 0200
Lowering 8
16 June 1972
Reel 8

FIGURE 3.4

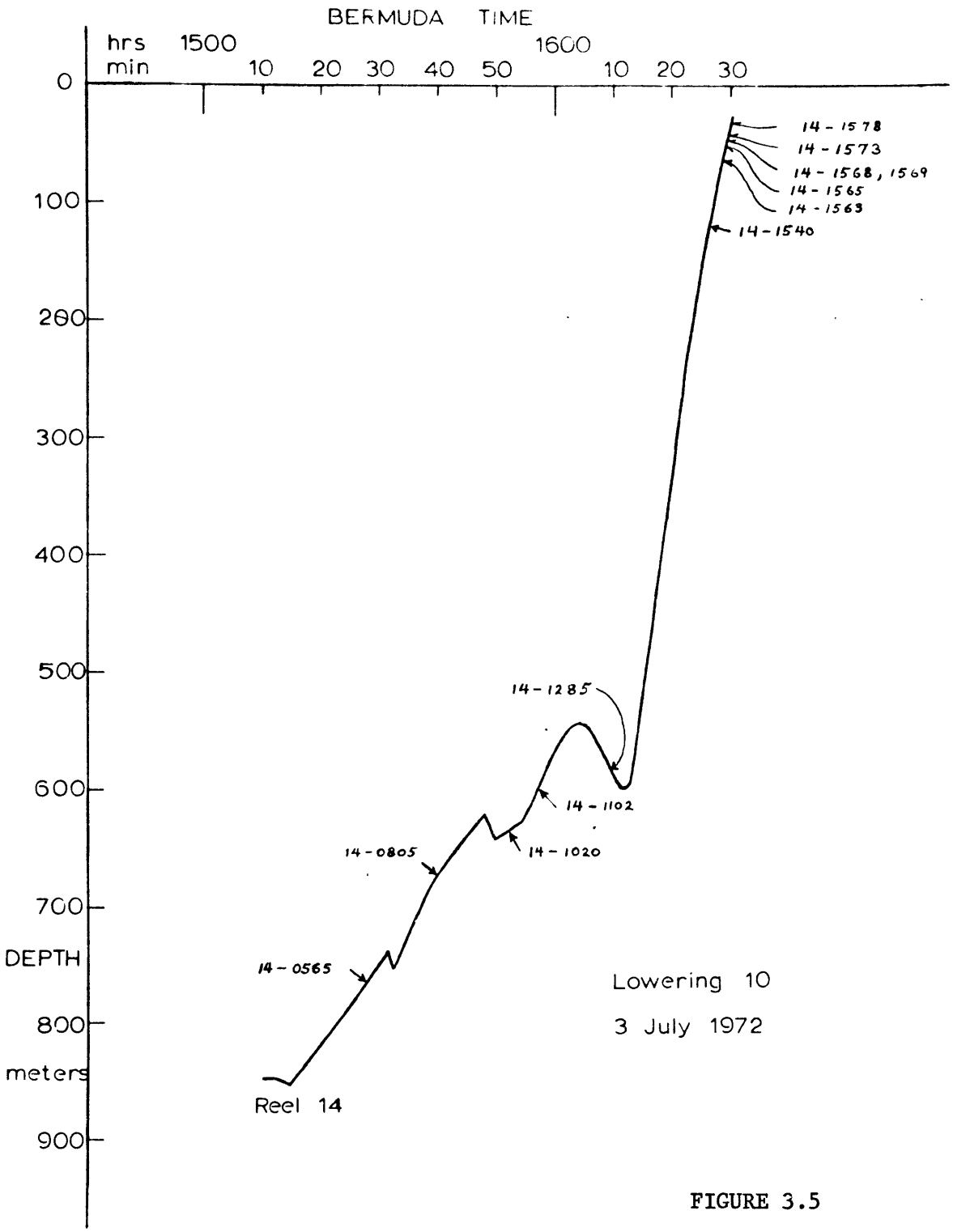
BERMUDA TIME
hrs
min
1500
1600
0
10
20
30
40
50
10
20
30
100
200
300
400
500
600
700
800
900
DEPTH
meters
14 - 1578
14 - 1573
14 - 1568, 1569
14 - 1565
14 - 1563
14 - 1540
14 - 1285
14 - 1102
14 - 1020
14 - 0805
14 - 0565
Reel 14
Lowering 10
3 July 1972

FIGURE 3.5

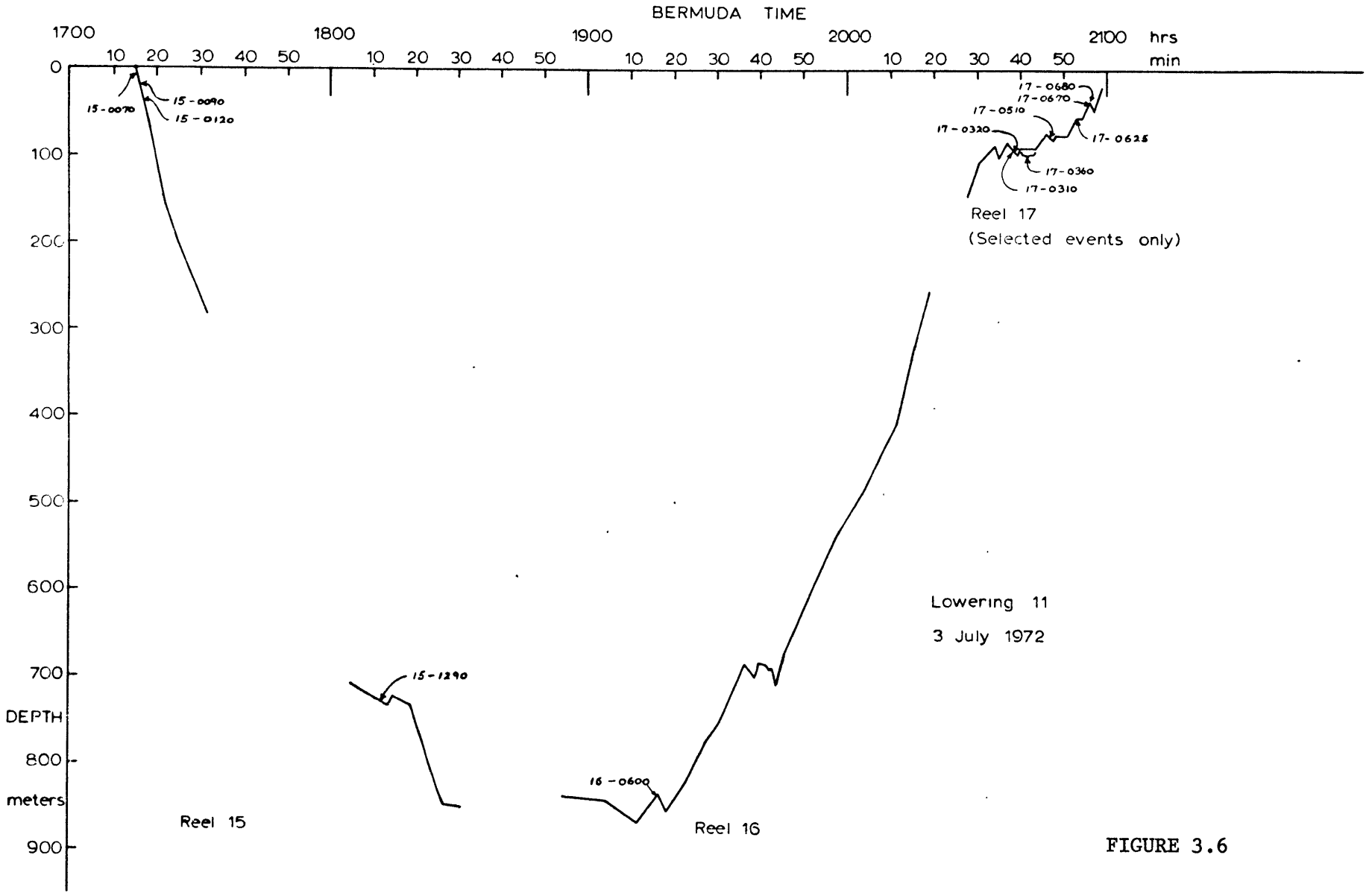
BERMUDA TIME
1700
1800
1900
2000
2100 hrs
0 10 20 30 40 50 10 20 30 40 50 10 20 30 40 50 10 20 30 40 50 min
0
100
200
300
400
500
600
700
800
900
DEPTH
meters
15-0070
15-0090
15-0120
15-1290
16-0600
17-0680
17-0670
17-0510
17-0320
17-0625
17-0360
17-0310
Reel 17
(Selected events only)
Reel 15
Reel 16
Lowering 11
3 July 1972

FIGURE 3.6

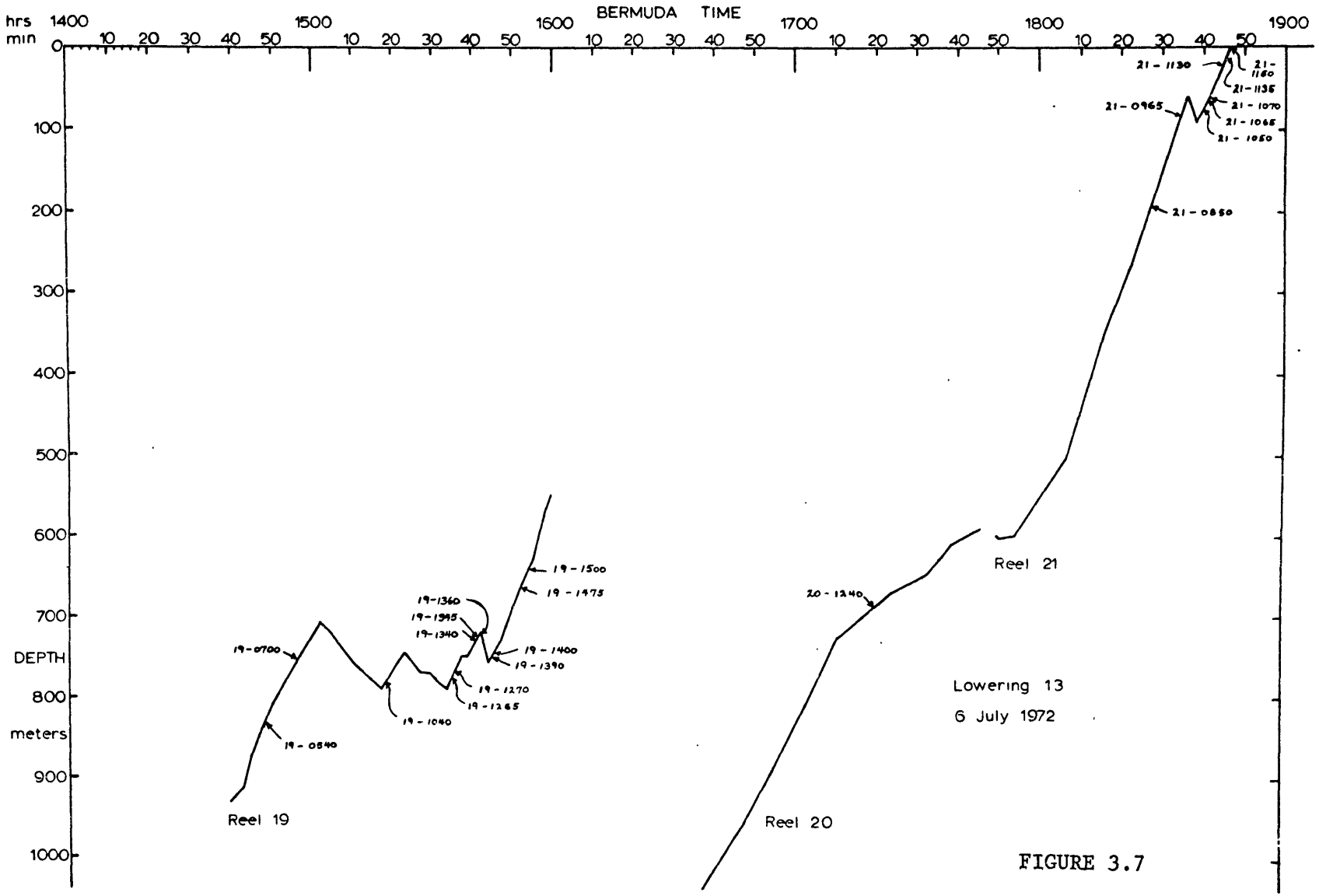
hrs
min
1400
1500
1600
BERMUDA TIME
1700
1800
1900
DEPTH
meters
19-0700
19-0840
19-1040
19-1360
19-1345
19-1340
19-1270
19-1265
19-1390
19-1400
19-1475
19-1500
Reel 19
20-1240
Reel 20
Reel 21
21-0850
21-0965
21-1050
21-1065
21-1070
21-1135
21-1160
21-1130
Lowering 13
6 July 1972

FIGURE 3.7

CHAPTER IV

PRELIMINARY DATA ANALYSIS

A. AN OVERVIEW OF THE DATA ANLYSIS

NATURE OF THE DATA

The conductivity microstructure record (C') consists mostly of background noise, with occasional "bursts" of high-frequency signal appearing above the noise level. The cause of these bursts is not immediately apparent; inspection using a high-speed chart recorder reveals that the bursts differ in amplitude, duration, and frequency content. The bursts all have a rather "spikey" appearance, as might be expected from a time-derivative signal; but some are rather more narrowband than others. The difficulties of eyeball interpretation are compounded by the fact that the towing speed is not constant; this influences both the amplitude and frequency content of the C' signal for a given conductivity field.

In the next section of this chapter we present some samples of the raw analog record, showing bursts of signal on C'. It is not feasible to present in this paper all the original data, because even at the slowest recording speed, a great deal of paper is required. Therefore the location of each significant burst has been marked on the lowering schematics, Figures 3.4 through 3.7.

OBJECTIVES OF THE DATA ANALYSIS

The primary objective of the data analysis is to determine the cause and significance of the bursts of

microstructure signal (C'), using the auxiliary data (Cg, Tg, Cz, Tz, Z, and V) to provide the necessary larger-scale information, without which the C' signal cannot be interpreted. In addition, the auxiliary data is informative in its own right, since it yields a picture of the vertical distribution of temperature and conductivity in the ocean. This information in turn is useful in understanding how the C' data fits into the overall picture.

BURST ANALYSIS STRATEGY

The analysis of the bursts proceeds, in essence, through a succession of increasingly complex models or theories, beginning with a passive-ocean model, then a salt-finger model, and lastly a turbulent model. The details of the burst analyses are given in Chapter V: Horizontal Microstructure Models.

The auxiliary data, particularly the vertical gradient data, is essential in distinguishing between the various models. But before this auxiliary data can be used in the C' analysis, it is first necessary to come to some understanding of it separately. This is done in the third section of this chapter. There, the gross temperature and conductivity, and the vertical gradients, are plotted as functions of depth. From these plots one can best comprehend the performance and limitations of the instruments, and thus avoid misunderstandings and confusion when the data is used in succeeding chapters in the C' analysis.

Moreover, by plotting the auxiliary data as func-

tions of depth, we can learn quite a bit about the distribution, variability, and horizontal extent of the vertical microstructure. These matters are also discussed in the third section of this chapter.

Finally, there is the all-important matter of the significance of the microstructure data with respect to vertical mixing in the ocean. The distribution of the microstructure as a function of depth is important in this connection; likewise the intermittency, or percentage of the ocean which is undergoing mixing, must be discussed for each dynamic model. From this an estimate may be made of the effective mixing coefficients for each type of convection. This analysis will be given in Chapter VI: Significance of the Microstructure.

B. BASIC APPEARANCE OF THE HORIZONTAL MICROSTRUCTURE

It is not feasible to present here all of the bursts of conductivity microstructure, since more than 300 more-or-less separate bursts have been catalogued. But an example might aid the reader in understanding what this analysis is all about, and in acquiring confidence as to the performance of the instrument. More examples will be presented later in the analysis to illustrate specific cases.

Figure 4.1 is an excerpt from Lowering 13, 6 July, 1972. The record shown is not the original monitoring record; rather it is a re-run of the data, played back as a function of time. Three variables are presented: C', Cz, and Z.

The record displayed here is a "yo-yo" experiment

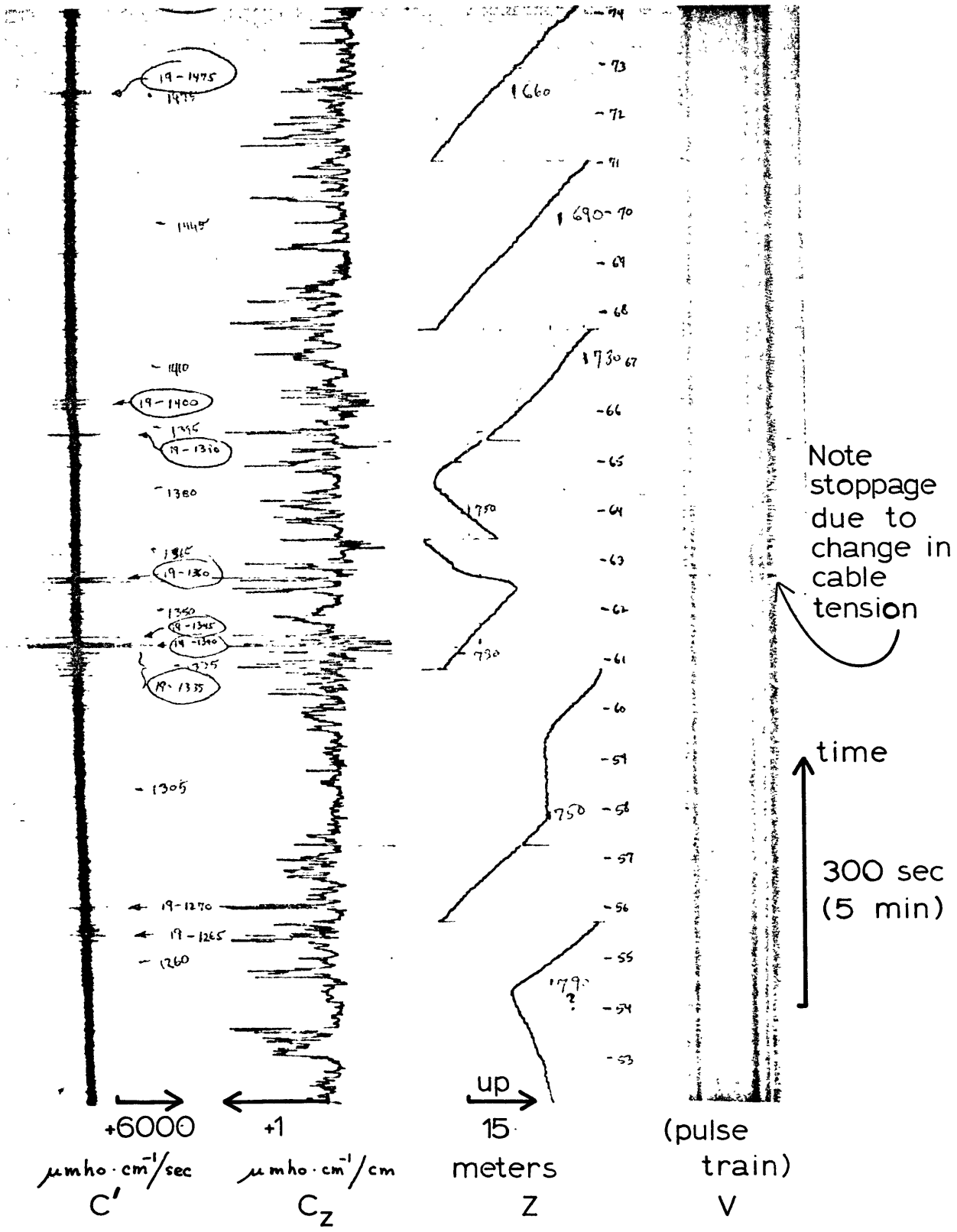

FIGURE 4.1 Horizontal Microstructure Example from Lowering 13

in the thermocline. From the records of these "yo-yo' experiments with the instrument we can estimate the horizontal extent of turbulent patches; this record represents the widest such patch. The microstructure region was intersected 3 times, at depths of 733 ±3, 726 ±3, and 746 ±3 meters, respectively. The distance between the first and second intersections was 110 meters; the average slope of the isopyncnal surface was therefore +1/16, with a range of 1/9 to 1/110. The distance between the second and third (less distinct) burst was 185 meters; the average slope was -1/9, with a range of -1/7 to -1/13.

The total distance between the first and last intersection is therefore about 300 meters horizontally. Since the first burst was the largest, and the last one was much smaller, it is reasonable to suppose that the instrument was approaching the edge of a mixing patch. If the patch were symmetrical, its horizontal extent would be 600 meters. It is possible, of course, that the 3 events are unrelated, in which case their horizontal extent must be less than 100 meters each.

It is more difficult to define the vertical extent of the patch. The first intersection contains many small events and one large one. Assuming that the interfaces are not tilted, the thickness can be inferred from the vertical velocity to be 10 meters overall for the entire event, and 1.4 meters for the large central burst. Of course if the interface was tilted these estimates will be too high.

The depth of successive intersections is seen to

vary by as much as 20 meters, although the errors in the depth sensors (primarily hysteresis) may reduce this somewhat. Assuming that the 3 intersections do indeed represent crossings of a single, wavelike interface, then we must postulate an internal wave having a 20 meter amplitude and a 300 meter (at least) wavelength. This is not inconceivable; but it is equally likely that the 3 events are merely local instabilities embedded in a larger turbulent region. In this case the differences in depth between the intersections would be irrelevant, although the range of depths would then imply that the turbulence had a vertical extent of at least 20 meters.

The largest burst shown in Figure 4.1, namely the one labeled 19 - 1340, is analyzed in detail in Chapter V to see if it is consistent with a turbulent model. This burst is shown in greater detail in Figures 5.4 and 5.5.

C. ANALYSIS OF THE VERTICAL PROFILES

This section provides a detailed look at the performance of the auxiliary or background sensors, namely, the gross temperature (Tg) and conductivity (Cg) and the vertical gradients of temperature (Tz) and conductivity (Cz). These data illuminate the environment in which the microstructure occurred; hence it is essential to investigate them first.

GROSS TEMPERATURE AND CONDUCTIVITY

Figures 4.2 throuth 4.5 are plots of gross temperature (Tg) and gross conductivity (Cg) versus depth (Z). Absolute values of temperature and conductivity have not been plotted; instead the sensitivity or scale factor is given. Neither Cg nor Tg was intended to be an accurate absolute sensor; as described previously, both of these outputs possess various sources of drift and error. The four-digit numbers again refer to tape footage.

The Cg trace, although distorted in the large scale, shows the same irregularities and even inversions as Tg, although the instruments are completely separate, even having separate power supplies; furthermore, these same irregularities and inversions are clearly visible as positive and negative gradients on Tz and Cz. For example, referring to Figure 4.5, note the inversion in temperature and conductivity near Z=840 meters. Then refer ahead to Figure 4.9 which is a chart of Cz versus Z, and observe the negative-going gradient signal at the same depth.

We may thus conclude from Figures 4.2 - 4.5 that:

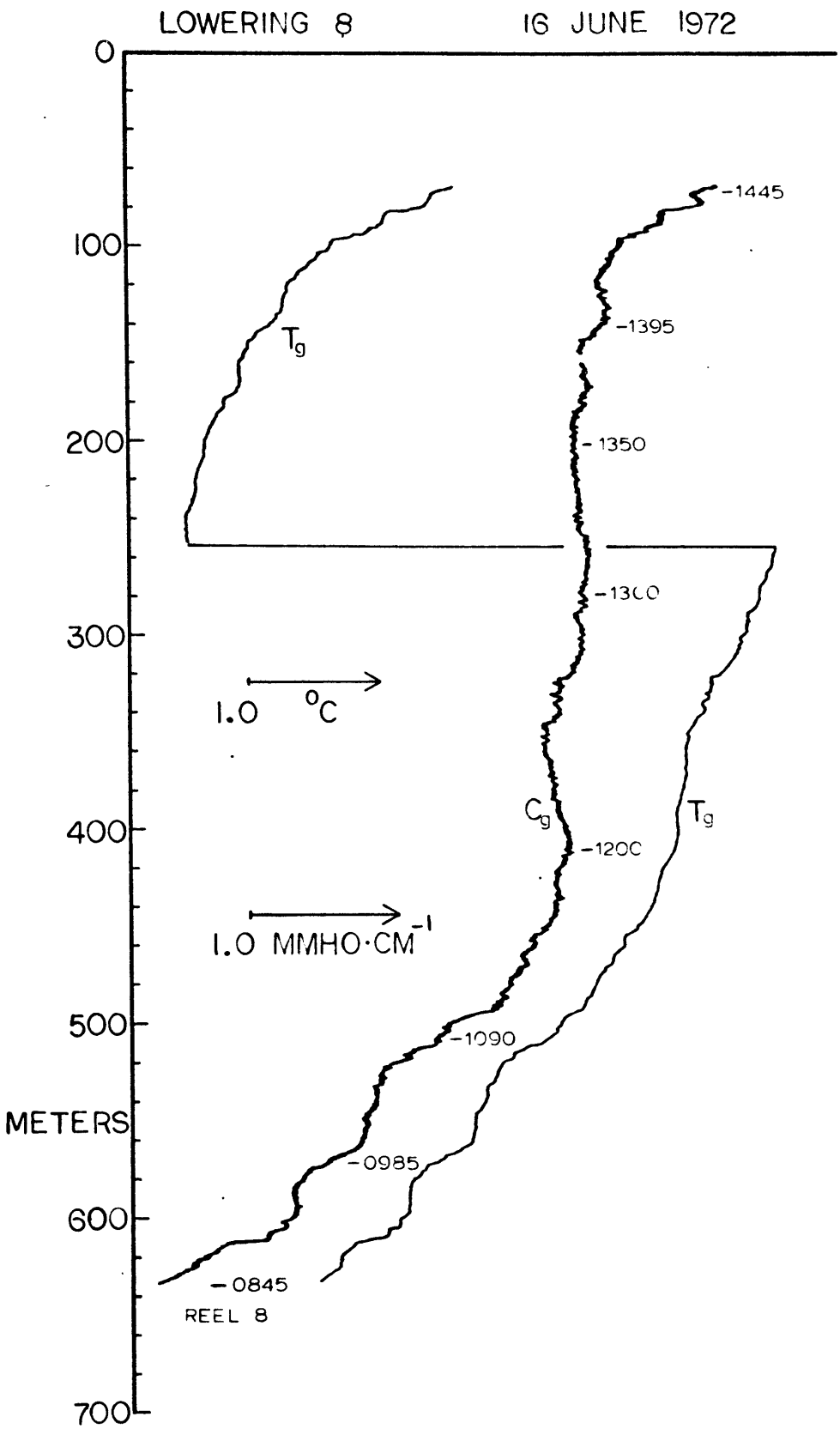

FIGURE 4.2 Vertical Profiles of Gross Temperature and Conductivity, Lowering 8.

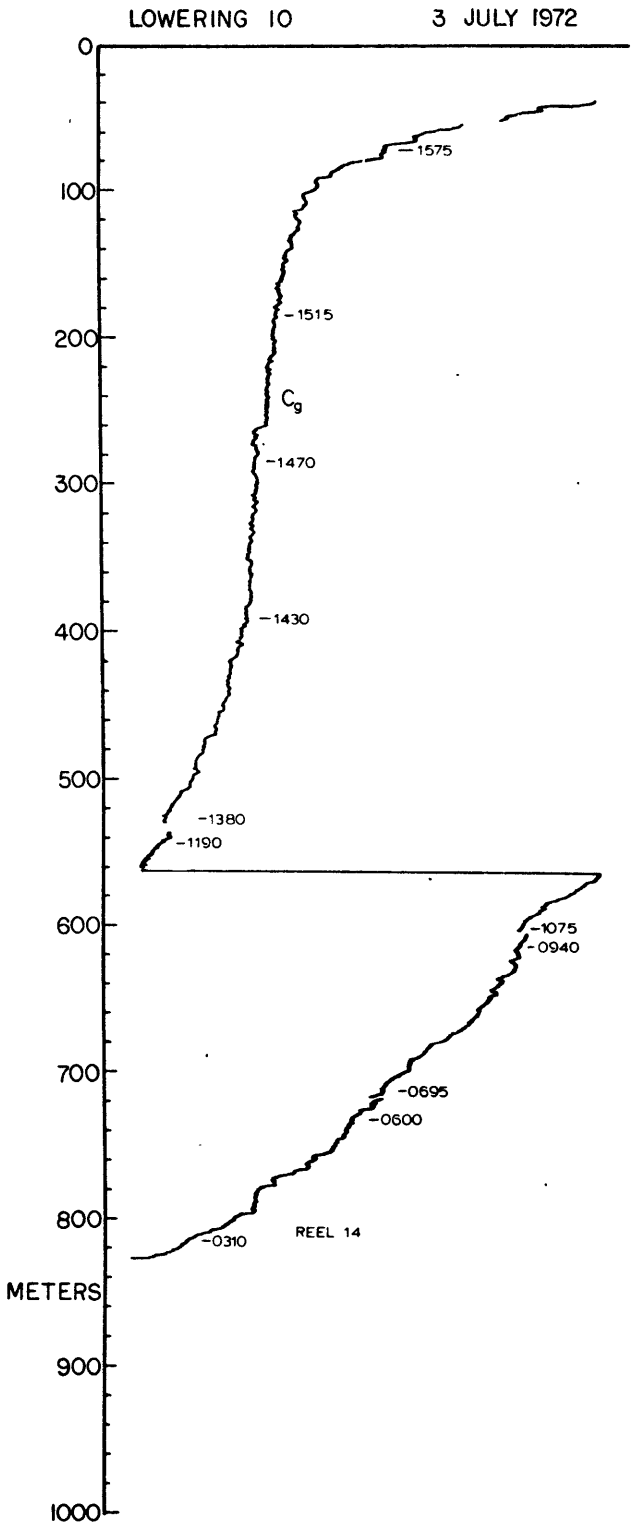

FIGURE 4.3 Vertical Profile of Gross Conductivity (no temperature data), Lowering 10.

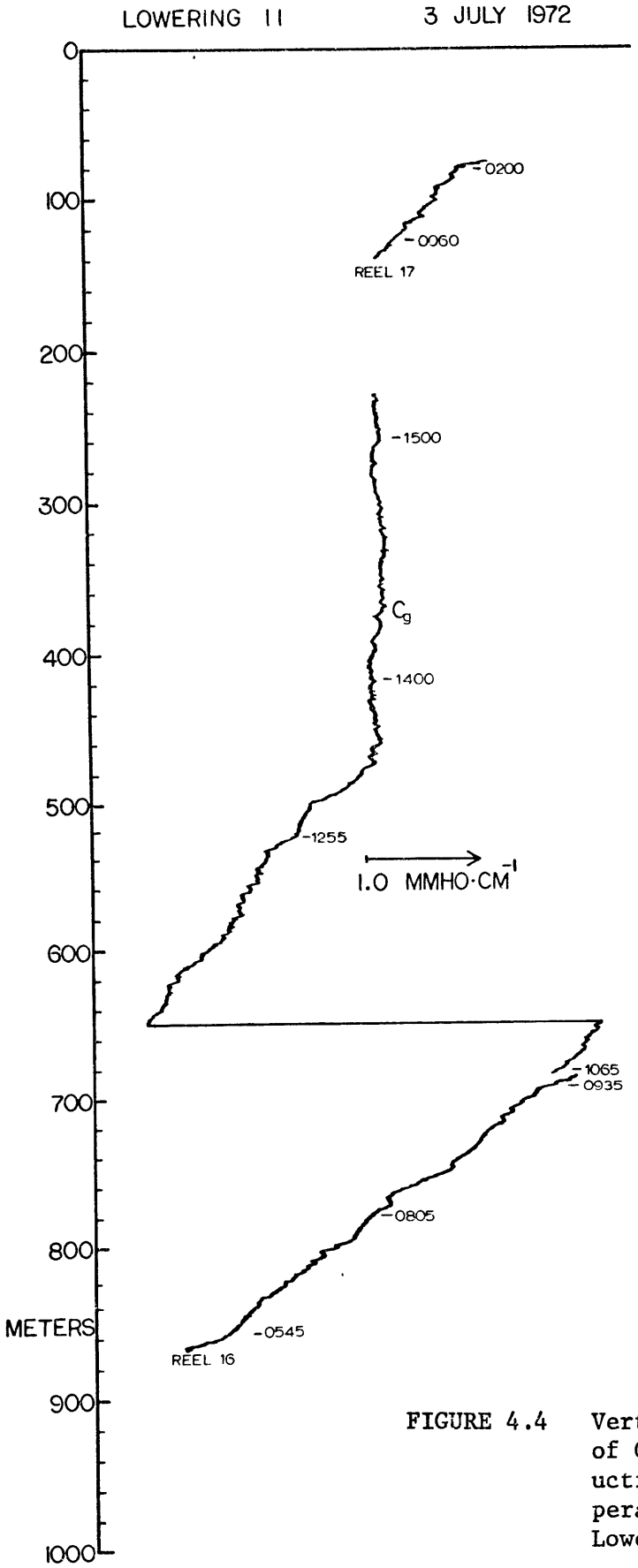

FIGURE 4.4 Vertical Profile of Gross Conductivity (no temperature data) Lowering 11.

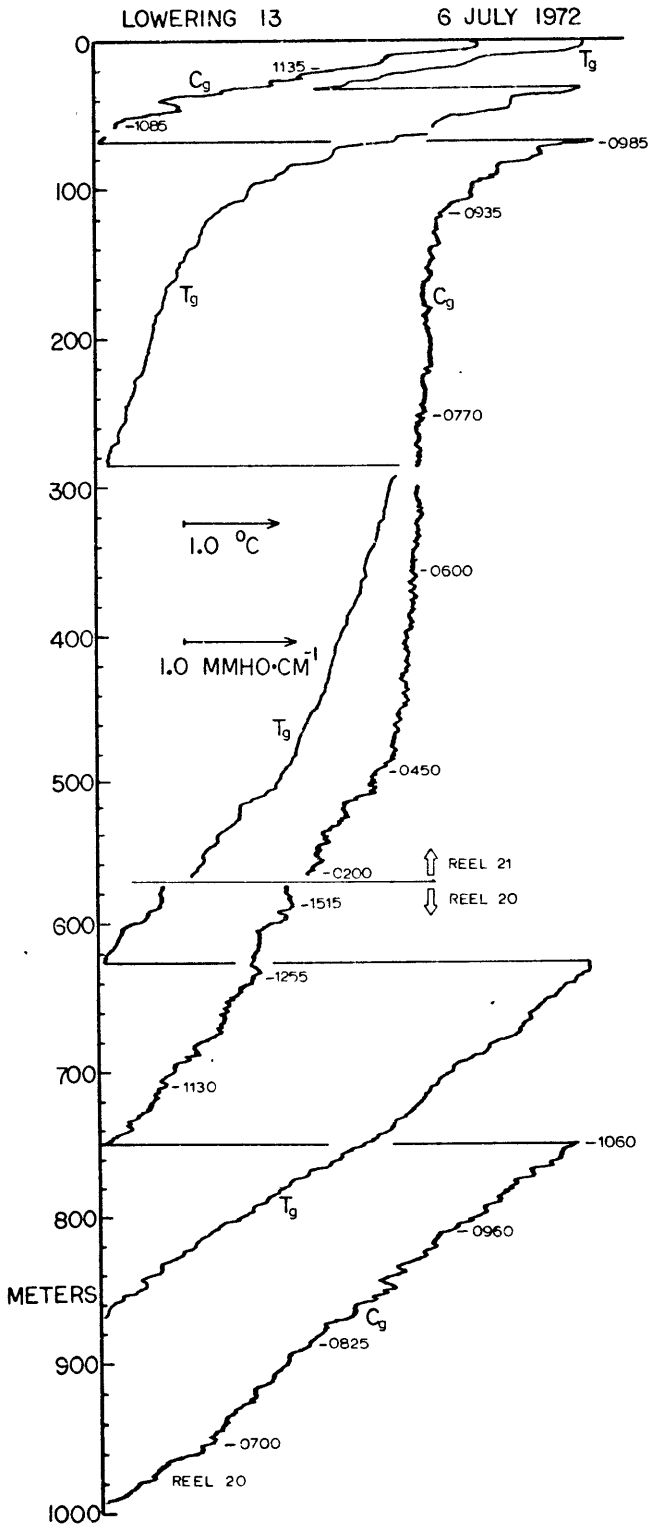

FIGURE 4.5 Vertical Profiles of Gross Temperature and Conductivity, Lowering 13.

first and most importantly, the conductivity microstructure probe was working correctly at least during the lowerings shown; secondly, that an irregular, vaguely step-like structure did exist, both in the thermocline and near the surface, at the time these lowerings were made; and thirdly, that infrequent inversions in temperature and conductivity did occur. The significance of this data will be discussed later in this chapter, following the analysis of the Tz and Cz data.

CONDUCTIVITY GRADIENT

In this section the data gathered by the vertical conductivity gradient sensor will be examined from several points of view. This instrument, described in Chapter II, measures the difference in electrical conductivity between two sensing heads separated vertically by 30 centimeters. The vertical conductivity gradient data is extremely important in the interpretation of the microstructure; hence it is essential to analyze and understand this data before proceeding to the C' data.

Figures 4.6 - 4.9 show the conductivity gradient signal (hereafter referred to as "Cz") plotted against depth (Z) for each lowering. It is clear from the Figures that the entire Cz trace is offset toward higher Cz values with increasing Z, a fact which does not accord with oceanic reality. Some probable reasons for this offset have already been discussed in Chapter II; among them is the presence of a spurious signal proportional to conductivity itself.

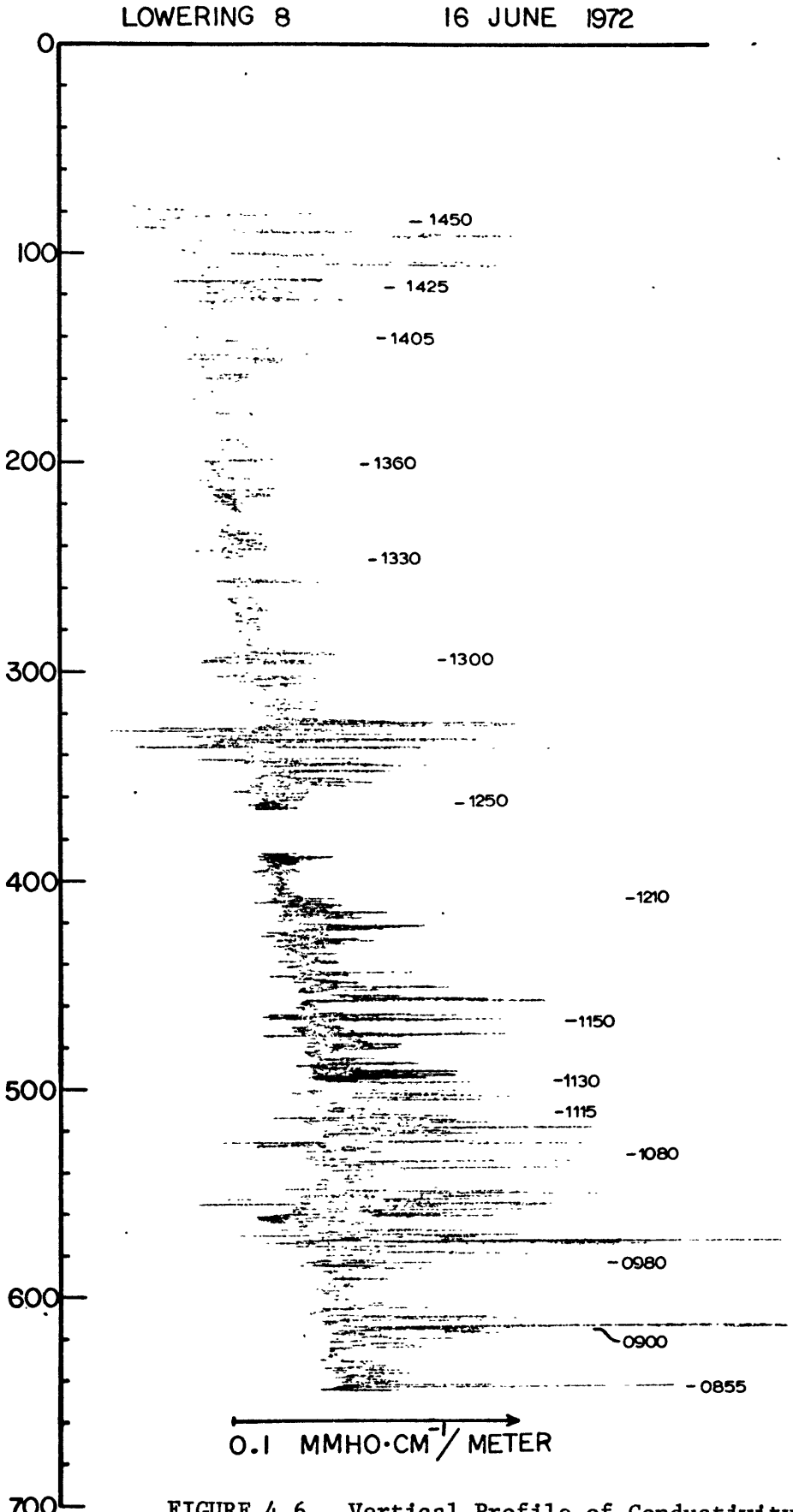

FIGURE 4.6 Vertical Profile of Conductivity Gradient, Lowering 8.

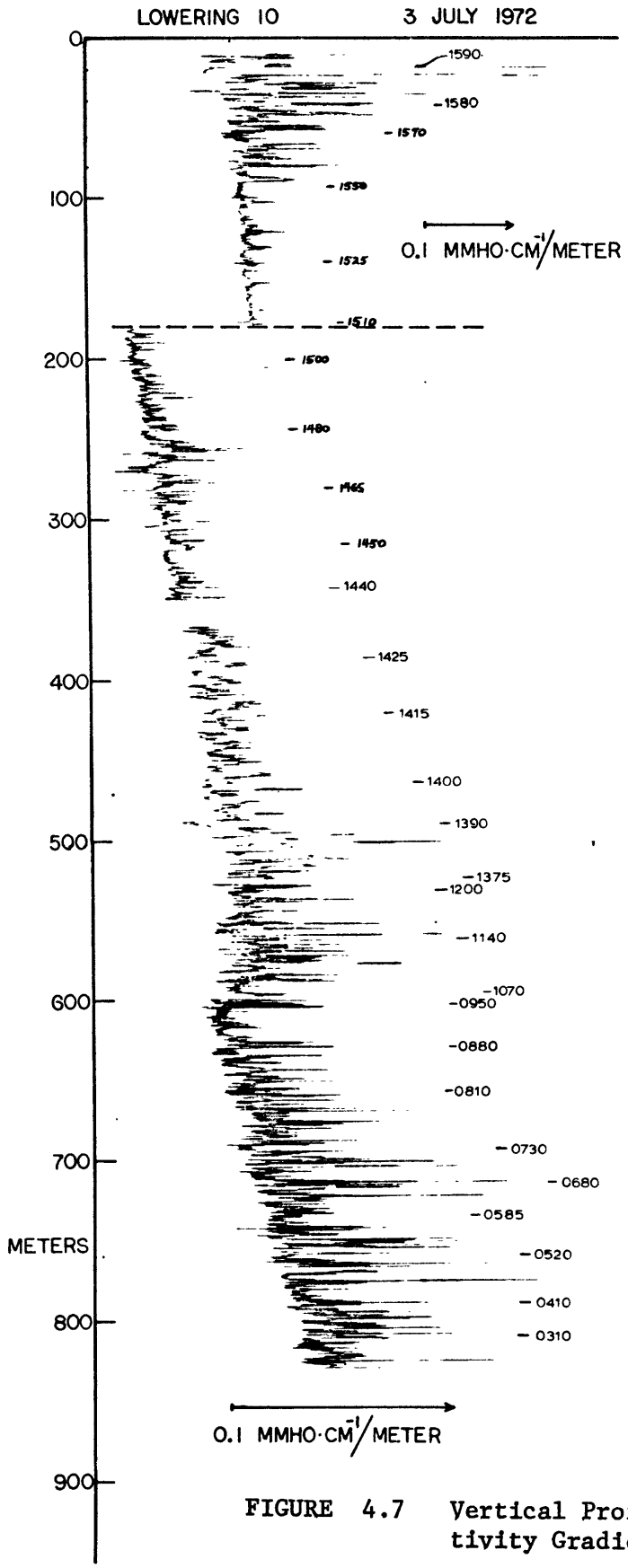

FIGURE 4.7 Vertical Profile of Conductivity Gradient, Lowering 10.

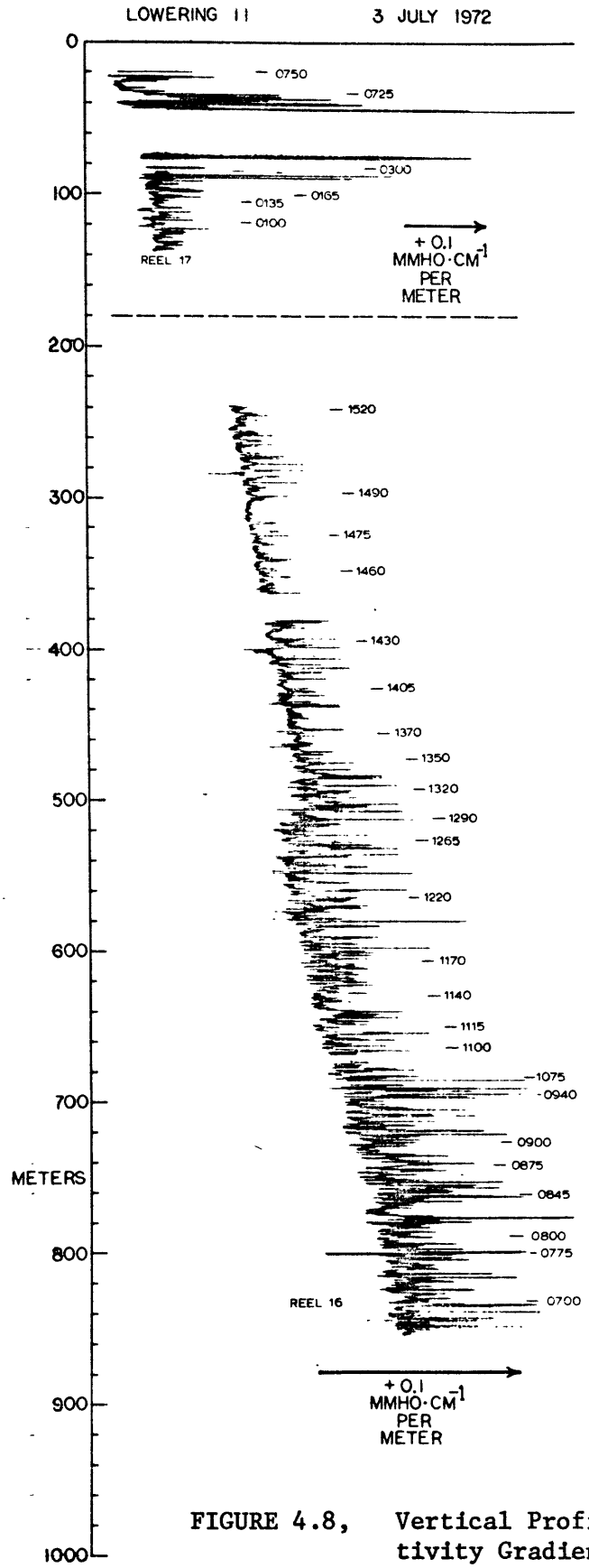

FIGURE 4.8, Vertical Profile of Conductivity Gradient, Lowering 11.

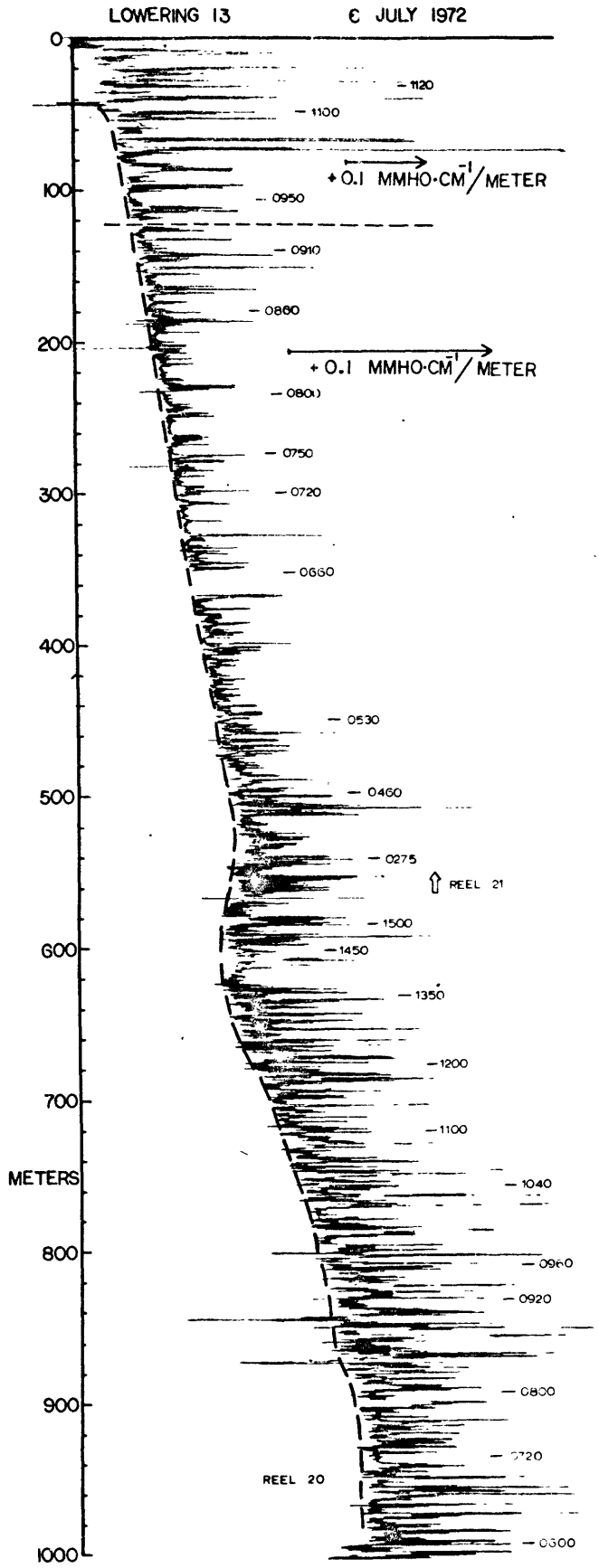

FIGURE 4.9 Vertical Profile of Conductivity Gradient, Lowering 13

METHODS OF CORRECTING THE C_z DATA

Efforts have been made to use the gross conductivity data, Cg, (properly scaled) to correct the error in the Cz data. The Cg data, however, is not sufficiently accurate in itself, as discussed previously in Chapter II, to be of much use as a corrective agent. Moreover, it was found that the residual error in Cz could not be explained by errors in Cg. The temperature data (Tg) effects a greater improvement in Cz; but significant error still remains. Consequently, it is concluded that the error in Cz is complex and cannot be cured by any simple additive correction.

Another method of correcting the Cz data is to compare its large-scale features with other independently-derived data. Refer to Figure 3.2, p. 74 which shows profiles of temperature, salinity, and conductivity as functions of depth. These data are from R/V Panulirus hydrographic station #362 (7 June, 1972), taken off Bermuda in the vicinity of the microstructure work and at about the same time. Nansen-bottle stations such as this do not reveal much detail, but average gradients may be calculated with considerable accuracy. The "knee" in the profiles is clearly visible at about 450 meters depth; above it the average conductivity gradient is nearly constant for 200 meters at 0.0056 mmho·cm.$^{-1}$ per meter (0.056 μmho cm.$^{-2}$), while below it in the main thermocline the gradient is 0.024 mmho·cm.$^{-1}$ per meter (0.24 μmho cm.$^{-2}$).

An examination of the Cz versus Z plot from lowering 13 (Figure 4.9) will reveal that these mean gradients are consistent with an envelope which passes near

the minima (leftward deflections) of Cz. Such a line is illustrated in Figure 4.9, and it may be seen to vary smoothly with depth, except in the vicinity of 500 meters where the structure is somewhat confused.

The conductivity gradient trace is quite asymetrical. Generally, the minima form a clearly defined envelope, except for an occasional negative-going aberration. The maxima, however, are not at all regular. One may well ask why there should exist such a well defined minimum of conductivity gradient, and whether this minimum is in fact zero. Figure 4.10 is a plot of density gradient and conductivity gradient in $\frac{dT}{dz}$, $\frac{dS}{dz}$ space. (This plot is entirely analogous to an ordinary T-S plot except that all the quantities are vertical gradients). Assuming that the water column is gravitationally stable (i.e., all points lie <u>above</u> the line $\rho = 0$) one can draw the following conclusions: (note that z is positive <u>upward</u>)

1. that if $\frac{dT}{dz} < 0$, then $\frac{dC}{dz} < 0$ always (Region 1).
2. that if $\frac{dT}{dz}$ is large and positive, it is extremely <u>unlikely</u> (but not impossible) for $\frac{dC}{dz}$ to be negative. This would require disproportionately large <u>negative</u> salinity gradients. This, plus the preceding conclusion, implies that the conductivity gradient is generally similar to the temperature gradient, except possibly for small positive temperature gradients.
3. that if $\frac{dT}{dz}$ and $\frac{d\rho}{dz}$ are small, as in a well-mixed layer, the <u>sign</u> of $\frac{dC}{dz}$ may be indeterminate, but

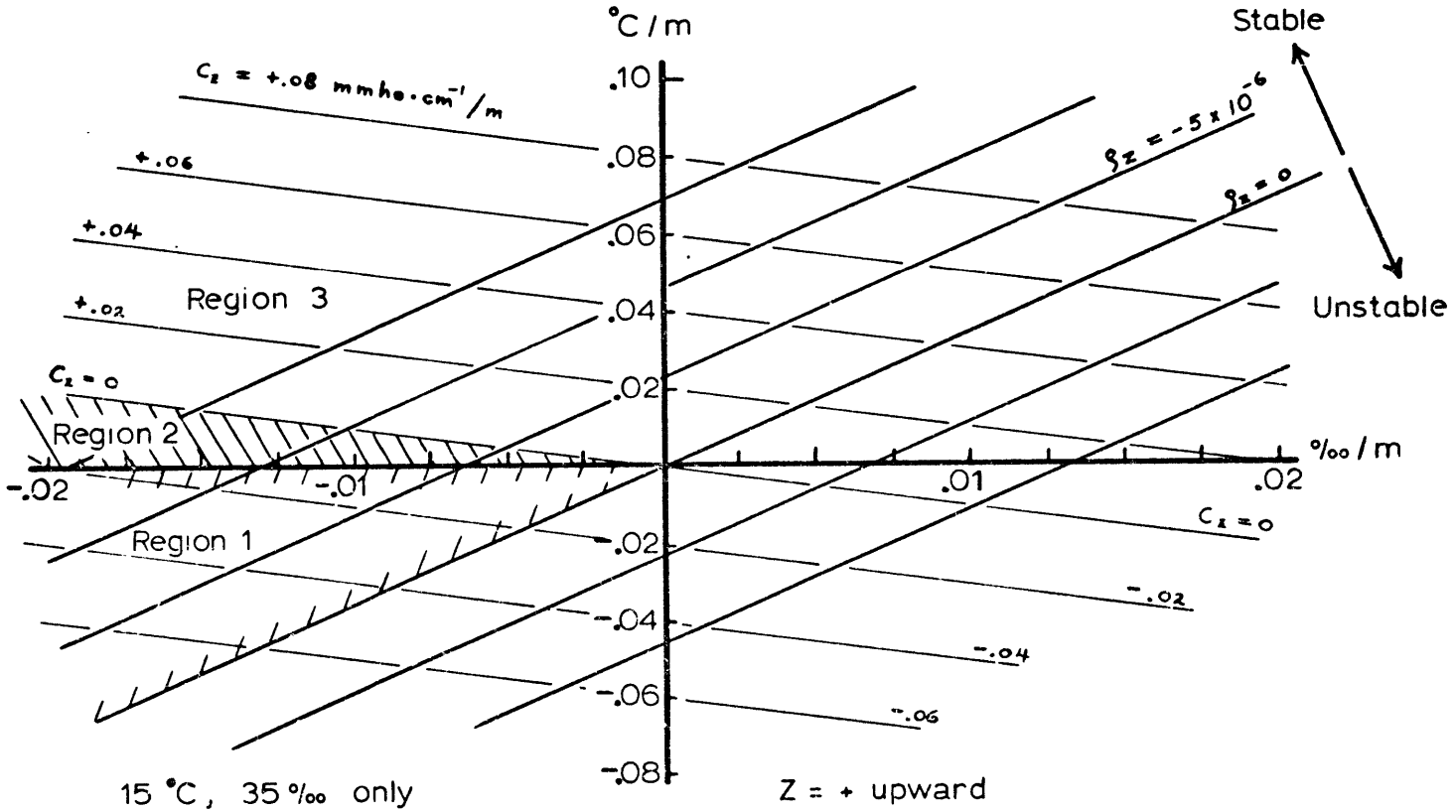

15 °C, 35 ‰ only

Z = + upward

Region 1: $T_z < 0$, $\rho_z < 0$

Region 2: $T_z > 0$, $C_z < 0$, $\rho_z < 0$

Region 3 $T_z > 0$, $C_z > 0$, $\rho_z < 0$

T_z , S_z Relationship

FIGURE 4.10

its magnitude is likely to be small; that is, $\frac{dc}{dz}$ may lie in Region 2 or Region 3, but in either case it will be small. Even with a small positive temperature gradient, however, it still requires a substantial salinity inversion to produce a negative conductivity gradient. No other investigator has ever observed such an inverse correlation between temperature and salinity gradients.

Consequently, we should expect the conductivity gradient to be similar in appearance to the temperature gradient, except that in mixed regions the conductivity gradient may occasionally become negative by a small amount, even though the temperature gradient remains positive. For a more quantitative illustration of the correspondence between temperature and conductivity structure, consider Figure 4.11 which shows a section of a microprofile record taken by another investigator in the Atlantic, southwest of Bermuda (28 02' N, 70 04' W) (Neil Brown, Private communication). The close relationship between temperature and conductivity variations on scales of meters is obvious. This particular record, however, shows no inversions in either temperature or conductivity. Note also that the temperature jumps appear to be smaller than those of Figures 4.2 - 4.5.

Finally, in order to verify that the peaks shown on the Cz records do fairly represent actual conditions in the ocean, consider Figures 4.12 and 4.13. The former is a section of the Cz versus Z data of Figure 4.9 (in the thermocline)enlarged along the depth axis to show greater detail; Figure 4.13 is a temperature

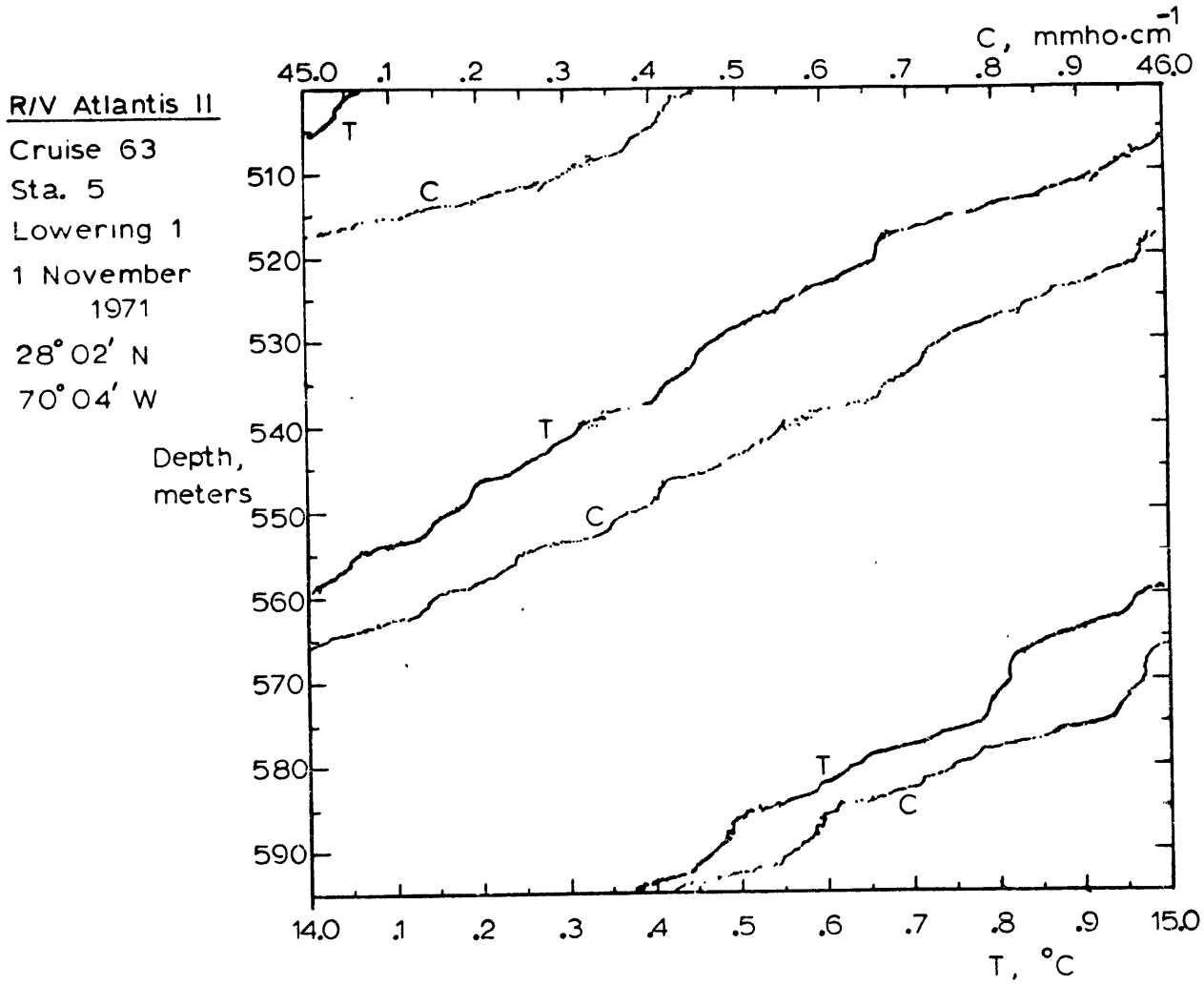

FIGURE 4.11 Neil Brown CTD Record, 28°02'N, 70°04'W (private communication)

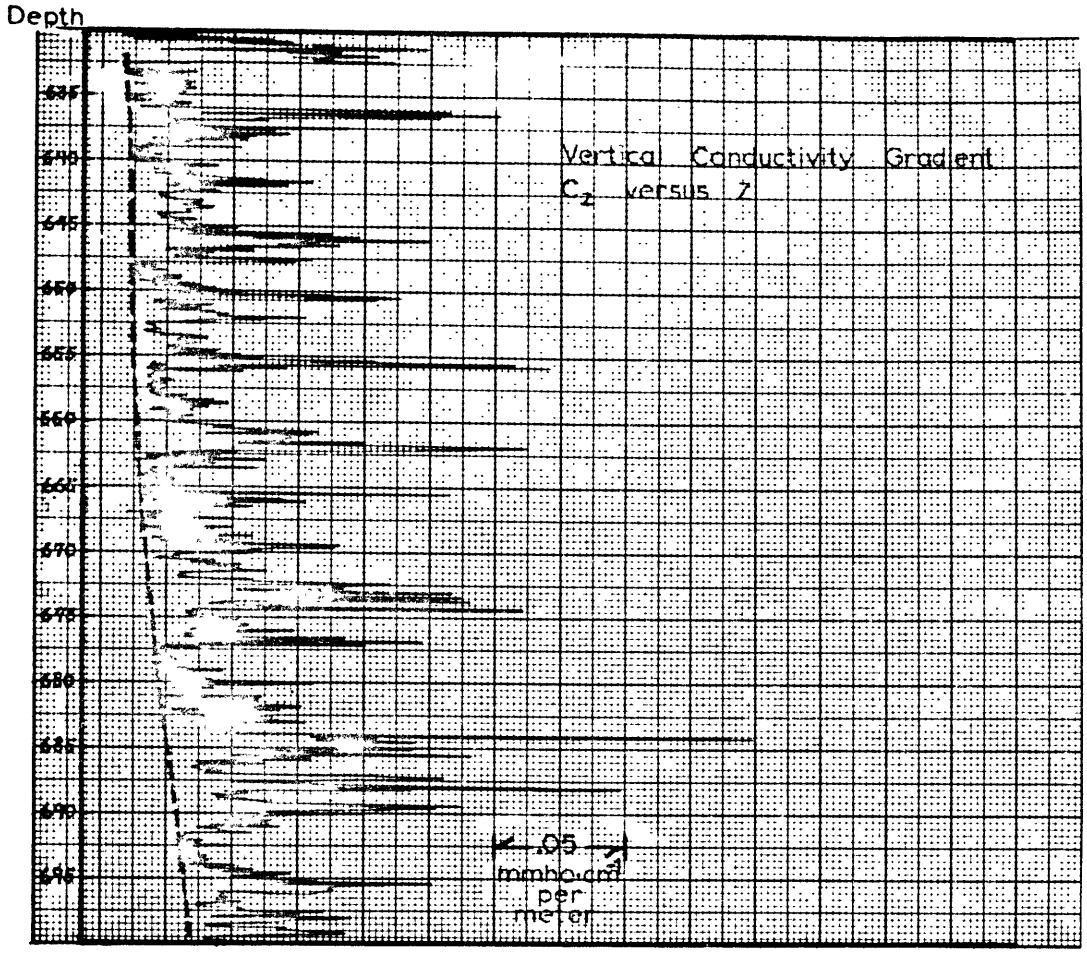

FIGURE 4.12 Section of Figure 4.9 (Lowering 13), enlarged to show greater detail.

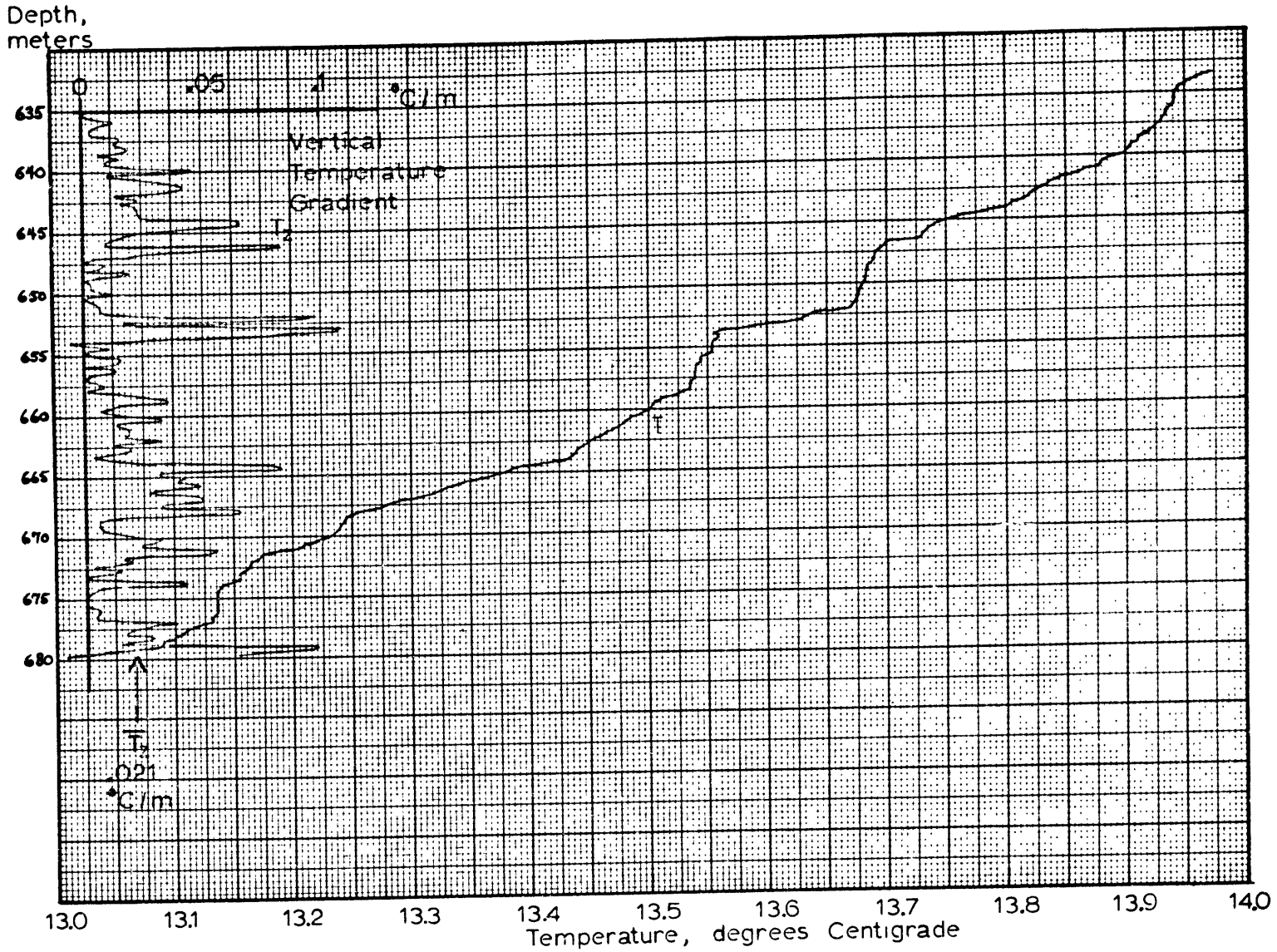

FIGURE 4.13 Neil Brown TD Record near Bermuda (32°10'N, 65°30'W) (private communication)

profile over a comparable depth interval, made in May, 1971, in the vicinity of Bermuda (32 10' N, 64 30' W) by the same microprofile device (conductivity data is not available) (Neil Brown, private communication). The gradient of temperature, computed on the basis of a 33 centimeter vertical separation, has also been plotted on Figure 4.13. Note that these two gradient plots are not supposed to be identical; indeed, the data were taken more than a year apart by entirely different instruments. They are, however, intended to show that the Cz trace is entirely consistent, both in amplitude and in the thickness of layers and interfaces, with previous observations from the same vicinity.

In conclusion, a simple rule may be stated for dealing with the Cz data, namely that the minima of Cz tend to lie on a slowly-varying line; and that line is the local origin of Cz within ±.01 mmho·cm.$^{-1}$ per meter. This rule is of great value when the data must be played back as a function of time, as for example in the analysis of C' signals. The Cz data thus corrected is entirely adequate to investigate possible correlations between the occurence of "bursts" of C' signal and the local vertical gradient; but it is not sufficiently accurate to enable the calculation of salinity gradient, even if the temperature gradient data (Tz) were perfectly reliable.

Since the salinity gradient cannot be calculated, there is no point in presenting both temperature and conductivity gradient data in later analyses. Cz and Tz may be regarded as equivalent insofar as this in-

vestigation is concerned. The choice of Cz as the preferred quantity is dictated, firstly, by the fact that the temperature gradient has short-term time-constant errors, and secondly, by the fact that the microstructure data (C') is itself a conductivity signal.

COMMENTS ON THE VERTICAL PROFILES

It is clear from the foregoing Cg, Tg, Cz, and Tz records that vertical "microstructure" is present at all depths in the ocean near Bermuda, if the definition of microstructure is taken to be the presence of thin "sheets" of high vertical gradient. But it is also clear that the 18-degree water is by far the least structured, in the sense that the sharp maxima in the gradient there are smaller in amplitude and much more widely spaced than in the water above or below. Typically, the gradient peaks in the 18-degree water are only one-third as great as those in the thermocline. On the other hand, the mean gradient in the 18-degree water is less than one-fifth of the mean gradient in the thermocline; thus the ratio of peak gradients to mean gradients is somewhat higher in the 18-degree water than in the thermocline.

The fact that the vertical profiles of temperature and conductivity are most steplike in the thermocline and the surface waters is not entirely in agreement with the conclusion drawn by Wunsch (1972). As the result of a hydrographic survey conducted in the Bermuda area, using an STD, Wunsch concludes that the 18-degree water contains more structure than the waters above or below.

Furthermore he asserts that a mechanical mixing process associated with the mean flow past the island is the source of the microstructure, and that this mixing process acts most strongly where the Richardson number is lowest, namely, in the 18-degree water on the side of the island that lies to the right of the current.

The reason for this discrepancy between our results and those of Wunsch is not entirely clear. There are probably several regimes for microstructure in the ocean, especially in the vicinity of islands; perhaps our data are typical of a different generating process than the one suggested by Wunsch. STD records from Wunsch's survey indicate that in regions other than those where mixing due to the mean flow is taking place, the conditions resemble ours much more closely; that is, the microstructure is less intense, and it is more evident in the thermocline than in the 18-degree water.

If this interpretation is correct, then it would appear that our experiment was carried out on a generally quiet side of the island. The observed microstructure may thus be regarded as the normal or undisturbed variety; it may be the result of the breaking of internal waves on the island slope, or it may be due to some other variety of mixing which is not directly related to the presence of the island.

The latter possibility deserves more attention. Wunsch's data indicates that in all cases the microstructure is more intense near the island than it is further out to sea. This implies that the island itself is somehow a cause of the microstructure. However, records from various deep-sea locations far from land

also show microstructure in the thermocline; an example has already been given in Figure 4.11. This figure, which shows vertical profiles of temperature and conductivity in an area 300 miles southwest of Bermuda, indicates that the vertical distribution of microstructure far from land is similar to the distribution found by the author near Bermuda, although generally less intense. Obviously, this microstructure cannot have been advected all the way from the nearest land; the process which generates it must be active everywhere.

Thus, on the basis of the evidence from various types of vertical profiles, it seems that microstructure is normally present in the ocean, especially in the thermocline; furthermore this type of microstructure tends to become more intense as an island is approached. The most likely interpretation of this is, not that the island is the cause of the microstructure, but rather that the process which generates the microstructure is merely strengthened near the island. Turbulence due to the breaking or shear of internal waves is certainly a likely suspect: it could be active everywhere; and it would be intensified over an island slope.

Of course, microstructure due to other causes may be present in addition to this observed "background" microstructure. Salt-finger convection may be active; and in the vicinity of islands and shorelines there is probably strong mixing due to the dynamics of flows around obstacles. This latter type of mixing, being mostly due to large-scale shear, will tend to occur in weakly stratified parts of the water column.

CHAPTER V

HORIZONTAL MICROSTRUCTURE MODELS

In order to help determine the cause or causes of the bursts of horizontal microstructure, we will analyze selected individual bursts on the basis of a series of models. We wish to establish the extent to which each model is applicable, if at all; and we must calculate the important parameters regarding the intensity of vertical mixing during such events. Inevitable, this model-matching technique involves a certain amount of sorting and categorizing of the bursts; but the bulk of the statistics regarding the occurence of events is reserved for Chapter VI: Significance of the Microstructure.

The analysis of individual bursts relies heavily on spectral analysis. Therefore a discussion of the spectral analysis method is given in Appendix 4. Particular attention is given there to the discussion of the noise spectra, and the error limits of the analysis.

A. MODEL ONE: PASSIVE LAYERS

ANALYSIS OF C' BURSTS ON THE BASIS OF HORIZONTAL LAYERS

In this section we shall postulate the first (and simplest) of a series of models or theories to account for the "bursts" of high-frequency signal that occur on the C' record. We shall test this model for consistency with the data. It will be shown unequivocally that this model is not valid.

This model assumes that the C' signals are caused

by the quasi-steady vertical motion of the instrument through a series of thin, gravitationally-stable layers. This is essentially a passive explanation of the bursts of C' signal: the water need not be in motion, and no dynamic process is involved. The ocean is assumed to resemble a stack of pancakes through which the probe moves at a shallow angle. We are not concerned with the origin of such layers.

The C' signal is the total time derivative of the electrical conductivity seen by the moving probe, which may be written thusly:

$$\frac{dC}{dt} = \frac{\partial c}{\partial t} + \vec{v} \cdot \nabla c$$

$$c = c(x, y, z, t)$$

where $\bar{v}$ is the velocity of the instrument, x and y are horizontal coordinates, and z is a vertical coordinate (positive upward).

In all that follows we shall assume $\frac{\partial c}{\partial t} = 0$, i.e., that conductivity in the ocean does not change at any fixed location during the time interval of interest. Moreover, we shall assume that the conductivity field is horizontally isotropic, and the X coordinate will be taken to represent the direction of forward motion of the instrument. Thus the C' expression may be simplified, becoming:

$$\frac{dc}{dt} = \vec{v} \cdot \nabla c = \frac{\partial c}{\partial x} \cdot \frac{dx}{dt} + \frac{\partial c}{\partial z} \cdot \frac{dz}{dt}$$

This model assumes that $\frac{\partial c}{\partial x} = 0$ and that $\frac{\partial c}{\partial z} = W$ is constant over the interval of the burst.

The actual C' signal as it is available for anal-

ysis contains the above information plus noise and offset. The first order of business therefore is to determine the location of the true zero line of C'. To do this we make use of the Cz signal and the vertical velocity:

$$\left.\frac{dc}{dt}\right|_{vert.} = \frac{dc}{dz} \cdot \frac{dz}{dt} = C_z \cdot W$$

The Cz signal is relatively slowly-varying compared to C', so in order to compare $\frac{dc}{dt}$ as seen by the microstructure probe with the $\frac{dc}{dt}$ calculated from the gradient sensor, it is necessary to filter the C' signal very heavily. Moreover the C' sensor does not have much sensitivity at low frequencies, so that it is necessary to select a C' signal which occurred in a region of high vertical gradients and/or high vertical velocity.

Figure 5.1 illustrates the calculation. The C' signal, played back as a function of time, is on the left. The same signal, filtered and amplified, is next on the right, followed by Cz and Z respectively. In this case a large peak in Cz occurs which is matched by a similar peak on C'. The vertical velocity is 29 cm/sec. (upward); the rate of change of conductivity from valley A' to peak B' is calculated from Cz to be 190 μmho$\cdot$cm.$^{-1}$ per second. The same variation is clearly visible in the filtered C' signal (note, however, the polarity inversion); here the change can be read off as 350 μmho$\cdot$cm.$^{-1}$ per second. The discrepancy between the amplitudes is due to the fact that the interfaces in question are thinner than the 30 centimeter spacing between the heads of the gradient sensor; this

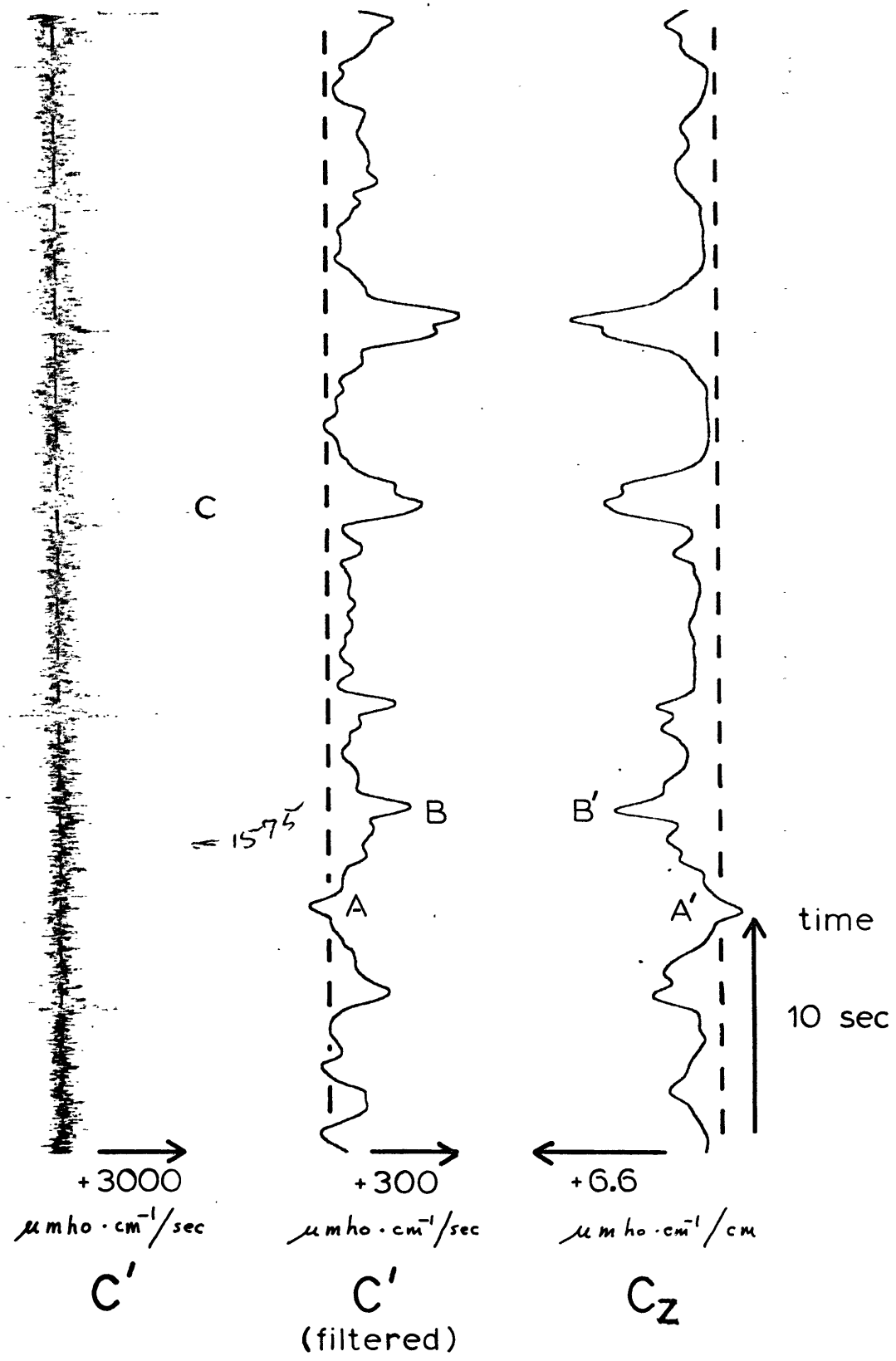

FIGURE 5.1 Section of Lowering 10 used to establish zero line of C'.

results in too low an output on Cz in terms of gradients. For example, it may be seen by inspection of the filtered C' trace in Figure 5.1 that the entire peak labeled B is over and done with in about one second (30 centimeters); the average value of this gradient over 30 centimeters, which is the quantity measured by the Cz sensor, will clearly be less than the peak value.

This exercise demonstrates in essence that the vertical gradient of conductivity as measured by the Cz sensor is also seen by the C' sensor; and since the zero of Cz is known, we can set the zero of C' to correspond. Such a zero line has been drawn on both C' records in Figure 5.1.

It is abundantly clear from the placement of this zero line that during the burst $\frac{dc}{dt}$ changes sign repeatedly and by a large amount. In fact, the zero line is buried in the background noise. Hence, we may conclude that any burst of signal on the C' record would represent micro-scale inversions in conductivity. The amplitude of such inversions is large: for the burst shown in Figure 5.1, labeled C, the peak amplitude of C' expressed as a verticle gradient is ± 3.4 mmho·cm.$^{-1}$ per meter. Positive and negative vertical conductivity gradients of this magnitude superimposed on a mean vertical gradient of .05 mmho·cm.$^{-1}$ per meter would be quite extraordinary. Certainly, such massive conductivity inversions would require ridiculously large salinity and/or temperature inversions. Intuitively, very thin stably-stratified layers having major inversions in temperature and salinity would not be stable in the long run anyway. Molecular diffusion would wipe

out the temperature differences between adjacent layers very rapidly, thereby destroying the stratification and causing the layers to break up and seek new levels.

In conclusion, it has been established that the bursts of C' signal cannot be explained as stable horizontal layers intercepted by the vertically-moving probe. These bursts must therefore be due to some dynamically-active convection process. Several different dynamic models will be examined in succeeding chapters.

B. MODEL TWO - SALT FINGERS

In this section we shall investigate the possibility that at least some of the bursts may be due to salt finger convection. The model we postulate is that of salt fingers across a sharp interface between two relatively mixed layers. This is not the only salt finger model that we could postulate; salt fingers are not constrained to occur only between mixed layers. But one of the original objectives of this project was to determine to what extent salt fingers are responsible for the creation and maintenance of the layered structure; hence it is most important to look for salt fingers on well defined interfaces. It is also easier to check for consistency between the data and the theory if the event is isolated.

Salt fingers are unique among oceanic phenomena in that they must have a bandlimited spectrum in wavenumber space. The convection depends upon the lateral diffusion of heat from the hotter, saltier, downward moving fingers to the cooler, fresher, upward moving ones; and if the system is to be quasi-stable, the diameter of the fingers must be about equal. This has been demonstrated repeatedly in laboratory experiments (Shirtcliffe and Turner, 1970), where the fingers appear to form in clumps; within each clump they have a roughly square planform, as viewed from above. Therefore they will have a horizontal spatial spectrum which is strongly peaked.

The horizontal spectrum which results from towing a probe through a salt finger field at a random angle

will be broader and less peaked than the intrinsic salt finger spectrum, but it will be bandlimited nevertheless. Thus the existence of a significant spectral peak above the ordinary background noise is strong evidence of salt fingers.

The analysis for salt fingers in this model has been done as follows. First, the records have been searched for C' bursts which are correlated with isolated positive peaks in the vertical gradient, Cz. These are denoted as "class A" events; there are 24 altogether, out of more than 300 separate bursts. Of this 24, 5 are in the surface water, above 200 meters (the surface water is confused and difficult to analyze, and there may actually be more class A events there). Of the 19 class A thermocline events, the majority are in the immediate vicinity of other, larger events. Only a few events could truly be described as occurring on an interface between two layers.

Secondly, all of these class A bursts (as well as other interesting events) have been subjected to spectral analysis. Those class A bursts whose spectrum exhibited a strong peak were considered to be possible salt fingers. There were only 5 which met this criterion.

Lastly, these 5 events were then tested for internal consistency and compared with salt finger theory, using the auxiliary data such as Cz. An example of such an analysis is given below.

First, in Figures 5.2 and 5.3, we see the C' signal as a function of time. Also shown are the vertical gradient of conductivity, Cz, and the depth, Z. The

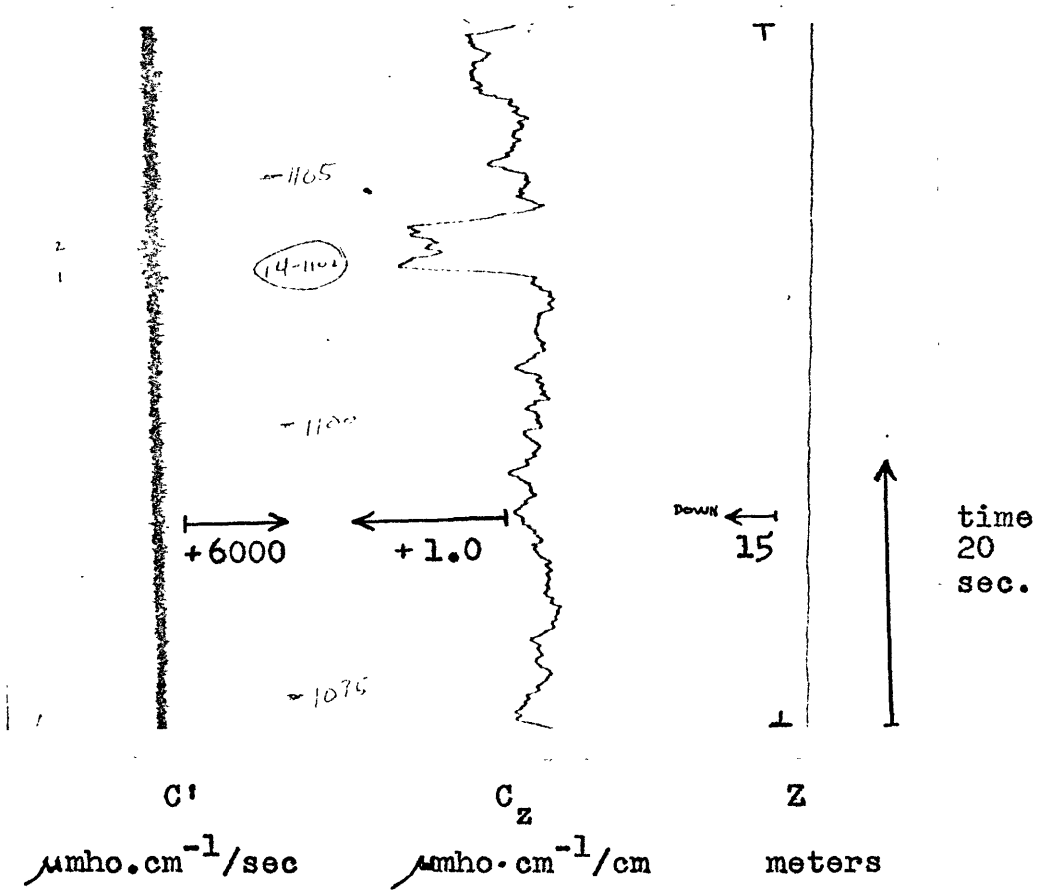

Depth of this event: 600 meters ± 5 meters.

Speed: 116 ± 10 cm/sec.

Vertical velocity: 18 cm/sec (up)

FIGURE 5.2 Time record, Event # 14 - 1102.

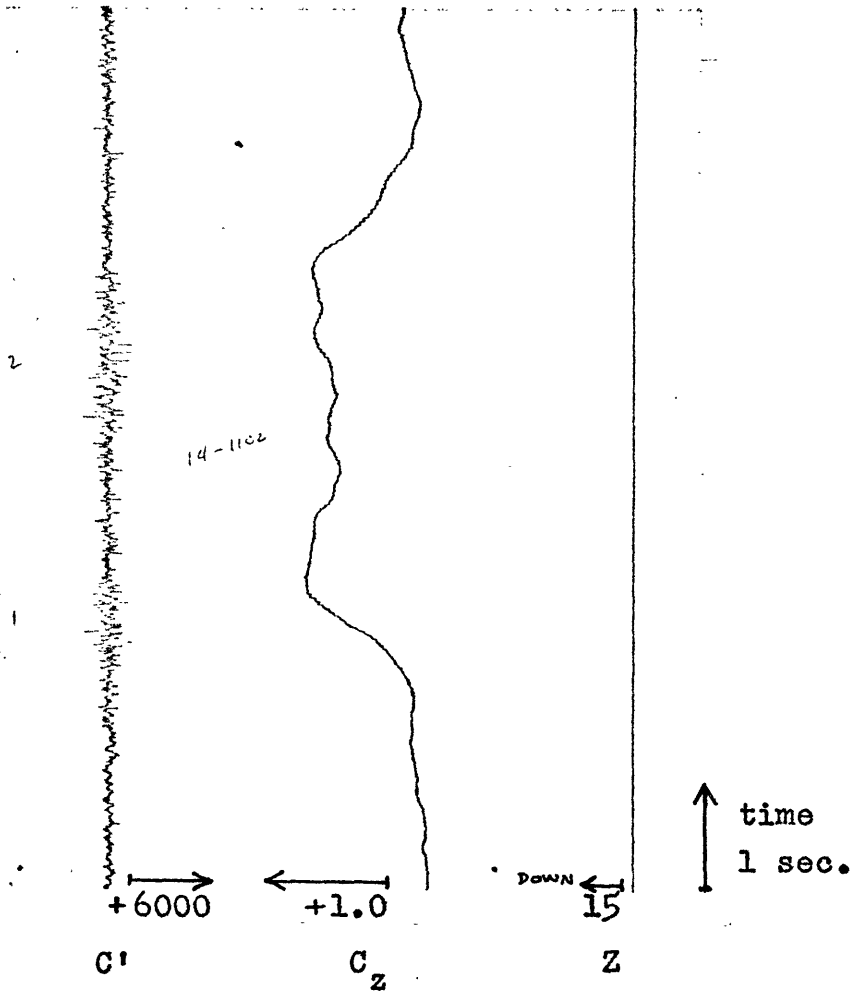

FIGURE 5.3 Detail of FIGURE 5.2, enlarged along time axis.

velocity signal, not shown, demonstrated that the instrument was gradually speeding up during the event. Actually, Figure 5.2 shows two quasi-separate bursts encompassed by the single peak in Cz. The spectrum of burst #14 - 1102 - 2 is shown in Figure 5.4. The information derived from all sources is summarized in Table II.

COMPARISON WITH THEORY

The first calculation is that of finer diameter,[9] which is given by the expression: (Stern, 1960)

$$\ell = \pi\sqrt{2}\left(\frac{\nu K_T}{g\alpha \bar{T}_z}\right)^{1/4}$$

where α is the thermometric coefficient of expansion of sea water; ν and K_T are the kinematic molecular viscosity and thermal diffusivity of sea water, respectively; and $\bar{T}_z$ is the average temperaturegradient across the interface.

We need to know $\bar{T}_z$, but we have only $\bar{C}_z$ available. However, if the water is stable, the ratio $\beta \frac{dS}{dz} / \alpha \frac{dT}{dz}$ is always less than unity. In the thermocline near Bermuda the average value of this ratio is 0.55. It may easily be shown that in consequence, any particular conductivity gradient in the thermocline is composed of about 6 parts temperature effect to 1 part salinity effect; that is, a $\bar{C}_z$ of 1 μmho$\cdot$cm^{-1}/cm <u>most likely</u> corresponds to a $\bar{T}_z$ of 0.86 x 10^{-3o}C/cm.

In this case $\bar{C}_z$ is 0.83 μmho$\cdot$cm^{-1}/cm. Therefore we should expect $\bar{T}_z$ = 0.71 x 10^{-3o}C/cm. This calculation is crude, but since all the parameters enter as

TABLE II

ANALYSIS OF POSSIBLE SALT FINGER EVENT

Lowering 10

3 July, 1972

Event # 14-1102-2

Time: 1558 hrs. Atlantic Standard Time (Bermuda Local Time)

FROM RECORD AS FUNCTION OF TIME:

Depth: 600 meters $\pm$ 5 meters

Vertical velocity: 18 cm/sec (upward) $\pm$ 1 cm/sec

Speed: 116 cm/sec $\pm$ 10 cm/sec

Burst #14-1102-2 only:

Maximum Amplitude of Burst, peak-to-peak: 26 μmho$\cdot$cm^{-1}/cm

Duration of Burst: 1 second

Number of cycles invelved in spectral analysis: about 20

Vertical Gradient Peak:

Amplitude: +0.83 μmho$\cdot$cm^{-1}/cm

Thickness, corrected for 30 cm vertical separation of sensor heads: 60 cm

Conductivity Differnece across interface: 50 μmho$\cdot$cm^{-1}

FROM POWER DENSITY SPECTRUM

Spectral Peak: centered at 0.21 cycles/cm

Bandwidth: approx. 0.16 - 0.27 cycles/cm

Amplitude: approx. $220 \dfrac{\left(\dfrac{\mu\text{mho-cm}^{-1}}{\text{cm}}\right)^2}{\text{cycle/cm}}$

Total Energy in peak: $20 \left(\dfrac{\mu\text{mho-cm}^{-1}}{\text{cm}}\right)^2$

RMS Horizontal Gradient at 0.21 cycle/cm: $4.47 \dfrac{\mu\text{mho}\cdot\text{cm}^{-1}}{\text{cm}}$

Calculated comductivity amplitude, peak-to-peak, at 0.21 cycles/cm: 9.6 μmho$\cdot$cm^{-1}

Cell size or finger diameter: centered on 2.4 cm

Bandwidth: 1.85 - 3.1 cm

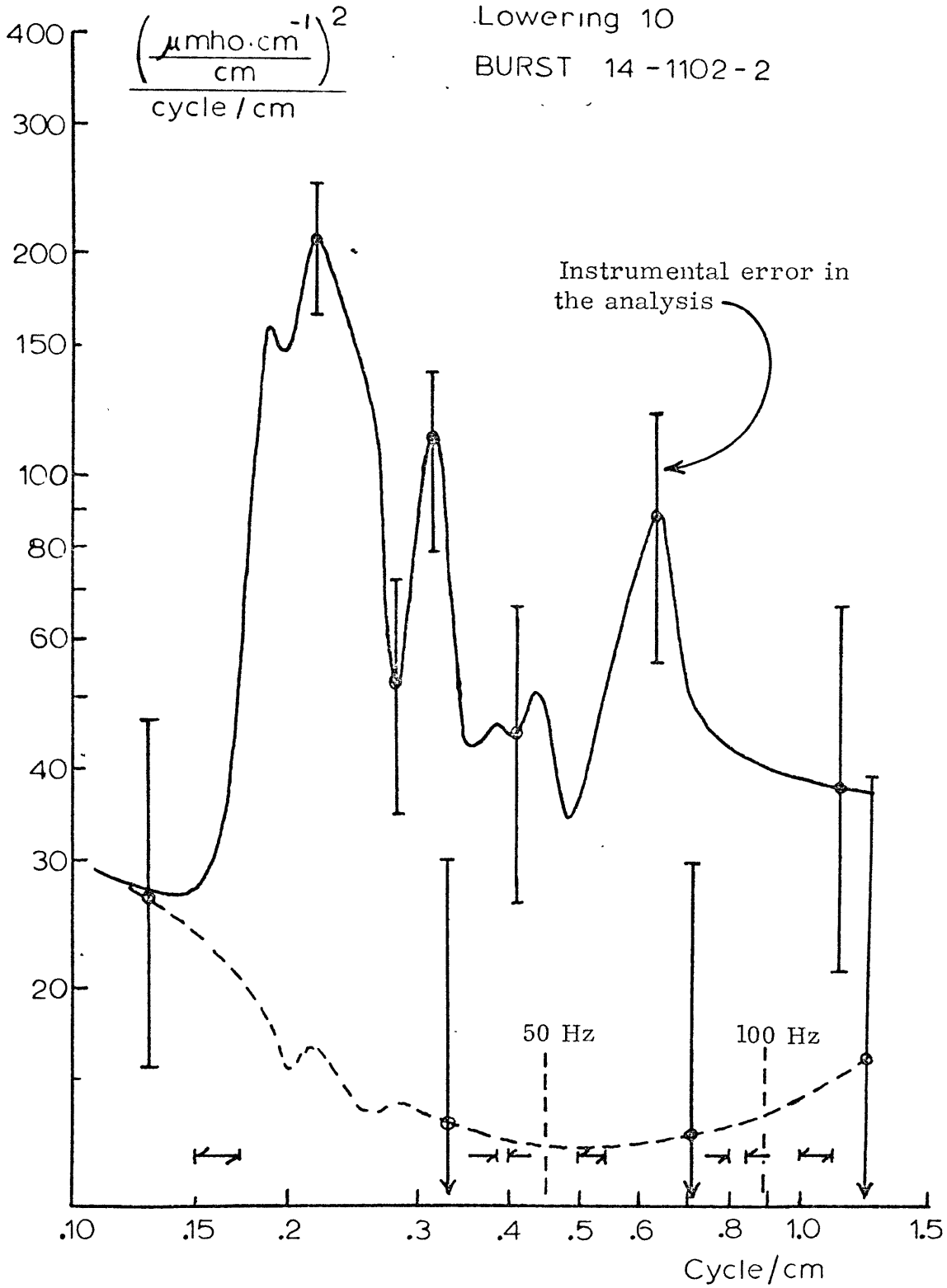

FIGURE 5.4 Conductivity Gradient Spectrum, Event # 14 - 1102 -2

The small arrows near the bottom of the figure represent the resolution bandwidth.

the fourth root, it doesn't really matter. Assuming $\nu = 10^{-2}$ cm^2/sec and $K_T = 10^{-3}$ cm^2/sec, we find that $\ell = 2.3$ cm. The agreement with the observed value is startlingly good.

The agreement between the calculated and observed amplitudes of the conductivity difference between fingers is not quite as good. With 50 μmho·cm^{-1} conductivity difference across the interface, there should be about 7 μmho·cm^{-1} difference due to salinity, by the above reasoning; this difference should appear between the fingers as well, since salt diffusion is negligible. Thus, unless <u>all</u> of the temperature difference should diffuse away laterally, we should see more than the observed 9.6 μmho·cm^{-1} difference between fingers. In fact, we should expect to see about 25 μmho·cm^{-1} between fingers, considering that there will be a temperature difference between fingers as well.

But the calculated amplitude is derived from, and is very sensitive to, the thickness of the gradient region. This thickness was calculated simply by multiplying the duration of the Cz peak by the vertical velocity. Clearly, however, if the interface is sloped so as to parallel the path of the instrument somewhat, the apparent duration of the Cz peak, and hence the apparent thickness, will be greatly increased. The instrument was ascending in this case on a 1:10 slope; consequently, if the gradient region is sloped at only 1:16, the Cz peak might appear to be 2.5 times thicker than it actually was. If this were the case, then the conductivity difference across the interface would be

only 20 μmho cm^{-1}, which would be consistent with the observed salt finger amplitude. The finger diameter seen by the instrument would be affected but little by these slopes. The ratio of finger length to diameter would be about 10.

An isopyncnal slope of 1:16, due to the presence of internal waves, is entirely reasonable. Garrett and Munk (1972) assert, on the basis of their universal horizontally isotropic energy spectrum, that the typical R.M.S. slope due to internal waves is 1:38. The peak slope due to random superposition of waves may be much higher. This line of argument, while certainly not conclusive, does indicate that the apparently small amplitude of the fingers need not be a serious flaw.

VERTICAL TRANSPORT DUE TO FINGERING

We will now estimate the vertical flux of salt by several methods. To do so we must make certain assumptions regarding the distribution of temperature and salinity. Let us suppose the observed conductivity differences between fingers, ΔC, which equals 9.6 μmho cm^{-1}, is composed of 2 parts temperature to 1 part salinity; for this case, that amounts to $\Delta S_1 = .0032$ 0/00, $\Delta T_1 = .0064^{o}C$. This is based upon the earlier assumption that for vertical gradients the ratio of temperature to salinity gradient is about 6:1, and further assuming also that only one third of the layer-to-layer temperature difference appears between fingers. Then we can calculate the amplitude of the vertical component of velocity in the fingers, after Stommel and

Fedorov (1967):

$$w_0 = \frac{g \Delta\rho \, l^2}{\rho_0 \nu \, 4\pi^2} = .011 \text{ cm/sec}$$

This result, however, is sensitive to the temperature and salinity differences assumed. The Reynolds number of this flow is about 3, so that the assumption of laminar flow is justified. The flux of buoyance due to salt transport may then be calculated as:

$$\beta F_{s_1} = \beta \Delta S \cdot \frac{w_0}{2} = 1.35 \times 10^{-8} \text{ cm/sec}$$

On the other hand, we can use the results of Turner (1967), in which he finds a flux law of the form

$$\beta F_{s_2} = C (\beta \Delta S_2)^{4/3}$$

where ΔS_2 is the salinity difference <u>across</u> the interface, and where $C \cong 10^{-1}$ by experiment. Using the same $\Delta S = .0032$ 0/00 as before, we find that $F_{s2} = 0.34 \times 10^{-8}$ cm/sec. Neither of these calculations is very reliable, however; Turner's experiments do not extend to high enough values of $\alpha \Delta T / \beta \Delta S$; and our value is very sensitive to the velocity calculation.

For comparison, if we assume that the entire conductivity difference between the fingers is due to salt, then $S = .01$ 0/00 . F_s calculated by the first method is 42×10^{-8}, and by method of Turner is 1.5×10^{-8}. These numbers demonstrate more than anything else how desirable it would have been to have measured the temperature field as well as the conductivity field!

The flux of buoyancy associated with heat may be calculated in the same way as the salt buoyancy flux.

We assumed $\Delta T = .0064$ C between fingers, and using $\alpha = 2.2 \times 10^{-4}/^{\circ}C$, we have

$$\alpha F_T = \alpha \Delta T \cdot \frac{w_o}{2} = .775 \times 10^{-8} \text{ cm/sec}$$

Thus the ratio of heat flux to salt flux is 0.57, which is not far at all from Turner's (1967) value of 0.56. Clearly, however, we can achieve nearly any desired value of this ratio merely by postulating a slightly different balance between ΔS and ΔT in the fingers; the point is only that a reasonable assumption regarding ΔS and ΔT does not lead to an inconsistency.

The simple molecular diffusion of salt across an interface 20 cm thick, having a salinity difference of .004 0/00, is

$$\beta F_{S_{MOL.}} = K_S \beta \frac{\Delta S}{h} = 2.6 \times 10^{-12} \text{ cm/sec}$$

EVALUATION OF THE SALT FINGER MODEL

The foregoing analysis has demonstrated that for this particular event, a salt finger model is entirely reasonable and consistent. The event chosen for this analysis, however, is the clearest such case of the five (out of 300) which were selected as possible salt fingers. From this we conclude: (1) that the instrument is capable of detecting, and the analysis technique is capable of resolving, salt fingers in the ocean; (2) that salt fingers are so rare in the thermocline near Bermuda that they must represent only a tiny

fraction of the vertical mixing. Strictly speaking, of course, the latter conclusion refers only to the thermocline near Bermuda, at the time the experiment was done; but insofar as we believe conditions at Bermuda to be typical of other parts of the ocean, we may apply these results more widely. It should be noted in this connection that some investigators, notably Cooper and Stommel (1968), have observed a far more regular layered structure in the thermocline near Bermuda than we did. It is possible that sometimes a different mixing regime is set up, and salt fingers might then be important. Further field work in a regularly-layered structure would be necessary to resolve this question.

C. MODEL THREE - TURBULENCE

A turbulent model is essentially a statistical model. Rather than searching through the data for individual events having distinctive features, as was done for the salt finger model, we now wish to look at the general spectral shape of a large class of events. We expect that no two bursts will be exactly alike; and we will not attach significance to the details of any individual spectrum. We do expect, however, that turbulent bursts should generally have wideband gradient spectra.

A PRIORI EXPECTATIONS FROM THEORY

According to the universal similarity hypothesis of Batchelor (1959), the turbulent power density spectrum of a weakly diffusive scalar property such as tem-

perature (or conductivity) can be divided into three regions. If ε is the average specific energy dissipation rate (the rate at which kinetic energy is being converted to heat), and if ν is the kinematic viscosity, and K the kinematic diffusivity, then Kolmogorov's wavenumber is defined to be:

$$k_K = (\varepsilon/\nu^3)^{1/4} \qquad \text{radians/cm}$$

For wavenumbers less than k_K the power density spectrum of the scalar field should follow a (-5/3) power law, thusly:

$$\varphi_T(k) = B\chi\varepsilon^{-1/3} k^{-5/3} \qquad \frac{(^\circ C)^2}{\text{cycle/cm}}$$

where B is a universal constant, and χ is the average temperature dissipation rate,

$$\chi = 2K\overline{(\nabla T)^2}$$

This is the so-called inertial subrange of turbulence. Clearly, this spectrum can be expressed in terms of gradients:

$$\varphi_{T_z}(k) = k^2 \cdot \varphi_T(k) = B\chi\varepsilon^{-1/3} k^{+1/3} \frac{\left(\frac{^\circ C}{cm}\right)^2}{\text{cycle/cm}}$$

If we define Batchelor's wavenumber as:

$$k_B = \left(\frac{\nu}{\kappa}\right)^{1/2} \cdot k_K = \left(\frac{\varepsilon}{\nu}\right)^{1/4} K^{-1/2} \qquad \text{radians/cm}$$

then according to Batchelor's theory, the spectrum falls off very rapidly for wavenumbers above k_B. This cutoff, which is associated with the dominance of diffusive processes on small scales, should cause the spectrum to go as (Grant, Hughes, Vogel, and Moilliet, 1968)

$$\varphi_T(k) \longrightarrow k^{+1} \cdot e^{-ak^2}$$

In terms of gradients, this region of the spectrum goes as

$$\varphi_{T_z}(k) \longrightarrow k^{+1} \cdot e^{-ak^2}$$

that is, it must go to zero eventually.

In between k_K and k_B the spectrum of temperature should show a k^{-1} dependence; this region of the spectrum arises because for water the Prandtl number $P_r = \frac{\nu}{K} \cong 7$ is not unity. Viscosity begins to cut off the motion on scales longer than the temperature cutoff scale; this means that temperature fluctuations will extend to higher wavenumbers than velocity fluctuations, before they too are cut off by diffusion. In this region the spectrum of the gradient should go as k^{+1}.

Cox, Hacker, Johnson, and Osborn (1969) estimate the diffusive cutoff, k_B^{-1}, to be typically 1.6 cm in the thermocline, based upon a dissipation rate, $\epsilon = 10^{-5}$ ergs/g.sec. On the same basis, Kolmogorov's scale, k_K^{-1}, is estimated to be 4.8 cm. Both of these scales are within the resolution of our conductivity microstructure probe, although it cannot resolve scales much smaller than k_B^{-1}.

CAVEATS

The foregoing discussion has been based upon the assumption of three-dimensional isotropy, which is probably not valid in a stratified ocean. Certainly the"inertial subrange" of the spectrum, if it exists at

all, must be valid only for wavenumbers greater than a typical buoyancy wavenumber, k_o , defined as:

$$k_o = \left(\varepsilon/N^3\right)^{-1/2}$$

where N is the Brunt-Vaisala frequency

$$N = \left(\frac{-g}{\rho}\frac{d\rho}{dz}\right)^{1/2}$$

In fact, however, such a length scale can easily be about the same as the Kolmogorov scale, particularly if one uses locally high values of N . Thus it is doubtful whether an inertial subrange can exist at all in the vicinity of high vertical gradients in the thermocline. Qualitatively, we would expect horizontal isotropy; but the stratification would tend to suppress vertical motions. A purely horizontal spectrum would no doubt differ greatly from a vertical spectrum, although both should show a sharp cutoff at k_B .

The matter is further complicated by the presence of salt, whose molecular diffusivity is nearly two orders of magnitude smaller than the thermal diffusivity. Thus, if the salt were merely a trace element, having no influence upon the dynamics of the process, we should expect to find a diffusive cutoff in the salt spectrum at a wavenumber of

$$k_{B_{SALT}} = \left(\varepsilon/\nu\right)^{1/4} K_s^{-1/2}$$

which is almost 10 times higher than the temperature cutoff wavenumber. This would correspond to scales of 0.16 cm. for salt. However, neither salt nor heat is a trace element; both affect the density and hence the

dynamics of mixing. We expect that at very high wavenumbers, where the temperature variations have diffused away, the salt variations will strongly influence the dynamics. The remnant salt variations will cause renewed density variations on those small scales, so that the water will tend to restratify itself instead of breaking up into infinitesimal filaments. What effect this has on the spectra of temperature and salinity is not clear. One might expect that since the salt tends to restore orderliness in the fluid, the spectrum would not extend to wavenumbers as high as it would if the salt were merely a tracer. This conclusion is highly speculative, however, since very little work has been done on the problem of turbulence in fluids as complex as sea water.

The spectral shape of a particular mixing event must also depend very strongly on its history. Mixing is intermittent in the ocean; we do not expect a statistically-stationary cascade of energy from lower to higher wavenumbers, as the theory assumes. "Older" turbulence, for which the driving shear has weakened, may also have greater vertical anisotropy than newly-minted turbulence.

As a final disclaimer, it should be remembered that the instrument moves vertically as well as horizontally, and at different rates. The spectra will contain contributions from horizontal and vertical conductivity variations; and if the statistics of the process do indeed differ from vertical to horizontal, the spectrum will be smeared.

REPRESENTATIVE SPECTRA

Three examples of possible turbulence are illustrated in Figures 5.5 through 5.12. For each case the burst is shown both as a function of time, together with the vertical conductivity gradient, and as a power density spectrum of the horizontal gradient of conductivity.

The similarity of the three events is unmistakable, even though the spectra are not identical in detail. Moreover, the difference between these spectra and that of the possible salt fingers, Figure 5.4, is very striking; the turbulent bursts have much more energy at higher frequencies. The energy in all three cases appears to peak somewhat between k=.5 and k=1. At higher wavenumbers it appears to decline.

Figure 5.13 is a composite gradient spectrum, made by graphically averaging the above three spectra. It shows more clearly the rolloff at wavenumbers above 0.5-0.6. Shown for comparison are the $k^{+1/3}$ line, which represents theoretically the spectral shape in the inertial subrange, and the k^{+1} line, which represents the viscous-convective subrange. The spectra are not inconsistent with these lines, but the agreement is not overwhelming.

If the rolloff at wavenumbers above 0.5-0.6 cycles/cm is assumed to be the diffusive cutoff, then we can calculate the energy dissipation from the formula for Batchelor's wavenumber, i.e.:

$$\varepsilon = \nu K^2 k_B^4$$

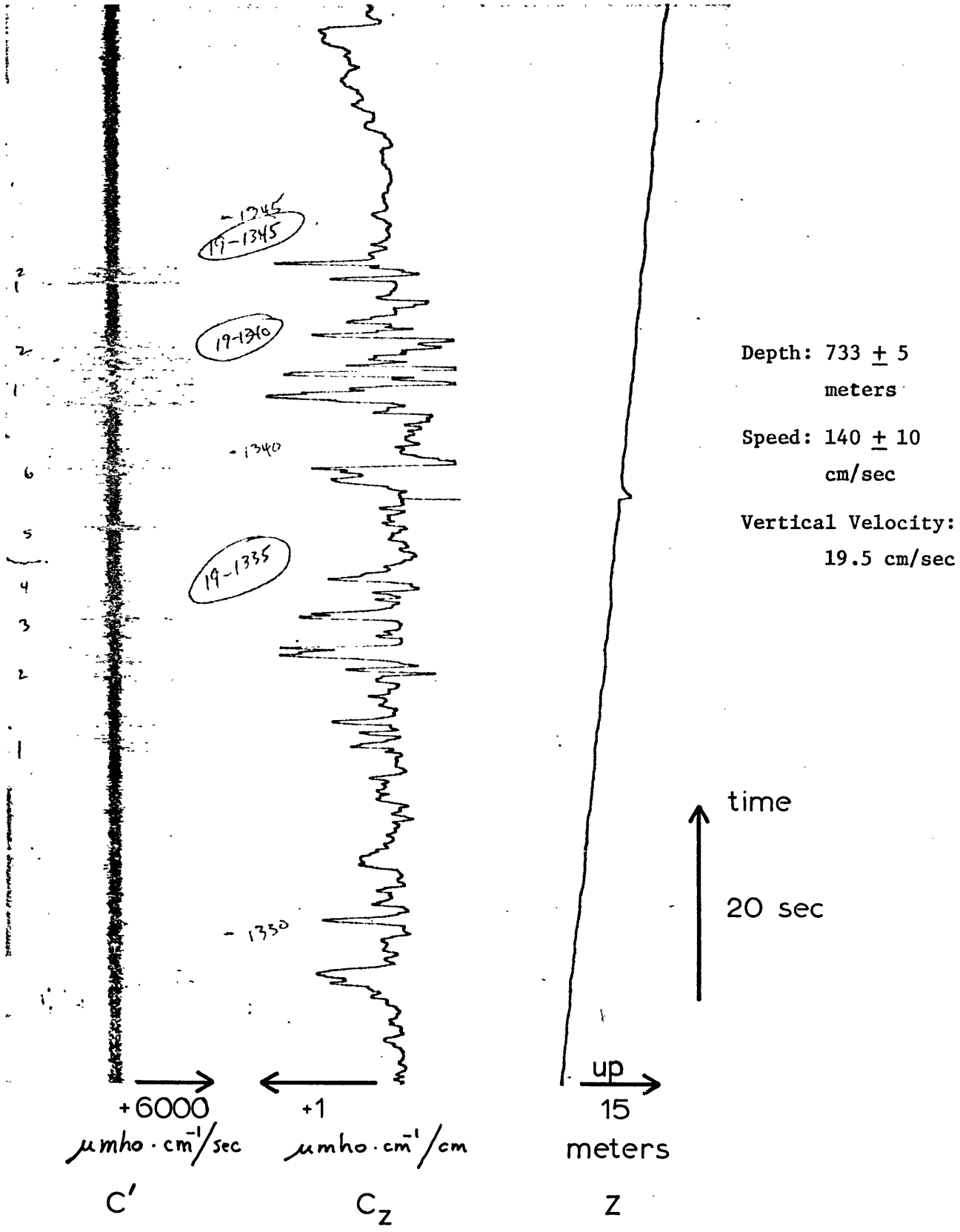

FIGURE 5.5 Time Record, Event # 19 - 1340, Lowering 13.

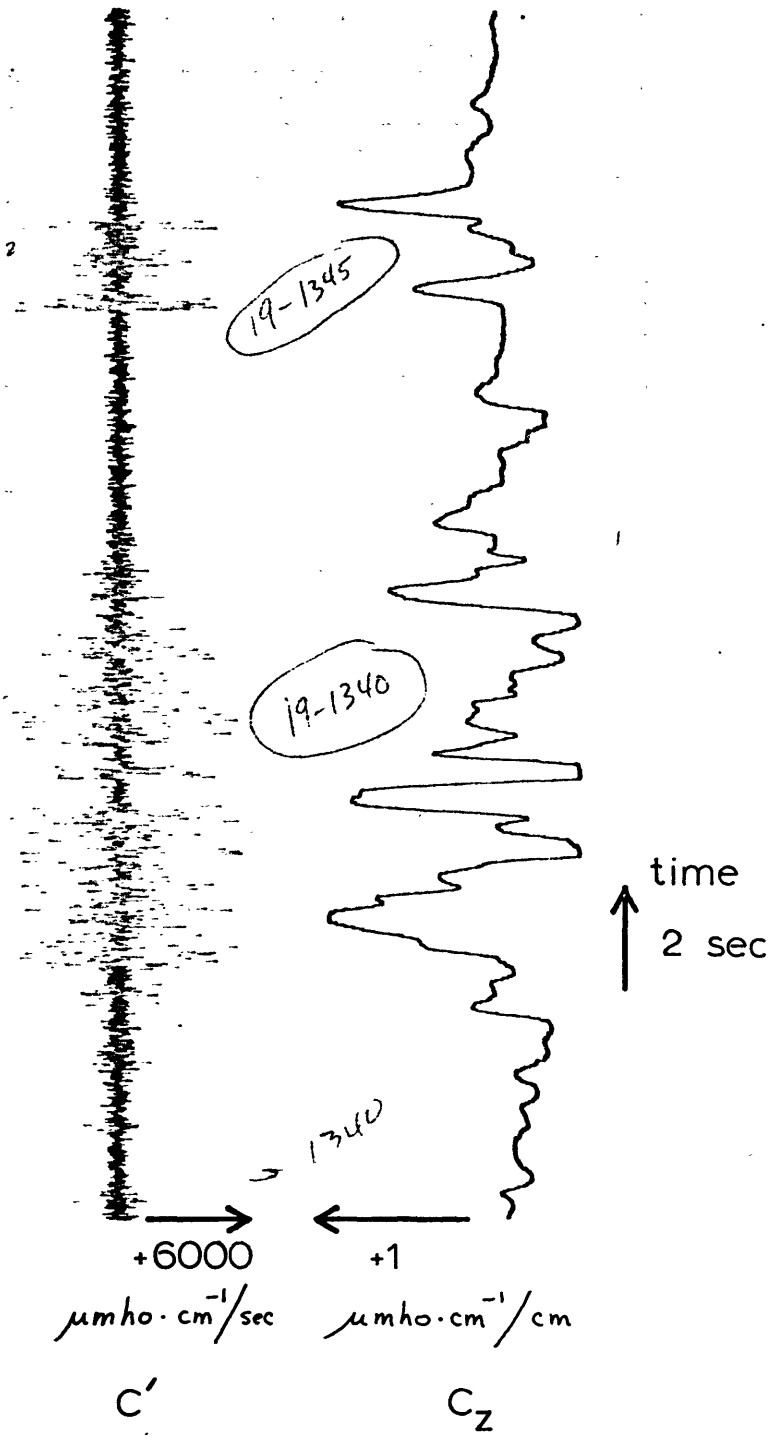

FIGURE 5.6 Detail of Figure 5.5, enlarged along the time axis.

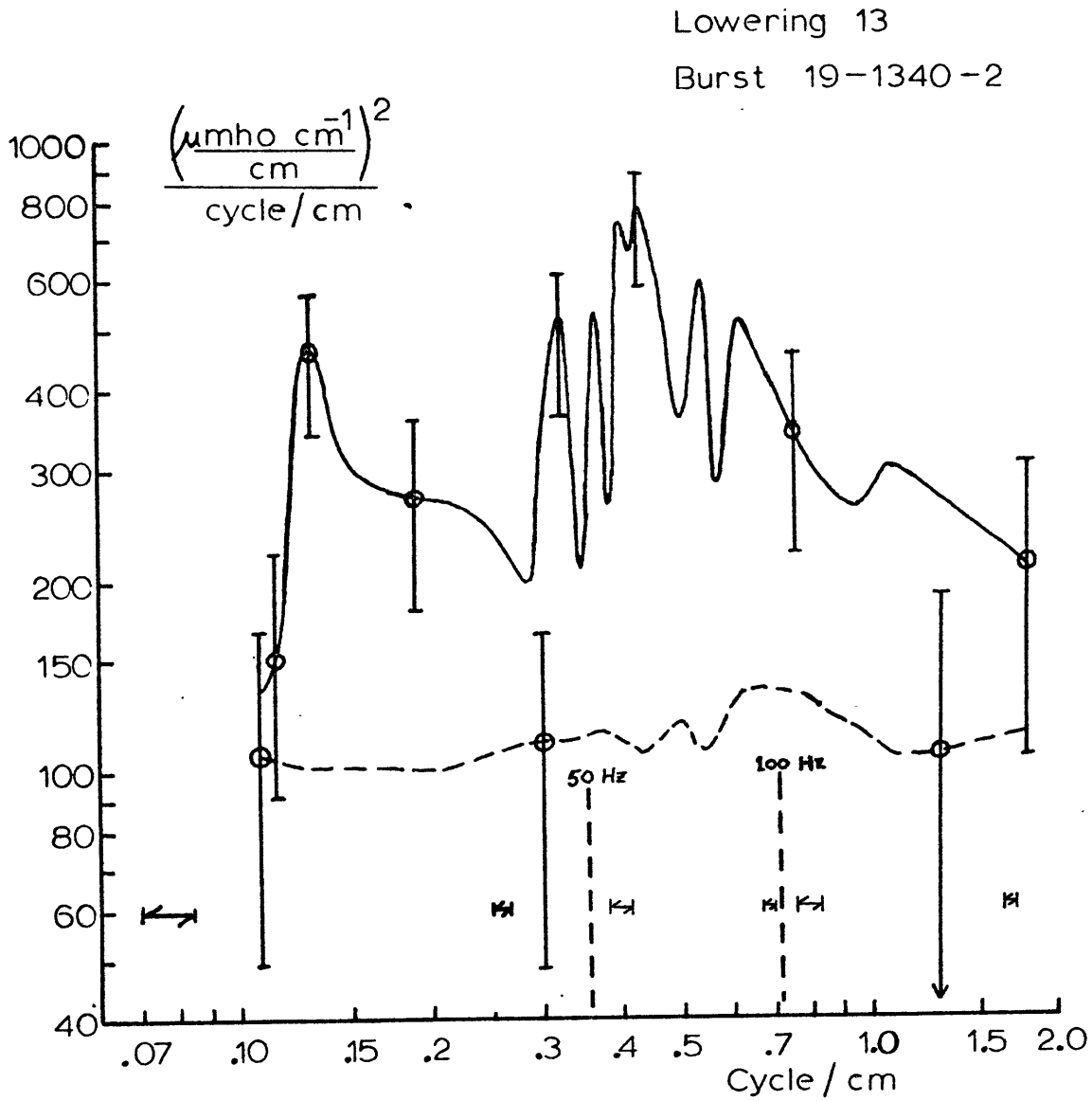

FIGURE 5.7 CONDUCTIVITY GRADIENT SPECTRUM, Event # 19 - 1340 - 2

On this and succeeding figures, the vertical bars represent the instrumental error in the analysis of the particular event. The small horizontal arrows represent the resolution bandwidth within each of the separate spectra from which the plots are made. For a full description, see Appendix 4.

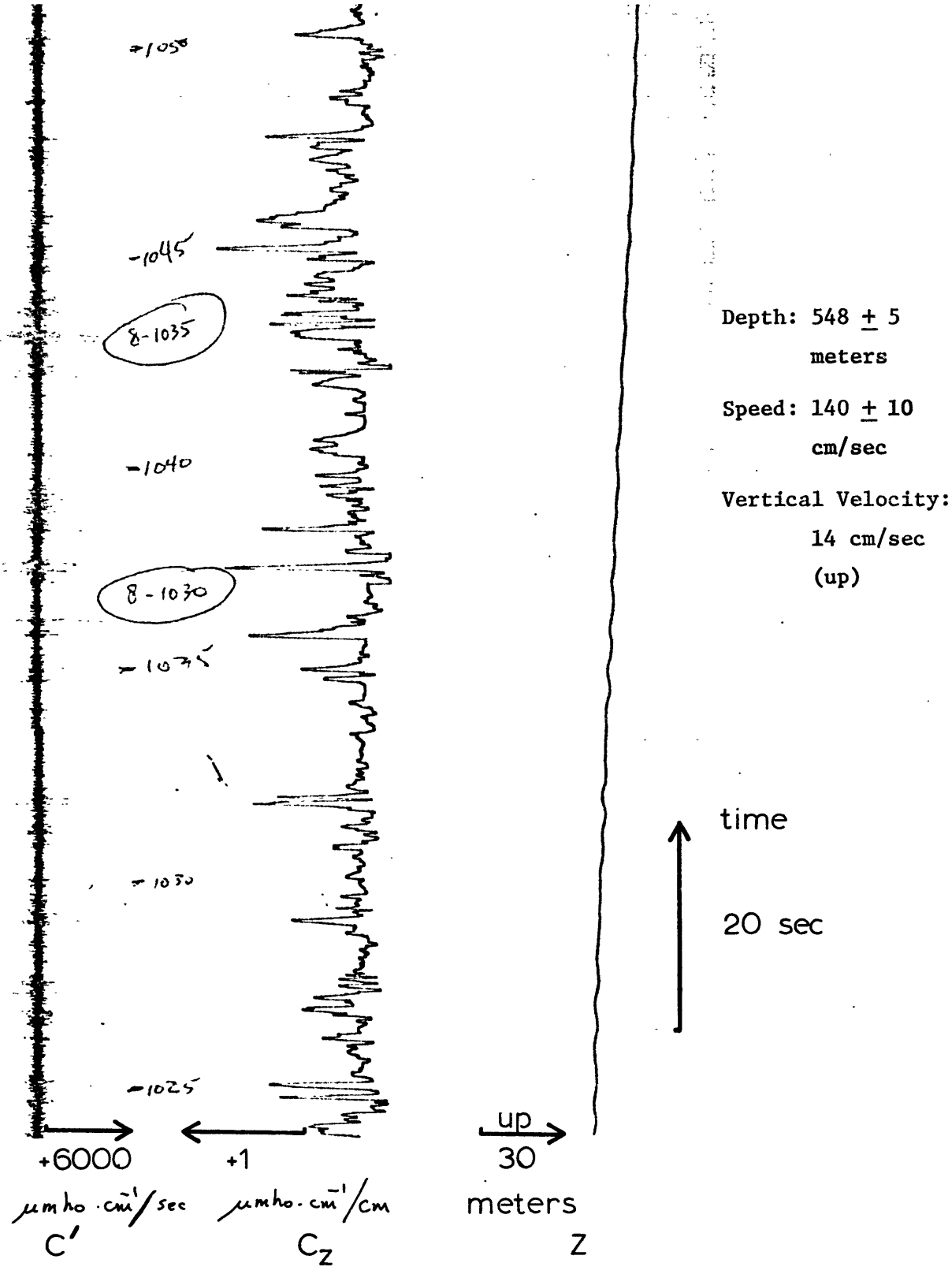

FIGURE 5.8 Time Record, Event # 8 - 1035 , Lowering 8.

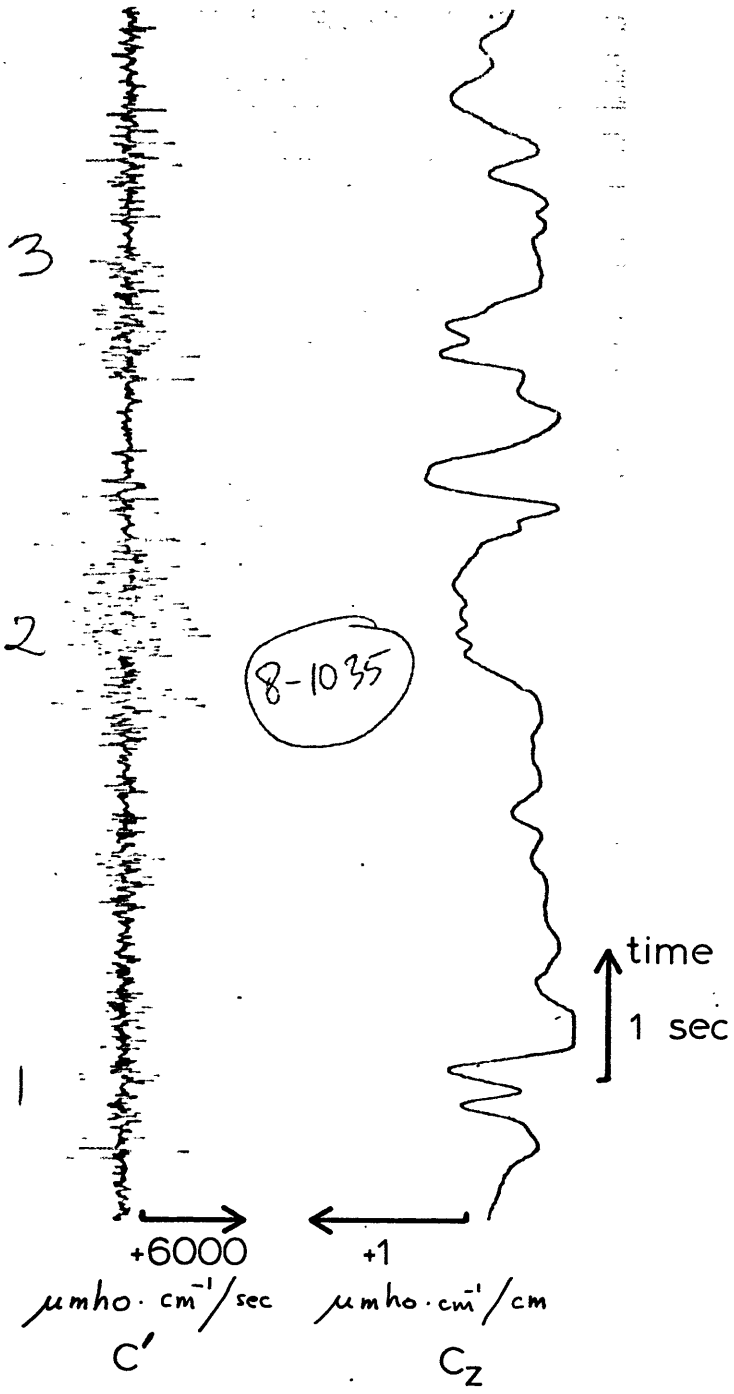

FIGURE 5.9 Detail of Figure 5.8, enlarged along the time axis.

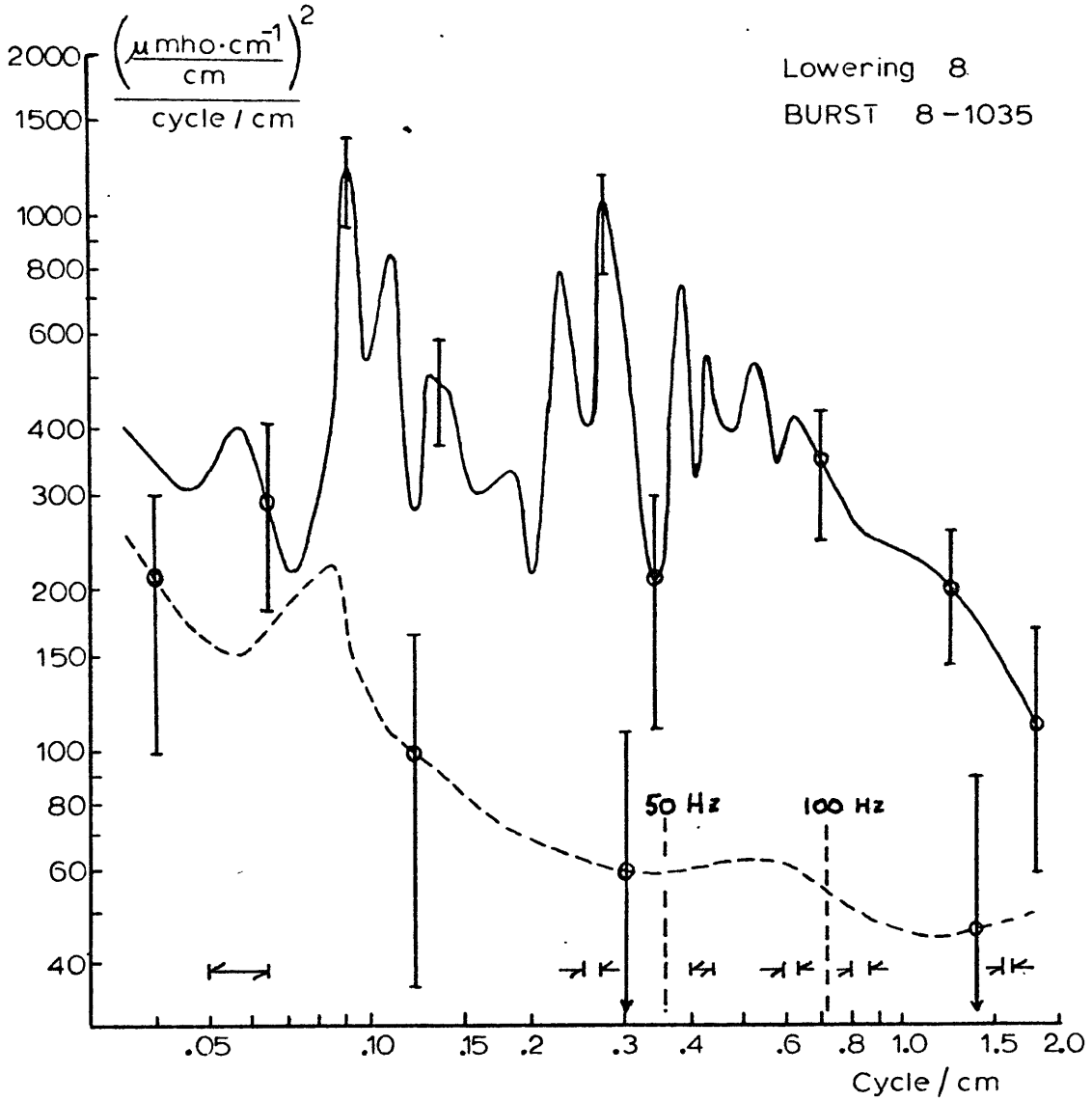

FIGURE 5.10 Conductivity Gradient Spectrum, Event # 8 - 1035

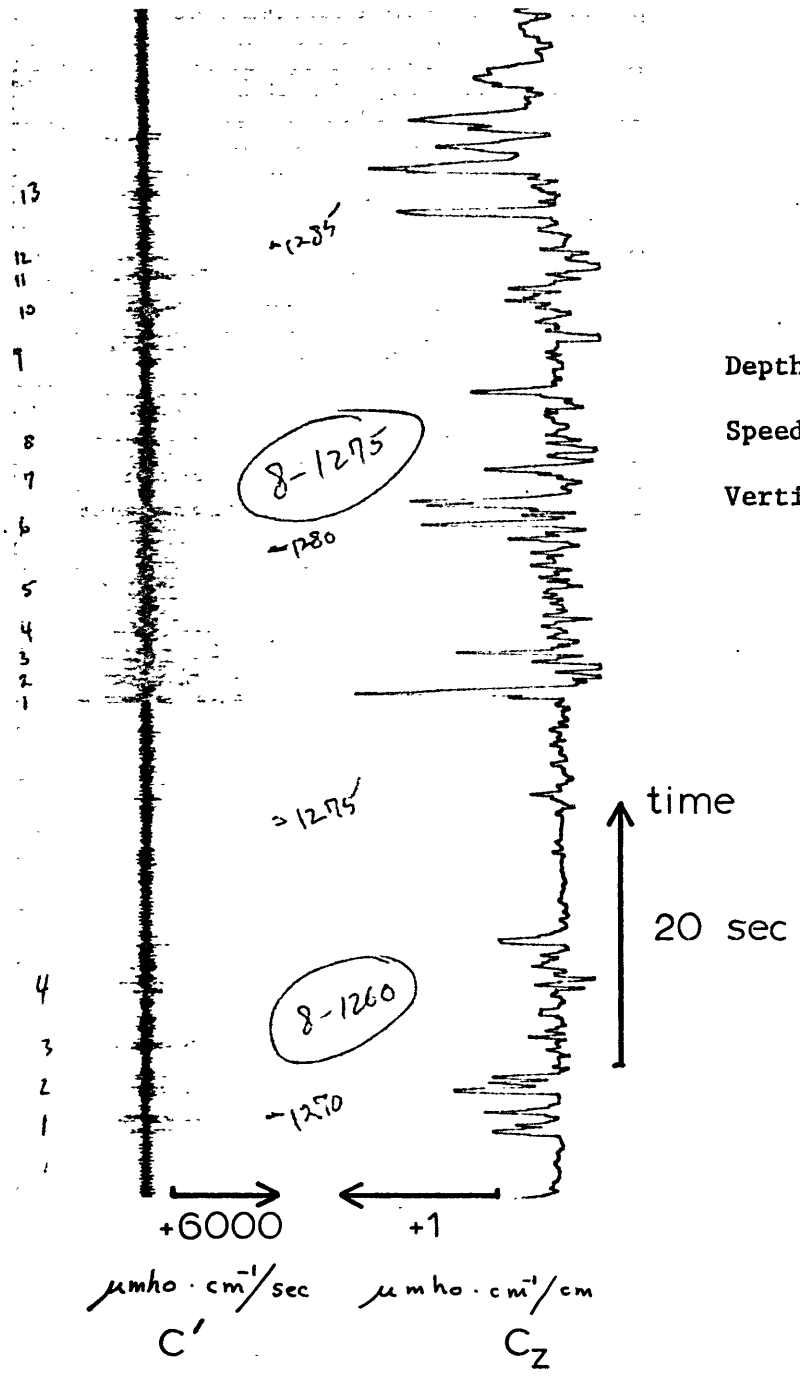

Depth: 340 ± 5 meters

Speed: 175 ± 10 cm/sec

Vertical Velocity: 31 cm/sec (up)

FIGURE 5.11 Time Record, Event # 8 - 1275, Lowering 8.

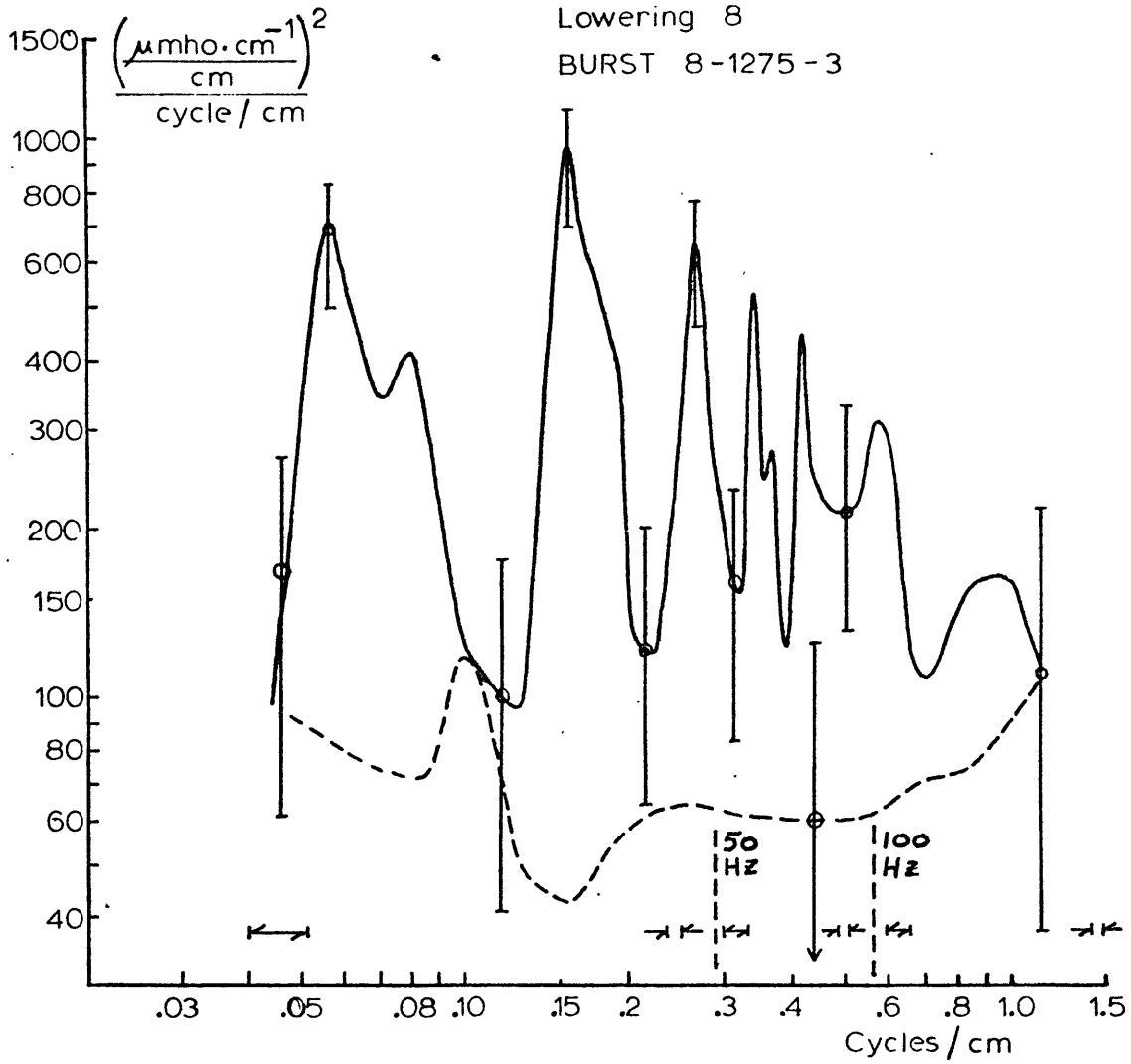

FIGURE 5.12 Conductivity Gradient Spectrum, Event # 8 - 1275.

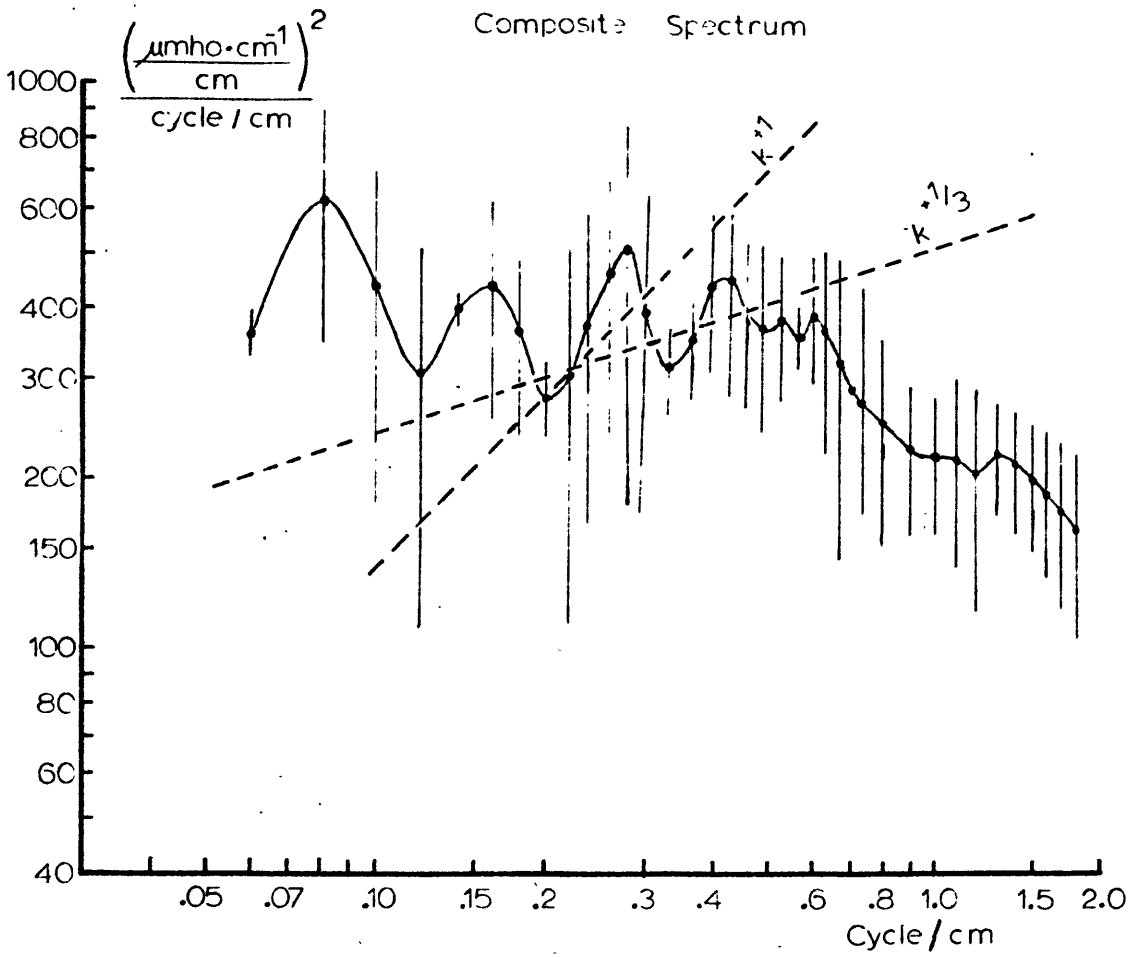

FIGURE 5.13 Composite Spectrum

This spectrum is an average of the preceding three spectra, Figures 5.7, 5.10, and 5.12. Before being averaged together, these spectra were smoothed individually in the wavenumber domain by averaging in bands equal to twice the resolution bandwidth.

Also plotted are lines of $k^{+1/3}$ and k^{+1}, whose slopes correspond theoretically with the inertial subrange of isotropic turbulence, and the viscous-diffusive subrange, respectively.

The vertical error bars represent twice the sample standard deviation at each averaging point; these have been computed by the formula:

$$2 \cdot \sigma_{k_n} = 2 \cdot \left[\tfrac{1}{2} \sum_{i=1}^{3} \left(x_i(k_n) - \bar{x}(k_n) \right)^2 \right]^{1/2}$$

where $x_i(k_n)$ is the value of the power density function at each wavenumber, k_n. Clearly, the sample size (3) is too small to obtain a meaningful spectral estimate in this case. Nevertheless, the basic shape of the spectrum is apparent.

The noise spectra (dotted lines in Figures 5.7, 5.10, and 5.12) have not been subtracted from the data before averaging and plotting.

We assume $\nu = 1.4 \times 10^{-2}$, $K = 1.5 \times 10^{-3}$ in e.g.s. units, and after converting the wavenumbers to radian measure, we get

$$\varepsilon = (.31 - .64) \times 10^{-5} \text{ ergs/gm} \cdot \text{sec}$$

This value seems consistent with the 10^{-5} value of Cox, Hacker, Johnson, and Osborn. But there is an inconsistency here. We have used spectral results from a few selected large bursts of activity to find k_B. Thus our calculated ε should refer to the rate of energy dissipation <u>within a turbulent patch</u>. The average dissipation rate over the whole thermocline must be several orders of magnitude less, since the turbulence is highly intermittent (say 1%, about which, more later). Therefore, ε_{ave} should be, very roughly, 0.5×10^{-7} ergs/gm·sec. This value is low by most previous estimates. Munk (1966), for example, calls for an energy dissipation rate in the thermocline of 1.8×10^{-6} ergs/gm·sec.

This inconsistency would be resolved if the measured value of k_B were only higher by a factor of three. It is possible that the observed spectral rolloff is due partly to the characteristics of the conductivity probe , whose spatial response is limited to structures of about 1 cm size for full output.

The important point here is that attempting to measure the energy dissipation rate by measuring k_B, if it is possible to do so at all, will require vastly more data than we have here, because of the 4th-power sensitivity of the dissipation to the measured value of k_B.

If we then assume that the diffusion cutoff scale is 1.7-2.0 cm, then Kolmogorov's scale must be 4.2-6.0 cm (wavenumbers 0.17-0.24 cycle/cm). In between Kolmogorov's and Batchelor's scales the spectrum of the gradient should, according to theory, go as k^{+1}. It is difficult to believe, from Figure 5.13, that it does so in these particular bursts. It is even more difficult to believe that the spectrum goes as $k^{+1/3}$ for wavenumbers less than 0.2. There appears to be more energy at lower wavenumbers than the theory calls for.

The mean value of N in the thermocline is 4.3×10^{-3} radians/sec., which implies a typical buoyancy wavenumber k_o=0.02 cycle/cm, if ε is taken to be 0.5×10^{-5} as calculated above. However, N can locally be as high as 10^{-2} on sharp interfaces in the thermocline, which implies that for turbulence occurring at an interface, k_o=.07 cycle/cm. The use of a locally high value of N is required by the fact that shear instability is most likely in regions of high gradient, and by the fact that the ε used is a local maximum value, not an average value. This buoyancy wavenumber is only a factor of 2 or 3 smaller than the Kolmogorov wavenumber itself; thus the inertial subrange would seem to occupy less than 1 decade in wavenumber.

What would be the effect of the stratification on the quasi-horizontal spectrum? Vertical motions will tend to be suppressed; this means that for a particular total energy dissipation, ε , horizontal motions will tend to be increased for wavenumbers less than k_o. Thus the purely horizontal gradient spectrum will qualitatively be increased at lower wavenumbers, in accordance

with our observations.

CHAPTER VI

SIGNIFICANCE OF THE MICROSTRUCTURE

Having looked in detail at individual events, we now turn to the larger scale, and try to reconcile the miscrostructure with the larger features of the ocean.

A. EVIDENCE AGAINST SALT FINGERS AS A MAJOR MIXING MECHANISM

In the first place, we must discard salt fingers as an important convective process. It is believed that salt fingers were observed in the main thermocline on several occasions, as described in Chapter V. But they occupied only about 10 seconds out of a total of 21,000 seconds of towing time in the thermocline. It was calculated in Chapter V that the vertical flux of buoyancy due to salt in the fingers was approximately 0.5×10^{-8} cm/sec. Purely molecular diffusion, assuming a typical thermocline salinity gradient of 3×10^{-5} % /cm, and $k_s = 1.5 \times 10^{-5}$, is 0.35×10^{-12} cm/sec. Thus the transport of salt due to fingering, averaged over the entire thermocline, is only about equal to the (negligible) molecular flux. We must regard salt fingers merely as a fascinating curiosity, at least at the time and place of this experiment.

Why are there not more salt fingers in the thermocline? Fingers should automatically form everywhere in the thermocline in the Atlantic Ocean, since the vertical gradients of temperature and salinity are in the right sense. But evidently they are inhibited almost completely, and the cause is probably externally-imposed

vertical shear. The exact mechanism of inhibition, however, is unclear. A great deal of theoretical and laboratory has been done to find how the fingers behave once they are started, but very little data exists on the question of how to prevent fingering. In light of our present results, this problem deserves further attention. Also, for further sea-going experiments it would clearly be desirable to construct a vertical velocity gradient sensor analogous to the vertical conductivity gradient sensor.

EVIDENCE FOR THE PRESUMPTION OF TURBULENCE

Turbulence is the remaining alternative. We have seen in Chapter V that the bursts are individually consistent with a turbulent hypothesis. In addition, evidence of the turbulent nature of the bursts comes from another source.

The bursts always occur in regions of irregular vertical gradient. This true without exception in the thermocline. Typically, the vertical conductivity gradient sensor, Cz, will show multiple sharp peaks in such a region. These peaks may have amplitudes as high as 1 μmho$\cdot$cm^{-1}/cm, and thicknesses ranging from 30 cm (the resolution of the instrument)to 100 cm. Half of the patches exhibit <u>negative</u> gradient peaks in these regions as well; these typically have a smaller amplitude, about -.3 μmho$\cdot$cm^{-1}/cm, but similar thickness. Some examples have already been shown (see Figures 5.5, 5.6 and 5.11). These patches of irregular gradient are rarely more than a few meters thick.

Those parts of the Cz record which contain multiple, sharp, but always positive, gradient peaks have been denoted as "class B" regions; irregular parts which contain both positive and negative gradients have been denoted "class C". Examination of the data reveals that: (1) every class C gradient region in the thermocline, without exception, is associated with a burst of horizontal microstructure (C'); (2) every burst of C' is associated with either a close B or a class C region in the thermocline; and (3) there are numerous class B regions which have no C' bursts.

We believe that irregular negative vertical gradients, in conjunction with horizontal microstructure, are the manifestation of active turbulence. Thus, every burst in a class C region is assumed to be turbulent; and since there is no apparent difference between bursts from class B regions and those from class C regions, the presumption is that they are <u>all</u> turbulent.

A plausible hypothesis is that class C regions are undergoing violent but temporary mixing. Class B regions are older, and although they are still turbulent, gravity has begun to re-establish the stratification; the motion here is probably mostly two-dimensional. When the turbulence has died out altogether, some gradient maxima are left; and if the shear is low enough, salt fingers may occasionally form across these remnant interfaces.

C. DISTRIBUTION OF MICROSTRUCTURE AS A FUNCTION OF DEPTH

Table III shows the number of bursts of microstructure, and their duration, in the thermocline, the 18°water, and the surface thermocline for each lowering. Lowerings 10, 11, and 13 are very consistent; Lowering 8 is quite unique. It is believed that the difference between Lowering 8 and the others is significant; and upon examination, this will be seen to provide further justification for the assumption that most of the bursts are turbulent.

D. DIFFERENCES AMONG THE LOWERINGS

Even a casual inspection of the records clearly shows that Lowering 8 differs significantly from the other three lowerings. This difference is apparent in the vertical profiles of Cg and Tg (see Figure 4.2), which appear to be qualitatively more irregular than those of the later lowerings. It is also apparent in the vertical gradient profile Cz (see Figure 4.6) which contains patches of high-amplitude gradient fine-structure, including negative vertical gradients; this is referred to as a class "C" gradient region. All of the lowerings contain such features, but they are far more prevalent in Lowering 8. Moreover, these patches occur even in the usually placid 18° water in Lowering 8, whereas no such patches were observed in the 18° water during any other lowering.

From the conductivity microstructure probe itself

TABLE III

DISTRIBUTION OF BURSTS AS A FUNCTION OF DEPTH FOR EACH LOWERING

Lowering #	No. of Bursts	Total Duration of Bursts (seconds)	Total Duration of Record (seconds)	Percentage of Time Occupied by Bursts
THERMOCLINE (Below 450 m.)				
8	73	124	3120	4
10	8	29	3600	0.8
11		22	4300	0.5
13	30	77	10,260	0.75
18° WATER (200 - 400 m.)				
8	22	37	900	4
10	0	0	720	0
11	0	0	1140	0
13	0	0	1080	0
SURFACE WATER (Less than 200 m.)				
8	5	10	420	2.4
10	9	28	360	7.8
11	130	222	2220	10
13	19	76	1080	7

comes further independent evidence of a significant difference in Lowering 8. With reference to Table III, which lists the burst statistics for the three main regions of each lowering, it may be seen that Lowering 8 had 5 times as much horizontal microstructure in the thermocline as the other lowerings, (although there appears to have been somewhat less horizontal microstructure in the surface layer). Furthermore there was extensive horizontal microstructure in the 18° water as well, a feature never observed on the other lowerings; and this microstructure occurs relatively as frequently as it does in the thermocline. Most significantly, this horizontal microstructure occurs in the patches of irregular, class "C" vertical gradient.

Naturally, the first question to be answered with regard to Lowering 8 is: are these features real or instrumental? That they are indeed real is proven in several ways. Firstly, the vertical temperature-gradient record (see Chapter II, Section B.3 for a discussion of Tz) exhibits the exact same structure as Cz in the patches, peak-for-peak, including the negative vertical gradients. The two gradient sensors are separate instruments in all respects, except that they share a common power supply. Secondly, the gross conductivity signal, Cg, shows a "bumpy" structure with inversions in these patches, indicating that it is the ocean itself which is irregular. The conductivity probe is a completely separate instrument, even having its own power supply. Consequently, there can be no doubt but that Lowering 8 is fundamentally different

from the others.

We can only speculate as to the reasons for this difference. Lowering 8 must stand alone; we have no large-scale survey to elucidate the context in which it occurred. Not even the direction of the mean flow past the island is known. But a likely conclusion can be drawn nevertheless.

Wunsch (1972) has found that conditions are not uniform azimuthally around Bermuda. He found that microstructure is present everywhere in the vicinity, but that one side of the island is generally quite different from the others. On this "active" side the vertical profiles are much more irregular, particularly in the 18 water, than the profiles from the "quiet" sides. The active region was always found on the side of the island lying to the right of the mean flow (Wunsch, 1972).

The vertical profiles from Lowering 8 very much resemble those from Wunsch's active region, whereas Lowerings 10, 11, and 13 more closely resemble those from quiet regions. The most likely hypothesis is, therefore, that a change in the mean flow pattern occurred between Lowering 8 and the others, and thatthe south side of the island, where the lowerings were made, was active at the time of Lowering 8.

Lowering 8 was made on 16 June, 1972, 17 days prior to Lowerings 10 and 11. It is known (Wunsch, 1972) that the mean flow can reverse direction completely in less than one week. On the other hand, Lowerings 10 and 11 were made on 3 July, and Lowering 13 was made on 6 July; it is not surprising that these lowerings resemble one

another more closely.

The consequences of this hypothesis are very important. Wunsch has asserted that the active side of the island is undergoing violent mechanical stirring due to large-scale, shear-induced instability. If this is correct, then it is inescapable that the horizontal microstructure and the patches of large positive and negative vertical gradients of Lowering 8 must be the actual mixing process itself, caught in the act, as it were. But similar events occur in the other lowerings; and so these events probably represent mechanical mixing also.

This conclusion is reinforced by the spectral evidence. Large bursts which occurred in class "C" regions generally have a wideband spectrum, consistent with a turbulent mixing process. This is true of such bursts from all the lowerings, not only Lowering 8. This correlation of wideband spectra with class "C" gradient regions must be regarded as qualitative and subjective, because there are not enough independent spectra to make a good statistical estimate. Moreover, we do not know the past history of any event. But no large burst in the thermocline was found to have a band-limited spectrum; and so the above conclusion seems intuitively right.

The details of two such mixing events from Lowering 8, including spectra, have been shown in Figures 5.8 through 5.12. The first of these is from the thermocline, and the second is from the 18° water.

E. VERTICAL MIXING DUE TO TURBULENCE

The mean-square conductivity gradient along the path taken by the probe, $\overline{\left(\partial c/\partial z\right)^2}$, can be found for each burst by integrating its power-density spectrum. The average value of $\overline{\left(\partial c/\partial z\right)^2}$ over all the thermocline bursts were analyzed is 115 ± 30 (μmho-cm^{-1}/cm)^2. The three-dimensional mean-square gradient, $\overline{|\nabla c|^2}$, would equal 3 x $\overline{\left(\partial c/\partial z\right)^2}$ if the turbulence were isotropic. We should not expect it to be isotropic except perhaps at high wavenumbers (ie, well above the buoyancy wavenumber); but since most of the energy in the gradient is in fact in the high wavenumbers, it seems reasonable to use the factor of three. This yields $\overline{|\nabla c|^2} = 345 \pm 90$ (μmho cm^{-1}/cm)^2. The square of the mean gradient, $(\nabla \bar{c})^2$, is 0.048 (same units) in the thermocline. The ratio $R_c = \overline{|\nabla c|^2}/(\nabla \bar{c})^2$ is therefore 7200 for thermocline bursts.

For want of a better assumption, it will be assumed that R_c is the same as the corresponding ratio for temperatures, R_T. This amounts to assuming that temperature and salinity fluctuations are proportional on all scales of motion, which is clearly wrong at very high wavenumbers. But conductivity is mostly temperature anyway; so the conductivity ratio, R_c, will at worst be a slight overestimate of the temperature ratio, R_T.

From Table III, it may be seen that turbulence occurred in the thermocline 0.69 percent of the time, not including the anomalous Lowering 8. Using the method of Gregg and Cox (1972) we compute the time averaged turbulent heat transport by the formula:

$$q = -\rho c_p K_T R_T (\nabla \bar{T}) I$$

where T represents the mean temperature, c_p is the specific heat of water, and I is the intermittency factor. For this case:

$\nabla \bar{T} = \frac{d\bar{T}}{dz} = 1.92 \times 10^{-4}$ °c/cm; $c_p = 0.95$ cal/gm; $K_T = 1.5 \times 10^{-3}$ cm^2/sec

The result is: $q = 13.6 \times 10^{-6}$ cal/cm^{2}sec. The effective eddy diffusivity, A, may then be calculated from the expression:

$q = \rho c_p A \frac{dT}{dz}$ which gives $A = 0.075 \pm 0.02$ cm^2/sec.

For Lowering 8, the equivalent calculation yields $q = 64.5 \times 10^{-6}$ cal/cm^{2}sec, and A = 0.36 cm^2/sec. Considering that Lowering 8 probably represents strong mixing due to the flow past the island, this value seems low.

For comparison, Gregg and Cox (1972) found that in the San Diego Trough, the eddy coefficient was 0.5 - 1.0 cm^2/sec in regions where localized overturning was suspected. However, the Trough is thought to be an area of very strong mixing, particularly in the upper layers where the measurements were made, so that their data may not be entirely comparable to ours.

In connection with global-scale thermocline theories, it has been postulated that the vertical eddy diffusivity should be of order (1) (Munk, 1966). But recent efforts to measure the effectiveness of vertical mixing, by Rooth and Östlund for example, have produced estimates of the vertical eddy diffusivity which are less than 0.2 cm^2/sec. Our data thus tend to confirm these lower measured diffusivities, rather than the higher theoretical ones. The low values from our data are presumed to be real, since no known quirks of the instrument or the data analysis procedure can account for an error in the mean-square gradient of a factor of 13, which is what would be required to produce an eddy diffusivity of 1 cm^2/sec.

Because the calculated eddy diffusivity depends directly upon the measured intermittency of the turbulent events, it is possible that a significant error could have arisen if by chance the instrument failed to pass through a representative number of turbulent patches. This would be a type of sampling error. The

fact that the frequency-of-occurrence statistics (Table III) are nearly the same for Lowerings 10, 11, and 13 would tend to discredit this objection, however. Also, the fact that data could only be gathered on calm days could conceivably have biased the measurements as well. But before these doubts can be fully resolved it will be necessary to know much more about the stationarity in time and space of the mixing processes. This will require much more data, and is clearly beyond the scope of this thesis.

The low measured value of the eddy diffusivity, and the virtual absence of mixing in the 18°water (except on the anomalous Lowering 8), are evidences of the sporadic nature of mixing in the ocean. Thus, strictly speaking, the results obtained in this investigation are only applicable to the waters south of Bermuda in the summer of 1972; and clearly further work in the field of vertical mixing must deal with this intermittency and localization of mixing, before reliable average diffusivities can be calculated.

BIBLIOGRAPHY

Batchelor, G.K. (1959) Small scale variation of convected quantities like temperature in turbulent fluid. J. Fluid Mech., Vol. 5, pp. 113-133.

Brown, N.D., private communication.

Cooper, J.W. and H.M. Stommel (1968) Regularly spaced steps in the main thermocline near Bermuda. J. Geophys. Res., Vol. 73, #18, pp. 5849-5854.

Cox, C.S., P.W. Hacker, B.P. Johnson, and T.R. Osborn (1969) Fine scale of temperature gradient. Trans. Marine Temp. Symp., Marine Tech. Soc.

Garrett, C. and W. Munk (1971) Internal wave spectra in the presence of fine structure. J. Phys. Ocean., Vol. 1, #3, pp. 196-202.

Garrett, C. and W. Munk (1972) Oceanic mixing by breaking internal waves. Deep Sea Res., Vol. 19, pp. 823-832.

Gibbon, C.H. and R.B. Williams (1972) Measurements of turbulence and turbulent mixing in the Pacific Equatorial Undercurrent. International Symposium on Oceanography of the South Pacific, Wellington, New Zealand.

Grant, H., B.A. Hughes, W.M. Vogel, and A. Moilliet (1968) The spectrum of temperature fluctuations in turbulent flow. J. Fluid Mech., Vol. 34, pp. 423-442.

Grant, H., A. Moilliet, and W.M. Vogel (1968) Some observations of the occurence of turbulence in and above the thermocline. J. Fluid Mech., Vol. 34, pp. 443-448.

Gregg, M.C. and C.S. Cox (1971) Measurement of the oceanic microstructure of temperature and electrical conductivity. Deep Sea Res., Vol. 18, #9, pp. 925-934.

Gregg, M.C. and C.S. Cox (1972) The vertical microstructure of temperature and salinity. Deep Sea Res., Vol. 19, #5, pp. 355-376.

Huppert, H.E. (1971) On the stability of a series of double-diffusive layers. Deep Sea Res., Vol. 18, #10, pp. 1005-1021.

Lambert, R.B and J.W. Demenkow (1972) On the vertical transport due to fingers in double-diffusive convection. J. Fluid Mech., Vol. 54, Part 4, pp. 627-640.

Munk, W.H. (1966) Abyssal recipes. Deep Sea Res., Vol. 13, pp. 707-730.

Orlanski, I. and K. Bryan (1969) Formation of the thermocline step structure by large-amplitude internal gravity waves. J. Geophys. Res., Vol. 74, pp. 6975-6983.

Osborn, T.R. and C.S. Cox (1972) Oceanic fine structure. Geophys. Fluid Dyn., Vol. 3, #4, pp. 321-345.

Prandtl, L. (1952) Essentials of Fluid Dynamics. New York: Hafner Publishing Co.

Riley, J.P. and G. Skirrow (1965) Chemical Oceanography, Vol. 1. New York: Academic Press.

Rooth, C.G. and H.G. Östlund (1972) Penetration of tritium into the Atlantic thermocline. Deep Sea Res., Vol. 19, pp. 481-492.

Shirtcliffe, T.G.L. and J.S. Turner (1970) Observations of the cell structure of salt fingers. J. Fluid Mech., Vol. 41, Part 4, pp. 707-719.

Stern, M.E. (1960) The "salt-fountain" and thermohaline convection. Tellus, Vol. 12, #2, pp. 172-175.

Stern, M.E. (1967) Lateral mixing of water masses. Deep Sea Res., Vol 14, pp. 747-753.

Stern, M.E. (1968) T-S gradients on the microscale. Deep Sea Res., Vol. 15, pp. 245-250.

Stern, M.E. (1969) Salt-finger convection and the energetics of the general circulation. Deep Sea Res., Suppl. to Vol. 16, pp 263-267.

Stern, M.E. (1969B) Collective instabilities of salt fingers. J. Fluid Mech., Vol. 35, Part 2, pp. 209-218.

Stern, M.E. (1970) Optical Measurements of salt fingers. Tellus, Vol. 22, pp. 76-81.

Stern, M.E. and J.S. Turner (1969) Salt fingers and convecting layers. Deep Sea Res., Vol. 16, pp. 497-511.

Stommel, H.M. and K.N. Fedorov (1967) Small scale structure in temperature and salinity. Tellus, Vol. 19, pp. 306-325.

Sverdrup, H.U., M.W. Johnson, and R.H. Fleming (1942) The Oceans. New York: Prentice Hall.

Tait, R.I. and M.R. Howe (1968) Some observations of thermohaline stratification in the deep ocean. Deep Sea Res., Vol. 15, pp. 275-280.

Tait, R.I. and M.R. Howe (1971) Thermohaline staircase. Nature, Vol. 231, pp. 179-180.

Turner, J.S. (1967) Salt fingers across a density interface. Deep Sea Res., Vol. 14, pp. 599-611.

Williams, A.J., private communication.

Woods, J. (1968) Wave-induced shear instability in the summer thermocline. J. Fluid Mech., Vol. 32, pp. 791-800.

Woods, J.D. and R.L. Wiley (1972) Billow turbulence and ocean microstructure. Deep Sea Res., Vol. 19, #2, pp. 87-121.

Wunsch, C. (1972) Temperature microstructure on the Bermuda Slope with application to the mean flow.

BIOGRAPHICAL SKETCH

Bruce Magnell was born on September 5, 1944 in Brooklyn, New York. He grew up there and in Franklin Square, Long Island, New York. He graduated with honors from H. Frank Carey High School in 1962. In September of that year he entered M.I.T., intent on becoming an oceanographer. Having discovered during his freshman year that there really is no such thing as undergraduate oceanography, he became an electrical engineer, receiving his S.B.E.E. in 1966. He then enrolled in the graduate oceanography program at M.I.T. Wishing to continue his engineering education in addition to learning science, he embarked upon a program which mixed engineering with oceanography. This culminated in the simultaneous receipt in September 1968 of two S.M. degrees, one in Oceanography and the other in Electrical Engineering. He continued at M.I.T. toward the Sc.D. degree in Oceanography, maintaining a strong experimental bent.

He married the former Patricia Frances Murphy in June of 1970, and they now reside in Cambridge.

APPENDIX 1

OPTICAL METHODS FOR DETECTING SALT FINGERS - A CRITIQUE

Salt fingers are an ordered spatial array of water columns moving alternately upward and downward, and the clearest demonstration of their existence would be a "photograph" of an array of vertical columns in the ocean. Apart from this subjective credibility of visual evidence, however, optical methods offer two great advantages, namely: that such methods can be extremely sensitive to variations in the index of refraction of light; and they can be used to investigate very small structures.

The shadowgraph technique has been used to investigate salt fingers in laboratory experiments with considerable success, particularly those involving sugar-salt solutions. This technique consists, in essence, of shining a collimated beam of light through the water onto a ground-glass plane. Gradients in the index of refraction cause the rays to bend, resulting in patterns of light and dark on the screen which may be photographed. Regularly-spaced structures of index of refraction result in geometric patterns on the screen (Stern, 1970).

Shadowgraph instruments are relatively easy to construct because they do not require precise alignment of the optical path; but they do require a rigid, bulky structure, which is difficult to tow through the ocean, enclosing the optical path. Moreover, it would be extremely difficult to avoid disturbing small structures in the water before the instrument could "see" them.

The only application of the shadowgraph in oceanic microstructure investigations to date has been as a vertically-dropped sensor. (A.J. Williams III, private communication)

The shadowgraph has, however, a more fundamental limitation than its mechanical configuration, namely that there are several sources of ambiguity in the interpretation of the photographs. Firstly, the index of refraction in sea water is a decreasing function of temperature but an increasing function of salinity, as given by the following:

$$\Delta n = \left.\frac{\partial n}{\partial S}\right|_{T=\text{CONST}} \cdot \Delta S + \left.\frac{\partial n}{\partial T}\right|_{S=\text{CONST}} \cdot \Delta T$$

$$\frac{\partial n}{\partial S} = +185 \times 10^{-6}/‰ \quad ; \quad \frac{\partial n}{\partial T} = -88 \times 10^{-6}/°C$$

(approximate values near 35 0/00, 15°C) (Riley and Skirrow, 1965)

Unfortunately the detailed temperature and salinity structure within salt fingers is not known; but since the difference of temperature and salinity across a thermocline interface may be, for example, 0.2°C and 0.03 0/00 (Tait and Howe, 1971), it is clear that the structure of the index of refraction in a salt finger field may have more inflection points than the salinity field. At best this may lead to an incorrect estimate of the diameter of the fingers; but, since the temperature must vary vertically as well as horizontally, it may result in a very confusing three-dimensional structure that would not be interpreted as fingers at all.

Furthermore, there may be an ambiguity due to a spatial filtering effect. This arises because, for a

given index of refraction field having a particular regular planform, there is one optimum position for the ground-glass screen, at which the rays diverge and converge most strongly. If the glass is not in this optimum position with respect to the sample, the image will be less clear, or may disappear altogether. Worse yet, this focus position of the glass is a function of the wavelength of the refractive index variations. Therefore the shadowgraph system is sensitive to a particular combination of refractive index amplitude variations, and the scale or wavelength of these variations, and the position of the groundglass. Different combinations of these parameters may or may not result in a focused image. This makes quantitative evaluation of the data very difficult, even if a clear image of fingers is seen.

Finally, shadowgraph data would be extremely difficult to interpret if no clearly-defined salt fingers are found. No structure larger than about one-half the diameter of the light beam can be resolved; and since the light beam in any practical device is unlikely to be very much larger in diameter than, say, 10 centimeters, it is clear that the shadowgraph would be poorly suited for a general-purpose microstructure sensor.

For these reasons the shadowgraph technique was discarded for this project. The Schlieren technique, which in essence senses the first derivative of the index of refraction rather than the second derivative like the shadowgraph, was also considered briefly. It was rejected because any slight misalignment of the optical path, due to temperature gradients affecting the supports for example, would result in no data at all. This danger was unacceptable.

APPENDIX 2

A SHORT HISTORY OF THE PROJECT

A brief calendar of events leading up to the 1972 Bermuda expedition is presented in Table A-1. A much more detailed calendar of events during the field operations in June and July of 1972 will be found in Chapter IV.

TABLE A-1

SHORT CHRONOLOGY OF THE MICROSTRUCTURE PROJECT

Summer 1969:	Discussions with H.M. Stommel, J.S. Turner, M.E. Stern regarding salt fingers and the desirability of trying to find them in the ocean.
Fall 1969:	Began feasibility study regarding microstructure probe. Optical methods investigated. Conductivity and methods of measuring it investigated.
Winter 1970:	Construction of first double-electrode type conductivity probe, after a suggestion by N.D. Brown.
Spring and Summer 1970:	Tests revealed the necessity

	of flushing water continuously through the probe. Design and testing of special sea-water transformer begun.
Fall 1970:	Design and construction of electronics and equipment.
Jan. - Feb. 1971:	Cruise to Barbados - R/V Atlantis II. Mechanical and electronic difficulties.
March - April 1971:	Ship time aboard R/V Knorr (buoy cruise). Electronics improved but still unsatisfactory. Poor launch conditions - instrument damaged.
May - July 1971:	Bermuda I. Debugging and testing. Instrument lost when cable parted, cause unknown. Some data obtained before loss, showing "bursts" of conductivity signal.
July - August 1971:	Analysis of records from Bermuda. "Bursts" were revealed to be instrumental, probably due to strumming of cable.

Sept. 1971 - March 1972:	Building new instrument of improved design. Laboratory tests carried out.
April - May 1972:	Towing tank tests at Woods Hole Oceanographic Institution.
3 May - 9 July, 1972:	Bermuda II. Details in Chapter III.

APPENDIX 3

INSTRUMENT DETAILS

Details of the instruments have been relegated to this Appendix to avoid cluttering up the text. However, the basic outline of the instrument designs has of necessity been included in the text, in order that the reader may understand how the data was obtained. Therefore, reference must be made to the block diagrams of the instrument in Chapter II, if the circuit diagrams in this Appendix are not self-evident.

Details are shown here only for those instruments which performed satisfactorily, and whose design was original.

PERFORMANCE OF THE CONDUCTIVITY GRADIENT SENSOR

As mentioned earlier, the gradient sensors had been constructed for another investigator and another project. Their electronics were modified slightly for use in this investigation, and laboratory tests were carried out to determine their performance.

The inductive heads used on the conductivity gradient sensor have an impedence of 116 ohms when the conductivity of the water is 50 mmho·cm.$^{-1}$. This sea-water impedance was modeled in the laboratory by using one turn of wire through each head coupled to appropriate resistances. One was a fixed resistor of 116 ohms; the other was variable. These resistors were adjusted for balance (zero output), then interchanged. By this means it was determined that the instrument error at balance was less than 0.005 mmho cm.$^{-1}$, which is one-fourth of

one percent of full scale.

Sensitivity was checked by placing 11,600 ohms in parallel with one of the resistors; this increased the effective conductivity by 1%, or 0.5 mmho cm.$^{-1}$. The output was adjusted to be 10 volts D-C.

It was discovered later that the designer of this instrument had not taken full account of the influence of temperature upon the electronics. A calculation by the author indicates that the drift of the zero point due to temperature may be as great as 0.067 mmho·cm.$^{-1}$ per meter over the 20 C oceanographic temperature range.

In addition, the two sensing heads apparently differed slightly in sensitivity when the instrument was mounted on the towing fish. The difference in sensitivities arose, not from the heads themselves, but from the relative proximity of the lower head to part of the vehicle frame. This effectively altered the cell constant of that head by substituting a metallic object for a part of the sea water loop. As a result, the lower head produced a higher output voltage for a given conductivity than did the upper head. Thus a signal is present at the output proportional to conductivity itself, i.e.:

$$C_z = a_u \cdot C_u - a_L \cdot C_L = \frac{(a_u + a_L)}{2} \cdot \Delta c + \frac{(a_u - a_L)}{2} \cdot (C_u + C_L)$$

$$C_z = a_1 \Delta c + a_2 \bar{c}$$

where subscript u refers to the upper head and "L" to the lower head. The first term of the last equation is the desired signal; the second is the error, which is due to the fact that a_u is not equal to a_L.

The sensitivities differ by only a small amount, but the error in the difference voltage is significant. In order to account for the average offset observed at the surface, one must postulate a coefficient for the error term in the above equation as follows:

$$C_z \text{ (volts)} = 20 \cdot \Delta c - \frac{1}{15} \bar{c}$$

where C and $\bar{C}$ have units of mmho·cm.$^{-1}$. These coefficients are also such as to account for most of the observed net drift over the entire depth range, at least in the large scale.

The proportion in which the two sources of zero drift enter into the data is not known. Moreover, the matter is complicated by the fact that there may be a considerable time lag in the temperature-related drift because the electronics is not in good thermal contact with the water; as a result the offset may depend upon the vertical velocity of the instrument. However, it is not known whether the temperature effect tends to augment or counteract the conductivity error.

The extent and significance of these errors did not become evident until the experiment had ended. Fortunately the data is not too seriously degraded, since it may be corrected to a certain extent by inspection. This process has been demonstrated in Chapter IV.

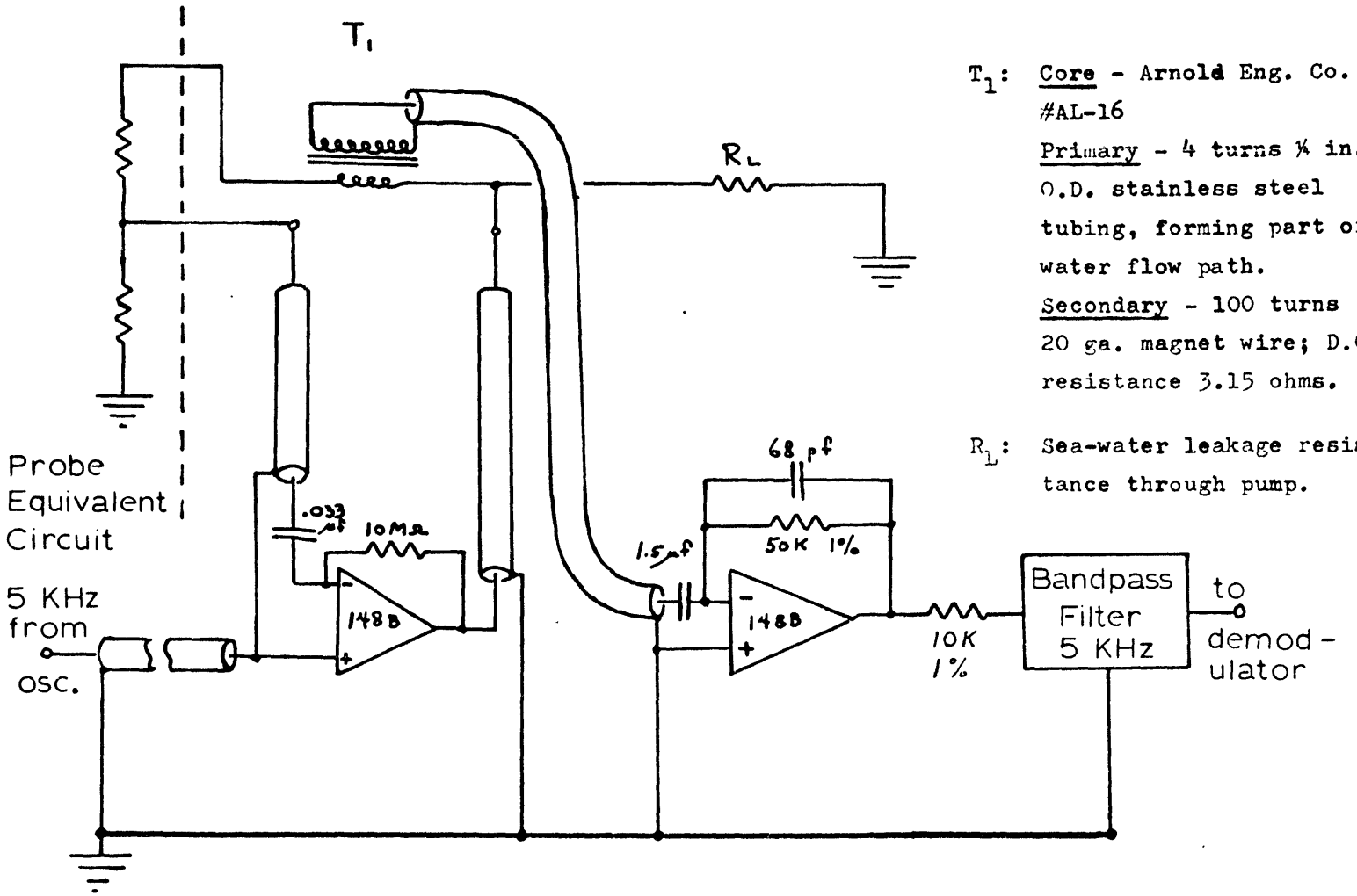

T_1: Core - Arnold Eng. Co. #AL-16
Primary - 4 turns ¼ in. O.D. stainless steel tubing, forming part of water flow path.
Secondary - 100 turns 20 ga. magnet wire; D.C. resistance 3.15 ohms.

R_L: Sea-water leakage resistance through pump.

FIGURE A-1

Conductivity Probe

Probe Driver &
Current–to–Voltage
Converter

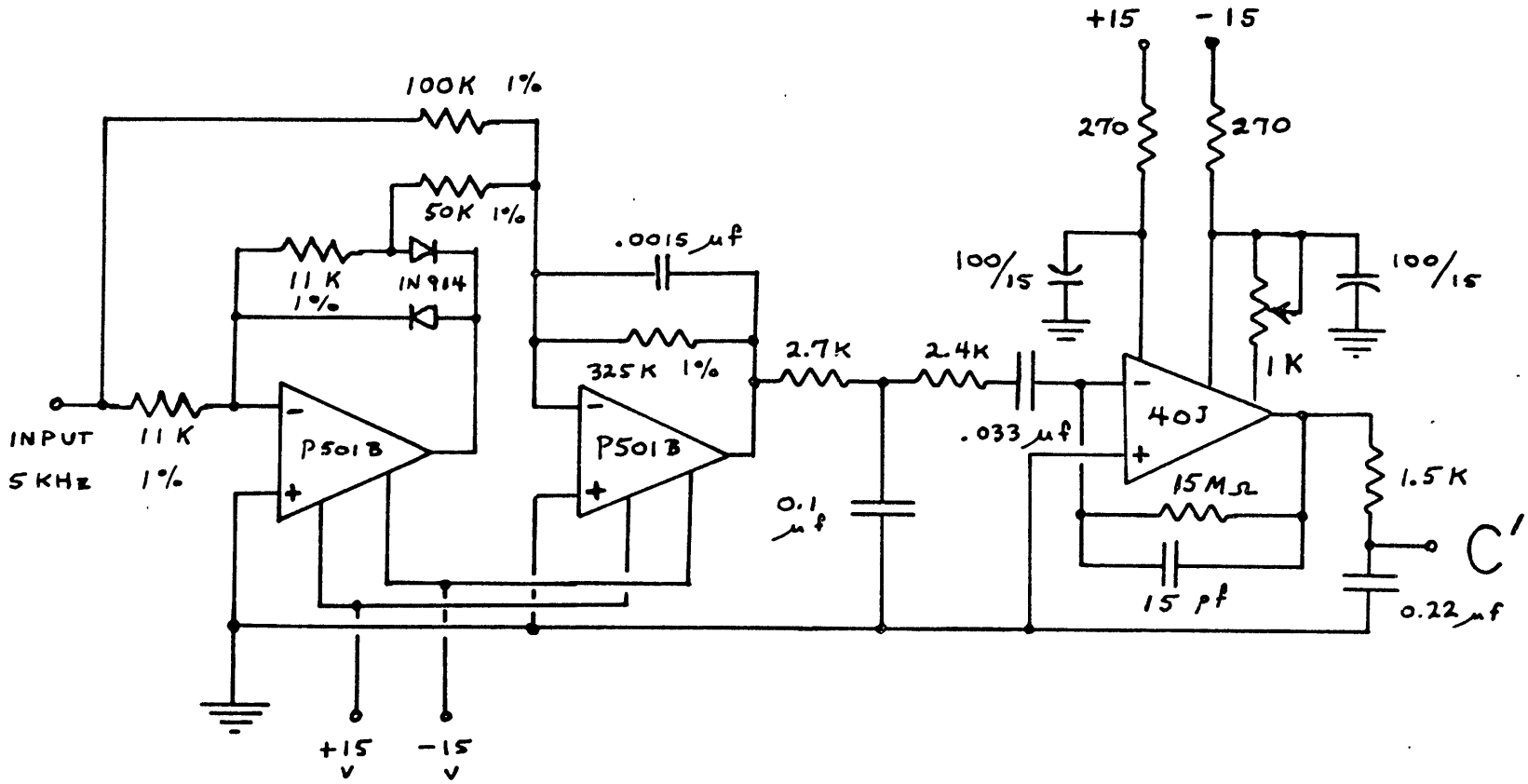

FIGURE A-2

Conductivity Probe

5 KHz Demodulator

&

Differentiator

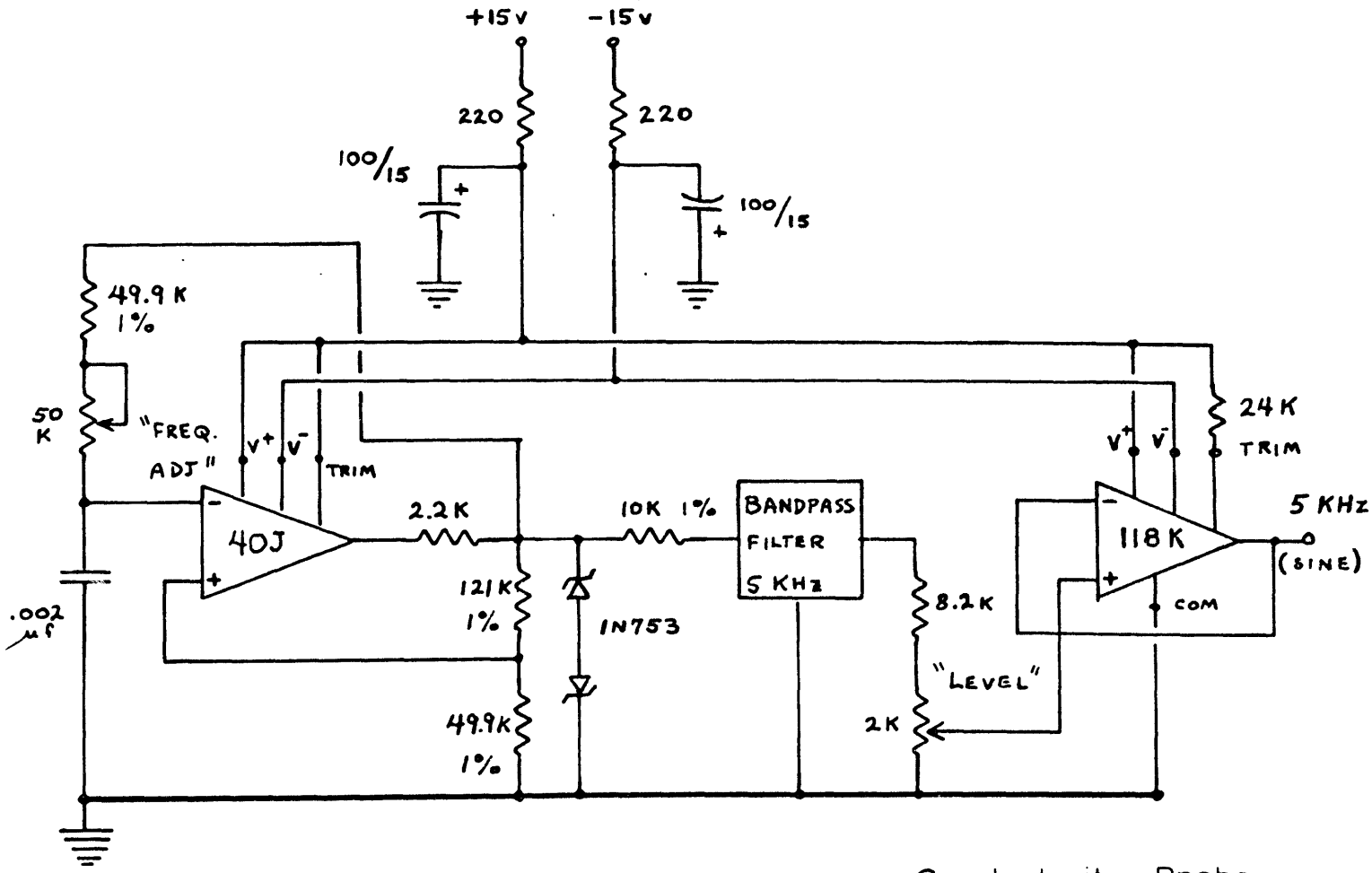

FIGURE A-3

Conductivity Probe

Oscillator with Amplitude Stabilization

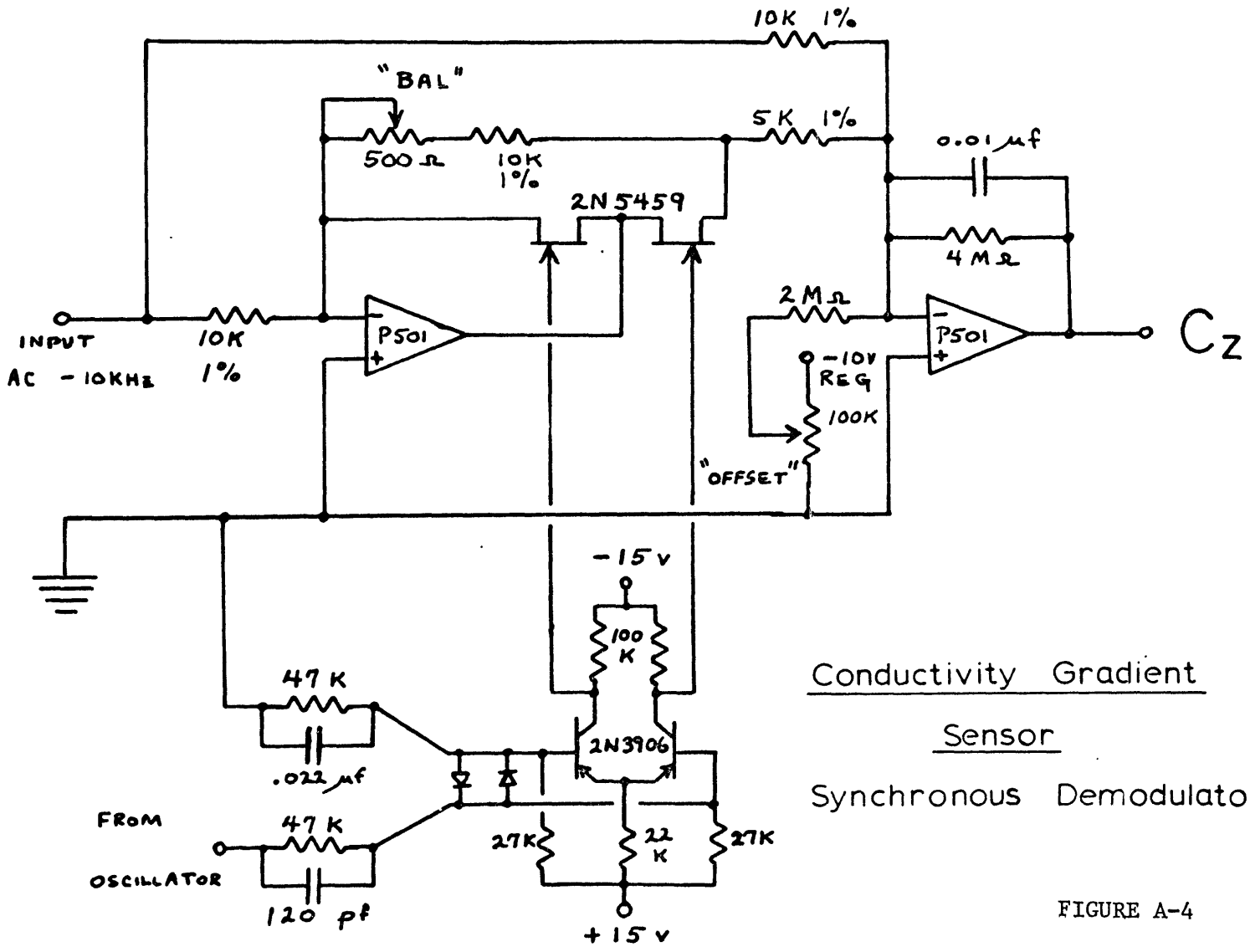

Conductivity Gradient

Sensor

Synchronous Demodulator

FIGURE A-4

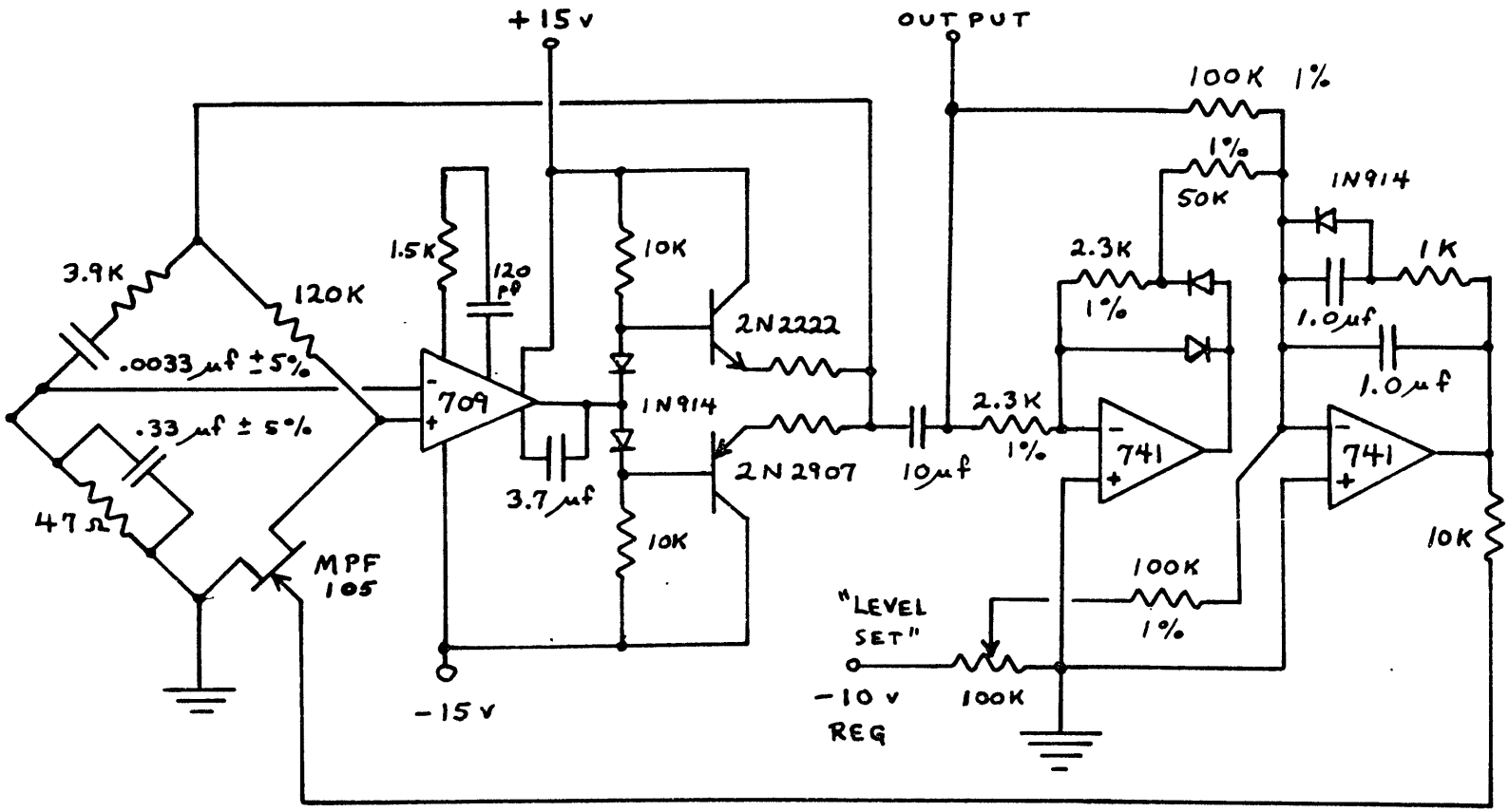

Conductivity Gradient Sensor

Oscillator with A.G.C.

FIGURE A-5

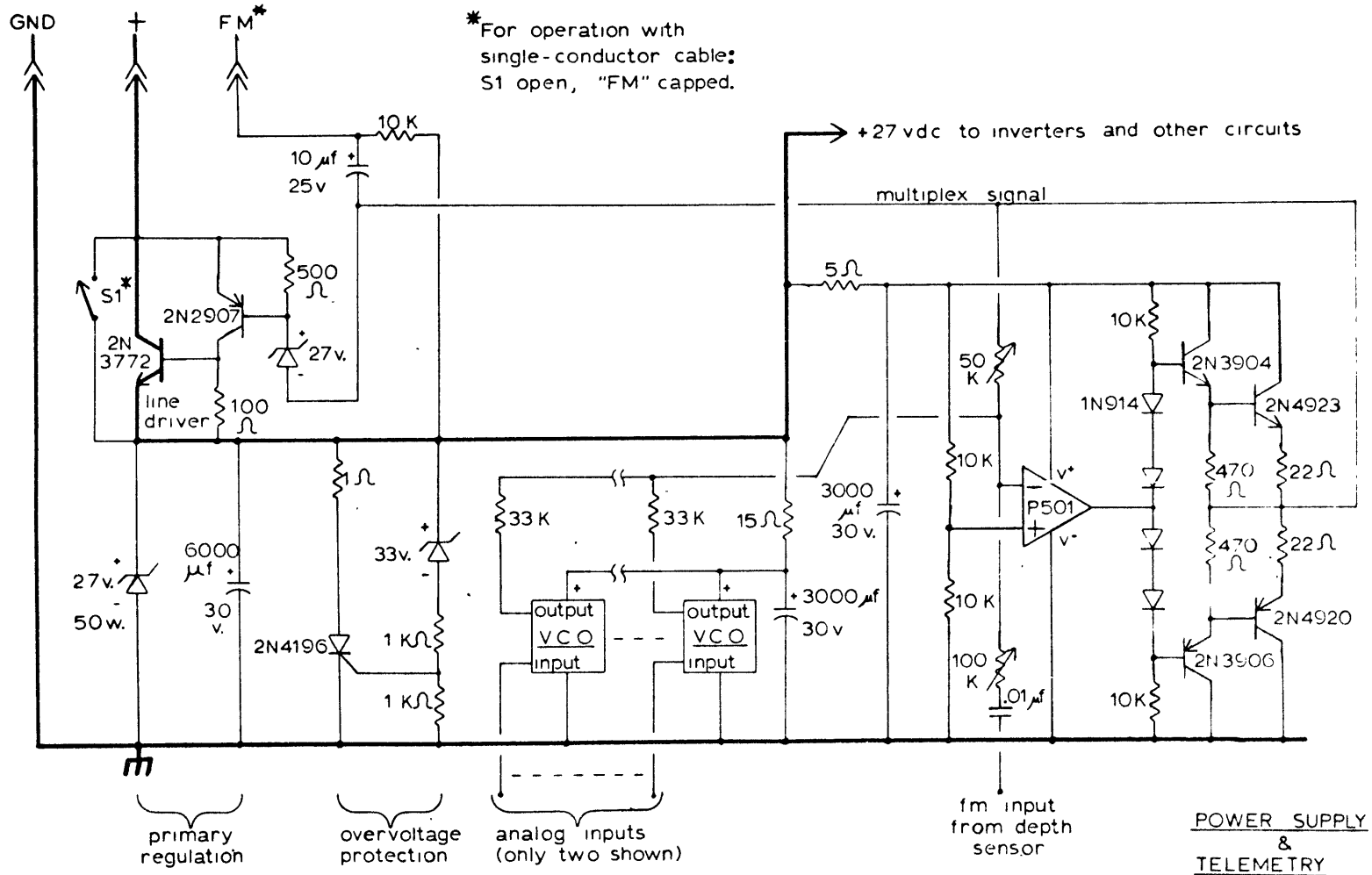

POWER SUPPLY & TELEMETRY SCHEMATIC

FIGURE A-6

TABLE A II

TELEMETRY SYSTEM FREQUENCIES

DATA	IRIG CH.#	f_o, Hz.	± DEVIATION	LBE, Hz.	UBE, Hz.
C'	14	22,000	1650	20,350	23,650
T'	13	14,500	1088	13,412	15,588
Z	12	10,500	788	9,712	11,288
V	11	7,350	551	6,799	7,901
	9	3,900	293	3,607	4,193
C	8	3,000	225	2,775	3,225
	7	2,300	173	2,127	2,473
T	5	1,300	98	1,202	1,398

It should be noted that the depth sensor provides its own frequency-modulated signal which is (conveniently) Channel 12.

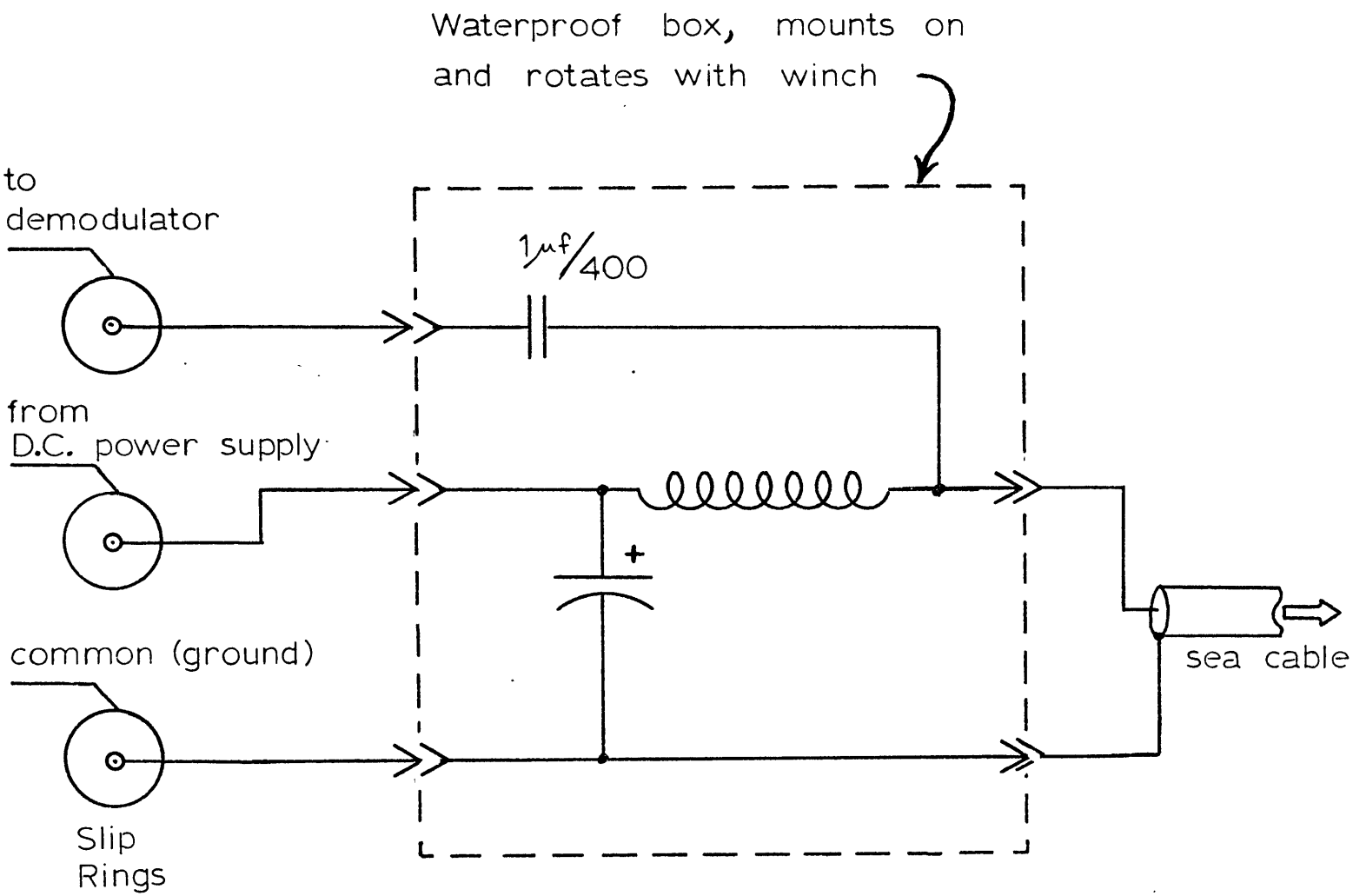

SIGNAL SPLITTER

FIGURE A-7

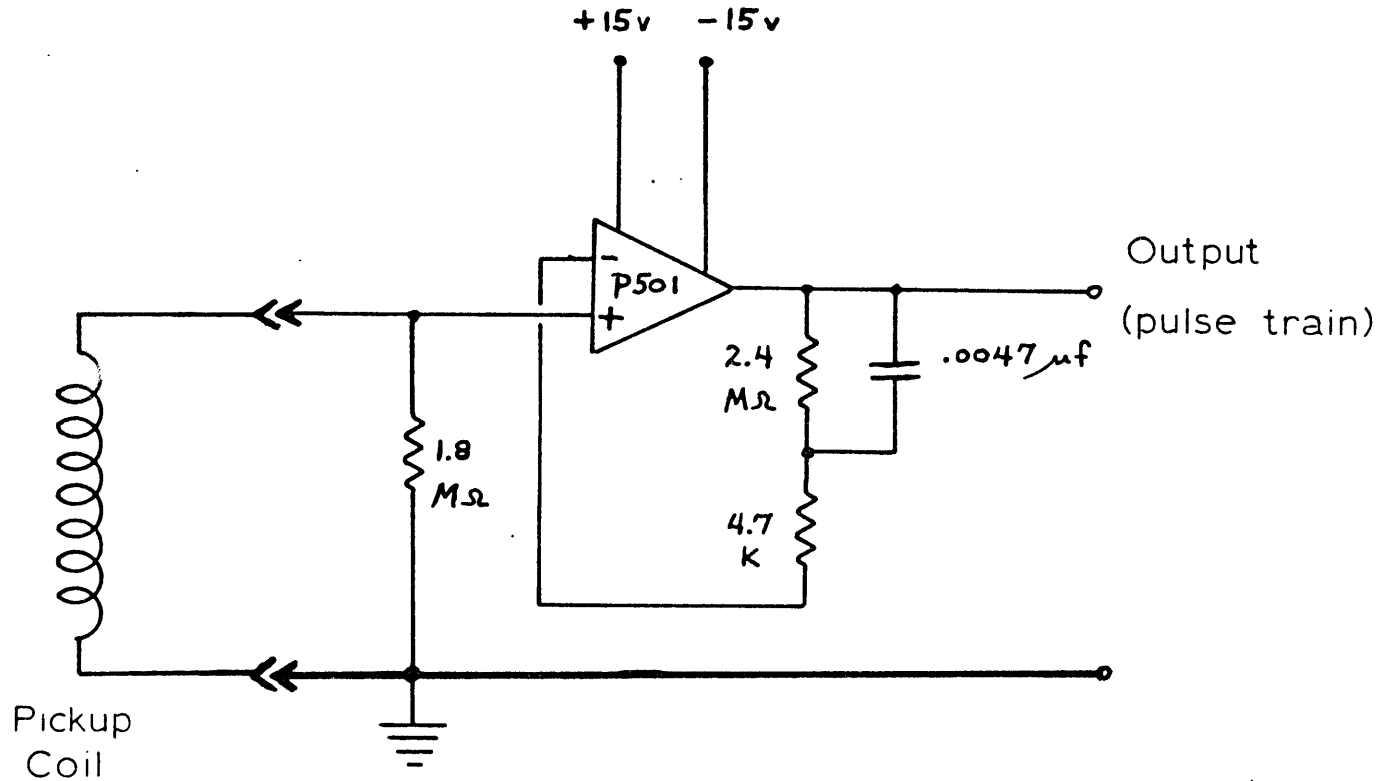

Velocity Meter Circuit

FIGURE A-8

APPENDIX 4

SPECTRAL ANALYSIS METHOD

For the purpose of this investigation the spectra were desired in the form of the power density of the spatial gradient versus wavenumber. The data, however, exists most conveniently as a function of time; and moreover the microstructure signal, C', is itself a time derivative, not a space derivative. For convenience, therefore, it was decided to perform the spectral analysis in the frequency domain first and convert to wavenumber space later. The spectra are made by feeding the time function C' into an electronic spectrum analyzer, which yields a spectrum whose axes have units of $(\mu\text{mho-cm}^{-1}/\text{sec})^2/\text{HZ}$, and HZ. Dividing both the frequency axis and the denominator of the ordinate by V (the local velocity in cm/sec) converts those quantities to units of cycle/cm. Dividing the numerator of the ordinate by V^2 converts it to a spatial derivative or a gradient. Thus, the desired spatial gradient spectrum in wavenumber space may easily be produced from the frequency spectrum of C' simply by scaling both axes by V^{-1}.

We are primarily interested in how the bursts differ from quiet regions; and in order to see this most clearly, all the spectra are plotted as dual spectra. The second spectrum in each case is that of an immediately-adjacent quiet region, made in exactly the same way and with the same settings as the burst spectrum itself. This technique is extremely useful in determining the significance of spectral features, and in

eliminating common and/or spurious peaks from the final plots.

DESCRIPTION OF THE SPECTRUM ANALYZING EQUIPMENT

Power-density spectra were computed for 25 bursts selected from various lowerings, using an electronic autocorrelator and Fourier analyzer (Princeton Applied Research Co., Inc., Model 101 Correlator and Model 102 Fourier analyzer). These machines use analog circuit techniques for the multiplication and storage of discrete or "quantized" information. Briefly, their operation is as follows: after the operator has selected a total delay time, T, the correlator samples the input signal 100 times in that interval. The sampling frequency is thus $\Delta\gamma = 100/T$, and the highest frequency that can be resolved is $50/T$ (the Nyquist frequency). Prefiltering of the data above this Nyquist frequency is done in each case to avoid aliasing; an RC filter having a 6-db/octave roll-off was found to be adequate. The samples, which are quantized, are clocked serially through a 100-position shift register. At each sample time, all the samples in the register are multiplied non-destructively by the current (instantaneous) value of the input data; then the samples are shifted one place, and the process repeats. The multiplied values are RC averaged in the output storage circuits. The resulting correlation function consists of 100 voltages, each representing the value of the autocorrelation function at a particular delay interval, $n\Delta\gamma$.

Many individual computations are required for the correlator's output to acheive its final values. Moreover, the correlator's output tends to degrade with time because an analog memory is used, so that it requires frequent updating. For these reasons the input data must be presented repetitively to the correlator via an endless tape loop. The bursts being analyzed in this work

are very transient and frequently do not completely occupy even a small tape loop; so it is necessary to gate or synchronize the correlator so that it only correlates when the burst is present.

The Fourier analyzer computes the transform of the correlation function; it presents the power density spectrum in the form of voltages (also quantized) which are used to drive an X-Y plotter. The frequency axis is quantized into about 500 discrete steps, and the amplitude is quantized into 100 levels. A single-sided Hanning window of the form $F_h(\tau) = \frac{1}{2}\left(1 + \cos \frac{\pi h \Delta \tau}{T}\right)$ is applied to the correlation function before the transform is taken, to prevent side lobes.

Owing to the rather low dynamic range of the correlator, it is crucial that the input signal be pre-amplified to be as large as possible without overloading the circuitry. Now, for this investigation it was desirable to compare the spectrum of a burst with an identically-made spectrum of an adjacent quiet region; but if the burst was amplified to the optimum level, then the quiet background signal was inevitably too small. In consequence, the background noise spectra shown in this thesis are more a measure of the spectrum analyzer noise level than of the true background signal strength.

The resolution in the frequency domain is 2/T; that is, it is a fixed percentage of the upper frequency limit, 50/T, of that particular plot. Each final plot, such as those shown in the text, is made by patching together on log-log scales a number of overlapping spectra of the same burst. This is why the resolution bandwidth on these final plots appears to change abruptly at certain wavenumbers. The exact wavenumber at which the crossover occurs depends on the velocity during that event.

Instrument velocities ranged from about 75 cm/sec to 250 cm/sec, with the median being about 150 cm/sec. In order to resolve wavenumbers as high as 2 cycle/cm, the upper limit of the

frequency analysis had to be tailored to the velocity in each case. For most of the bursts, an upper frequency limit of 250 Hz was about right. This corresponded to a total delay time, T, in the autocorrelator of 0.2 sec. Overlapping spectra having upper frequency limits of 100 Hz (T = 0.5 sec) and 50 Hz (T = 1.0 sec) were generally made also, to obtain better resolution at the low end.

ERRORS IN THE SPECTRAL RESULTS

Owing to the manner in which the autocorrelator performs its multiplications (which will not be discussed in detail here) the correlation function exhibits fluctuations at each of its 100 points. The amplitude of these fluctuations is normally distributed, and is proportional to the output amplitude. In consequence, the amplitude of the power density spectrum is slightly different with each sweep of the frequency scale. Thus if repeated spectra are made from the same input data, an ensemble of spectra is generated whose amplitudes may differ somewhat in a random fashion. The best estimate of the true spectrum is an average over this ensemble. The variance of the spectral ensemble around its mean value provides an estimate of the instrumental error in the analysis. These are the error limits shown on the figures in the text. It should be borne firmly in mind that although this error arises randomly, and requires averaging in the frequency domain to obtain a good spectral estimate, it is nevertheless solely instrumental in nature, since only one particular chunk of input data is involved in each spectrum (except for the composite spectrum, Figure 5.13). That is, each burst has been analyzed separately, in the manner of a deterministic function, to determine its frequency content; however, each determination is imperfect due to analyzer noise and error.

In the case of the composite spectrum, there is an estimation error as well, due to the fact that only a finite number of individual spectra are contained in the composite. This estimation error would exist even if there were no instrumental error.

Furthermore, the correlator output decays in time, although it is continuously updated; but this degradation is not the same for all values of delay, $n\Delta\tau$. As a result, the spectrum shows spurious peaks at certain fractions of full scale frequency. But these peaks have been proven to be completely additive; and the use of the dual spectrum technique allows their removal completely within the rated accuracy of the equipment.

It should be noted that spectral analysis using an analog-to-digital converter and a digital computer to calculate the spectra would have provided greater dynamic range and flexibility, and hence better performance on wideband signals. However, the original intention of the investigation was to determine whether or not salt fingers are present in the thermocline, and therefore an analysis technique having the capability of positively detecting the presence of bandlimited energy was deemed satisfactory. Moreover, in view of the limited amount of data (limited from a statistical viewpoint, anyway), it is doubtful whether the improved resolution of digital processing could have provided much better understanding of the causes of the wideband processes. It was recognized from the start that a proper statistical treatment of turbulence in the ocean would require vastly more data than this project could gather; but that even a simple measurement such as the intermittency of turbulence would be extremely valuable.

PLOTTING PROCEDURE

The final spectra which are presented here are made in the following way: each burst is played into the spectrum analyzer repetitively by means of the tape loop. The analyzer scans over the

desired frequency range, producing an ensemble of spectra for each burst. A similar ensemble is generated for the background noise spectrum. Then an average smooth curve is drawn through each ensemble, one curve for the burst and one for the noise. These smoothed spectra are then replotted, after being purged of the spurious peaks, and scaled correctly including the V^{-1} factor.

DISCUSSION OF THE NOISE SPECTRA

The noise spectra shown here are intended as a reference, to indicate clearly the difference in frequency content between a burst and a quiet region. The noise spectra in most cases are not well resolved; nor should they be interpreted as oceanic structure. The true oceanic background noise is masked by instrument noise.

The output noise of the conductivity microstructure sensor is approximately constant in amplitude, and independent of velocity. This noise is mostly electronic in origin. The telemetry, recording, and playback system introduce a small amount of additional noise (mainly 60 Hz), also independent of velocity, of course. Thus, even if the spectrum analyzer could resolve this noise fully, the result would not have any oceanographic significance. But the spectrum analyzer also introduces noise of its own, which is dependent on the various control settings; this noise can be equal to or greater than the actual noise being analyzed.

Consequently, the noise spectra shown are mostly analyzer noise, especially in cases where the burst itself is large relative to the background noise. In such

cases the true signal-to-noise ratio is much greater than the plots indicate. In other cases, where the burst itself is relatively small, the noise spectrum is closer to the background noise; but, as described above, this noise has no oceanographic significance either.

To further compound the confusion, the magnitude of the noise signal is divided in each case by the magnitude of the velocity, in order to convert the time derivative, C', into the spatial gradient, Cx. Because of this, the background noise level, in terms of gradients, is not constant from spectrum to spectrum, when in fact the noise voltage actually is constant.